UNIVERSITY OF KWAZULU-NATAL

PERFORMANCE OF INSULATORS UNDER HVDC STRESS

Olanrewaju A. Lasabi

Supervised by:

Dr. A. G. Swanson

2018

PERFORMANCE OF INSULATORS UNDER HVDC STRESS

Olanrewaju Adedamola Lasabi

A DISSERTATION SUBMITTED TO THE SCHOOL OF ENGINEERING, UNIVERSITY OF KWAZULU-NATAL, DURBAN, IN FULFILMENT OF THE ACADEMIC REQUIREMENTS FOR THE DEGREE OF MASTER OF SCIENCE IN ELECTRICAL ENGINEERING.

AUGUST 2018.

Supervisor: Dr. A. G. Swanson

DECLARATION 1 – PLAGARISM

As the candidate's supervisor, I agree to the submission of this dissertation.

Name: Dr. A. G. Swanson

Signed: ..... Date: 20/08/2018

I, Olanrewaju Adedamola Lasabi, declare that:

1. The research reported in this dissertation, except where otherwise indicated, is my original research.

2. This dissertation has not been submitted for any degree or examination at any other university.

3. This dissertation does not contain other persons' data, pictures, graphs or other information unless specifically acknowledged as being sourced from other persons.

4. This dissertation does not contain other persons' writing unless specifically acknowledged as being sourced from other researchers. Where other written sources have been quoted, then:

a. Their words have been re-written but the general information attributed to them has been referenced

b. Where their exact words have been used, then their writing has been placed in italics and inside quotation marks and referenced.

5. This dissertation does not contain text, graphics or tables copied and pasted from the Internet, unless specifically acknowledged, and the source being detailed in the dissertation and in the References sections.

Signed: …… Date: 20/08/2018

Olanrewaju Adedamola Lasabi

DECLARATION 2 – PUBLICATIONS

Details of contributions to publications that form part and/or include research presented in this dissertation:

Paper 1: O. A. Lasabi, A. G. Swanson and I. E. Davidson, "Surface charge accumulation on DC insulators: an overview", *In Proceedings of the 25th Southern African Universities Power Engineering Conference*, vol. 1, pp. 38-43, January 2017.

Paper 2: O. A. Lasabi, A. G. Swanson and K. G. Ilunga, "Performance of Insulators under Impulse, AC and HVDC Voltage", *8th International CIGRE Southern Africa Regional Conference*, November 2017.

Paper 3: O. A. Lasabi and A. G. Swanson, "Performance of Insulators under AC and HVDC Voltage", *Fifth Eskom Power Plant Engineering Institute Student Workshop*, August 2018.

Signed: …… Date: 20/08/2018

Olanrewaju Adedamola Lasabi

DEDICATION

It is in Him we live and have our being. He is the one who has been busy working behind the scene seeing to it that the stage-play comes out perfect.

I dedicate this workpiece to the Lord Almighty.

ACKNOWLEDGEMENTS

All glory to Almighty God who made the compilation of this dissertation possible. I would like to express my sincere and deepest appreciation to my supervisor, Dr. A. G. Swanson, for his guidance and support. He has been of a great help and inspiration right from the inception of this investigation. I have certainly grown under his supervision and I hope that we will still work closely together in the near future.

My profound gratitude also goes to my mother, Mrs. K. A. Lasabi, for her love, prayers, immeasurable support and impact in my life. It is my prayer that you will live long to enjoy the fruits of your labour. Also to my siblings, Folakemi and Oloruntoba, I appreciate all your prayers, advice, patience and support.

I would also like to extend my gratitude to the Specialisation Centre in HV Engineering (DC) and FACTS as part of the Eskom Power Plant Engineering Institute (EPPEI) at the University of KwaZulu-Natal, Durban, for the funding provided all through the course of this research investigation.

I wish to also thank all my friends, colleagues and academic mentors at the University of KwaZulu-Natal for all their encouragements and insightful advice.

Lastly, I would like to appreciate Pastor Gabriel Adejimi and every member of The Redeemed Christian Church of God, Chapel of Praise, Durban, for their prayers, love, support and kindness toward me. All is well that ends well.

Thank you all.

ABSTRACT

Ongoing industrialization and expansion in developing economies around the world calls for an upgrade and reinforcement of the current electrical power systems with the use of high voltage direct current (HVDC) transmission and distribution systems. A major factor for these systems is the choice of suitable insulators required by the transmission lines. Insulators under HVDC are expected to function irrespective of the various stresses associated with their use, varying and extreme environmental conditions. The electric field distribution around insulators under HVDC stress is different to that of insulators under an AC stress due to electrical characteristics (resistivity and permittivity) and the space charge accumulation in the air-solid interface of the insulation system. This contributes to the mechanism of breakdown for insulators under DC stress. This study contributes to the knowledge and understanding of insulator breakdown voltage under HVDC stress.

Experiments were carried out with a 22 kV silicone rubber insulator according to IEC 60060-1 standards, to understand the breakdown voltage under impulse, AC and HVDC in both dry and wet conditions. The results indicated that the impulse breakdown occurred at a higher voltage, compared to DC and AC, as expected due to the short duration of the applied voltage. It was noted that the breakdown voltage for negative DC was higher than the positive DC, an indication that the space charge generation and distribution may be the cause.

Breakdown tests were carried out on 22 kV silicone rubber and glass cap-and-pin insulators under AC, negative and positive polarity HVDC stress where the effect of the surface charge was investigated. The course of these surface charges was modified through a corona source and quantified by measuring the leakage current along the insulator surface. The results were analyzed and showed that the choice of insulator material plays a crucial role in DC insulation system: silicone rubber being an organic material exhibited more current than the non-organic glass insulators.

To further aid the understanding of the differences in the electric field, the test arrangements were analysed using finite element models. The simulation results showed that under the application of DC voltage, the presence of space charges on the insulator surface distorts the electric field distribution along the insulators and the field becomes resistive as against capacitive under AC voltage when there is an increase in surface conductivity.

TABLE OF CONTENTS

LIST OF FIGURES

LIST OF TABLES

LIST OF ABBREVIATIONS

ATH	Aluminum Trihydroxide
ATR-FTIR	Attenuated Total Reflection Fourier Transform Infrared Spectroscopy
ECR	Electrical grade Chemical Resistant
EPDM	Ethylene Propylene Diene Monomer Rubber
ESDD	Equivalent Salt Deposit Density
FRP	Fiberglass Reinforced Polymer
FEM	Finite Element Method
FEMM	Finite Element Method Magnetics
FOV	Flashover or Breakdown Voltage
HTV	High Temperature Vulcanized
HVAC	High Voltage Alternating Current
HVDC	High Voltage Direct Current
IEC	International Electro-technical Commission
LI	Lightning Impulse
LMW	Low Molecular Weight
LTV	Low Temperature Vulcanized
MVDC	Medium Voltage Direct Current
NCI	Non-Ceramic Insulators
NSDD	Non-soluble Deposit Density
PDMS	Polydimethylsiloxane
RMS	Root Mean Square
RTV	Room Temperature Vulcanized
SDD	Soluble Deposit Density
SEM	Scanning Electron Microscopy

SiR	Silicone Rubber
UV	Ultra-violet
XPS	X-ray Photo-electron Spectroscopy

LIST OF SYMBOLS AND UNITS

U_{50}	50% Flashover or Breakdown voltage
η	Attachment coefficient
cm	Centimetre
σ	Conductivity
I	Current
E	Electric field
K_{det}	Electron detachment
F	Electrostatic Force
q	Elementary charge
kV	Kilo-Volt
KVA	Kilo-Volt Ampere
mm	Millimetre
min	Minutes
P	Pressure
β_{ei}	Recombination coefficient of electron-ion
β_{ii}	Recombination coefficient of ion-ion
∅	Scalar voltage potential
s	Seconds
T	Temperature
α	Townsend's first ionization
V	Voltage

CHAPTER 1
INTRODUCTION

1.1 Background Knowledge

The electric power system serves to generate, transport and distribute electrical energy to consumers in an efficient, economic and reliable manner. When contemplating electricity delivery, a choice must be made between alternating current (AC) and direct current (DC) system. AC has been used as the desired platform for transmission and distribution of electricity for over a century, including lower voltage (LV) distribution systems that supply electricity to serve industrial, commercial and residential loads. Its intrinsic advantage of easy voltage level conversion which can be carried out by a power transformer coupled with the emergence of poly-phase circuits, induction motor and flexible alternating current transmission systems (FACTS) devices also contributes to further advancement of the AC system.

There are however various drawbacks that limit the utilization of AC transmission systems. These include transmission capacity, distance constraints as well as the impossibility of directly connecting two AC power networks of different frequencies. Although not as popular as AC transmission, HVDC systems offer other special technical advantages as all angular stability problems now disappear and even connection of systems at different frequencies is entirely feasible [1]. In HVDC transmission systems, the concept of skin effect is also not found which allows for power transmission between unsynchronized AC transmission systems. Additionally, harmonics, transients, and oscillation issues are minimal. The effortless control of power flow in HVDC system makes thermal capacity and maximum power of transmission lines attainable. HVDC also eliminates problems of cable charging current, thus cables can readily be used for underwater crossings [2]. These great merits in the HVDC system would offset the high costs of the DC inverters and rectifiers. In this new energy era, HVDC is expected to grow beyond its traditional position as an enhancement to AC transmission and play a dominant role in the electric power system, most especially in the smart grid (SG) system [3]. One key issue to this advancement in the power system is the selection of appropriate insulators for HVDC transmission lines. Due to the high and increasing operating voltage, the insulation system will be exposed to stronger electrical stresses than ever before.

Various studies have been carried out on the technical and technological properties of HVDC insulators but there are some practical aspects which are still unclear, in particular, the breakdown (flashover) mechanisms due to the different electrical characteristics (resistivity and permittivity) and in the presence of space charges accumulating on the insulator surfaces. Surface charging is

a phenomenon in HVDC systems and may affect the performance of insulators. Surface charge accumulation and its distribution along the insulator surface allow for the flow of leakage current which reduces the effective resistance of the insulator surface [4]. The localized electric field, along the insulator surface, may become distorted and thus may affect the breakdown characteristics of the insulator. These phenomena should be considered in the design and application of insulators for HVDC systems. This would result in a more secure and reliable system.

1.2 Motivation for the Research

At the time of writing, the only operational HVDC link in South Africa is Cahora Bassa link with a power rating of 1920 MW at a rated nominal voltage of ± 533 kV. The link runs between South Africa and Mozambique. Both composite and glass (cap-and-pin) insulators are used in the scheme for the insulation. There are some unpredictability of the integrity of the air gap and insulation and investigation is required into the breakdown mechanism under HVDC stress [2]. Furthermore, should a new scheme, whether HVDC or even MVDC, be developed in South Africa, there is a need to understand the breakdown mechanism to improve design or specification of the insulation.

1.3 Problem Statement

The electric field distribution around insulators under HVDC is different from that of insulators under AC and impulse; the capacitive field distribution considered under AC or impulse becomes a solely resistive field distribution under DC. This is due to the characteristics of the materials of the insulator (resistivity and permittivity) as well as the accumulation of space charge in the air-solid interface along DC insulators [4]. This field distortion may lead to reduction in the breakdown voltage across DC insulators. The insulator interface is inherently a part of the gas-solid insulation system. The problem is that the breakdown mechanism for insulators under HVDC stress has not been fully understood.

1.4 Research Objectives

The objective of this research investigation was to carry out laboratory experiments and develop a simulation model that would be both repeatable and representative of outdoor HVDC insulation system. The research objectives were as follows:

- To investigate and evaluate the breakdown performance of polymeric insulator under high voltage AC, standard impulse and DC. This will help to understand the differences between the mechanism of breakdown under DC and other voltage types.

- To investigate and evaluate the breakdown and leakage current performance of both composite and glass (cap-and-pin) insulators under HVDC stress. This will give a better understanding of the differences between the insulator material characteristics and space charges.
- Development of both composite and glass (cap-and-pin) insulator models based on finite element methods to aid in the understanding of the differences in the electric field.

1.5 Outline of the Dissertation

This dissertation is divided into five main chapters.

Chapter 2 provides a literature review of types of insulators used in high voltage transmission, their failure modes and several factors responsible for the degradation of insulator material. Mechanisms of charge deposition, accumulation and transport of charges on the surface of high voltage insulators, charging mechanisms, effects of surface charges on insulator flashover characteristics, leakage current and flashover criteria are also discussed.

Chapter 3 describes the experimental set-up and procedures used during the course of this research investigation in the laboratories. Also, a discussion on the computer simulation models developed to aid in the understanding of the electric fields are also provided.

Chapter 4 presents the results and analysis of all the experiments and simulation models undertaken during the investigation.

Chapter 5 presents conclusions and recommendations that were derived from the findings and propositions for future work.

CHAPTER 2
LITERATURE REVIEW

2.1 Outdoor Insulators

In high voltage power transmission, insulators render mechanical reinforcement to the lines and electrically isolate the transmission lines from the tower to prevent the flow of current to the earth. Flashovers occur on outdoor insulators resulting in a breakdown of the insulation system and this can stop the continuous progress of the flow of power. A flashover can be explained as a disruptive discharge taking place along the gas (air)-solid interface of the insulation system resulting in a high voltage short circuit between two electrodes. The gas-solid interface is the breakdown path which becomes conducive for ionization resulting in a sustained electric arc [5]. This arc tends to bridge the two end-fittings of the solid insulator. Environmental conditions such as pollution, humidity, temperature and pressure can affect outdoor insulators resulting in their breakdown. Insulator design, construction, and material may also contribute to the failure of the insulation system.

In overhead transmissions, materials employed for the manufacturing of insulators are generally inorganic and organic. Organic materials are mainly utilized in non-ceramic insulators and inorganic in ceramic insulators. Insulators made of glass and porcelain material are grouped as ceramic while either polymer or composite insulators are grouped as non-ceramic. Ceramic insulators were used before the emergence of the power system for telegraphic purposes [6]. With the development of the AC power systems, the need for ceramic insulators increased greatly. The modernization of the power system which involves utilization of HVDC system coupled with the increasing transmission voltage has caused a shift to the use of polymeric insulators due to their great insulating performance over ceramic insulators [7]. Polymer insulators have excellent insulating properties and great tensile strength-to-weight ratio.

2.1.1 Porcelain Insulators

Porcelain insulators can be classified into two categories; the cap-and-pin as well as the long rod suspension insulators. The cap-and-pin insulators are fabricated with the porcelain insulating shell, galvanized malleable iron pins and caps which are assembled together with cement. Porcelain cap-and-pin insulators can also be categorized into two parts, namely: stacking and non-stacking units [8]. The difference between the two is the number of sheds between one pair of electrodes, the stacking unit has more than one shed while the non-stacking unit only has one.

The long rod suspension insulators are fabricated to circumvent the punctures which are experienced by the insulating media and with the increased leakage distance, they are able to

withstand more harsh or critical environmental conditions [8]. All the components of both types of porcelain insulators influence the mechanical capabilities of the insulators and they require a heedful treatment. The surface and volume properties of the insulators govern their electrical capabilities [9].

2.1.2 Glass Insulators

When exposed to electrical stress, the glass type of insulators are susceptible to fracture. This breakage that occurs on the glass surface results in poor mechanical performance of the insulator, it also affects both the electric field distribution and properties of the insulator interface [10]. As a result, glass insulators yielded both poor mechanical and electrical capabilities in their early ages. Research carried out over the years on glass insulators has however improved their performances. Presently, the addition of barium, potassium and aluminum to the glass material have toughened the insulator. When compared to other insulator types, the toughened glass insulators have better mechanical performance and the ability to withstand electrical stresses also increased by 40% [9].

The toughened glass insulators have greater ability to prevent erosion when compared to porcelain insulators and during manufacture, glazing is not required [10]. They can be grouped into three categories namely: multi-cone post insulators, pin-type glass insulators and suspension glass insulators [8]. Out of the three, the suspension glass insulators are the most prevalent type.

2.1.3 Polymer Insulators

Polymer insulators can be referred to as either composite or non-ceramic insulators, with their mechanical and insulation material merged together. Distinctive attributes such as light-weight, cost-effectiveness, ease of fabrication, viability for different shapes, recycling, high dielectric strength coupled with the capacity of allowing other materials to be added to it for the formation of composites have led to a drastic increase in their usage around the world in high voltage insulation systems, where there is great need for reliability [11, 12]. However, due to the nature of the material being used for polymeric insulators (i.e. organic materials), they are liable to leakage currents and this makes them more prone to ageing [12, 13].

Polymeric insulators are composed of three main parts [9]: Fiberglass Reinforced Polymer (FRP) rod, metal end-fittings and polymeric weather sheds. The FRP rod is located at the center of the insulator and is a very crucial component of composite insulators because it provides support for the mechanical load. Either epoxy resin, polyester or vinyl ester can be used to strengthen the rod. The fiberglass used for the rod are also Electrical grade Chemical Resistant (ECR) so as to avoid fracture. The end-fitting hardware parts are grooved to the rod at both ends, they are made up of either forged steel, malleable iron or cast, forged or machined aluminum. They can be attached to

the core by swaging or gluing. To protect the FRP rod from electrical failure when subjected to harsh environmental conditions and electrical stresses, weather sheds of various polymeric materials with excellent ageing resistance are shaped and spaced over it [14]. This also produces the needed leakage distance.

Polymeric materials used for the weather sheds are ethylene propylene rubber, ethylene-propylene-diene monomer and silicone rubber. Silicone rubber proved to have the best performance when subjected to harsh environmental conditions and this is due to its great hydrophobic characteristics [15]. They can be categorized as: line post type and suspension type insulators [10]. The line post type of insulators is analogous to the suspension types in terms of its component features. The diameter of its fiberglass core is more than that of the suspension type of insulators [8] and this made the line post type more useful for heavy mechanical loads.

In high voltage transmission system, the operation of non-ceramic insulators over a long period of time has become more challenging as their breakdown can lead to a halt or disruption in the supply of electric power. Several factors can influence their breakdown such as wetting and electrical treeing, dielectric losses, accumulation of space charge, etc. This factors may lead to an increase of unwanted conduction processes in the polymer material [16, 17]. Furthermore, the amplification of the local field may occur due to some imperfections such as protrusions, non-homogeneous dielectric properties, voids, cavities, etc. All these may result in events such as partial discharges, unanticipated flashovers and eventually breakdown of polymeric insulators [17]. In addition, the performance of polymeric insulators used in high voltage transmission systems can be influenced by other factors, such as corona, the formation of electrolytic solution on the insulator surface due to water and dust accumulation, electrode-material contact corrosion and environmental conditions such as temperature, humidity, pressure, ultraviolet radiations, etc. This may unavoidably cause degradation of polymeric materials in a very short time frame [18, 19, 20].

2.2 Insulator Failure Modes

The rate at which high voltage insulators fail nowadays depends not only on the standard of the design and the process of manufacture but also on the choice of the insulator, in terms of the material, that is being selected for a particular service condition. Failure modes are peculiar with each insulator type, due to the different types of materials and design involved [21]. The most common failure modes associated with the different types of insulator outlined earlier are discussed in this section.

2.2.1 Mechanical Failure and Shattering

Mechanical failure is one of the usual failure modes experienced by high voltage insulators in operation. Virtually this type of failure mode can be associated with all types of insulator material, even though the causes of the failure are usually related to individual insulator design and material [21].

Shattering is a usual mechanical failure mode found in ceramic insulators. It is as a result of accumulated impurities during the fabrication process of the insulators [21]. Stress concentrations on the insulator are the result of these impurities and these stresses lead to the unprompted shattering of the insulators. The glass type of insulator is vulnerable to experience internal mechanical stresses developed by the movement of ions introduced under HVDC application.

In the case of porcelain insulators, shattering as a result of thermal stresses is another usual appearance of mechanical failure. A sudden change in temperature such as those encountered during power arcs is known to easily damage the porcelain material [21]. This damage can take different forms such as glaze cracking or breakage of the insulator sheds. Arc horns can be used on porcelain insulators as a protective device.

A distinctive kind of mechanical failure associated with the core of composite insulators can occur at the load levels far lower than the critical level. It takes place in the presence of both acid and tensile stresses and it can be called brittle fracture [21]. The core axis is perpendicular to the area of fracture which looks smooth over almost all the cross-section. A small irregular area that will not be able to withstand the load and consequently fail in conventional tensile mode will be created [22]. Clearly, brittle fracture can take place when moisture exists in the core, thus using water-proof for isolating the core is important. Brittle fracture can also be averted by making use of glass fibres which are corrosion resistant and less vulnerable to acid erosion [21].

Vandalism and damages that exist on insulators as a result of transportation, shipping and insulator handling can also be another cause of mechanical failure [23].

2.2.2 Thermal Runaway

This failure mode is specifically found on glass type of high voltage insulators operating under DC transmission lines, where electrical conductivity through the insulator is achieved by ionic conduction. Upon the application of a DC voltage, movement of ions within the insulator material is being aggravated in relation to material resistivity and temperature. As electrical current flow, the material temperature increase while its resistivity decreases and this process continues to iterate itself until the thermal capacity of the insulator is reached [21]. This results in the failure of the insulator.

2.2.3 Erosion of Insulator Material through Electrical Discharge

This failure mode is probably the most commonly found mode on any insulator in the field. It is usually caused by contaminants present on the insulator interface. During light rain, in the case of ESDD, the contamination layer becomes electrically conductive as a result of electrolyte formation and paves way for current to flow along the insulator interface. NSDD do not form electrolyte, but it can act as binding material for the conductive pollution and also contributes to the area available for leakage current flow. This leads to the emergence of small width dry bands areas which are exposed to the voltage of the transmission system [23]. Due to these dry bands, the field intensity surpasses that of the air enclosing the insulator and results in an electric discharge which causes the deterioration and erosion of the insulation material as a result of the huge quantity of heat energy involved. The material's relative affinity for water is also another factor that may influence this process.

Extreme Erosion can be found in close proximity of the pin for glass and porcelain insulators as a result of the high current in this area [21]. Mechanical failure exists in the insulator as a result of this severe erosion at the metal pin of the insulator. Zinc rings can be used to minimize this risk.

In polymeric insulators, electrical stresses coupled with environmental elements will not only result in the erosion of the insulation material but also tracking. This is in relation to the chemical composition of the organic material of the insulator [21]. Tracks are conductive immutable carbonaceous pathways [24]. They result in a permanent reduction of the insulator leakage distance which increases the risk of flashover and insulator failure. Proper covering of the core is very important as they can generate internal discharge that can result in erosion and tracking of the insulator when the core is contaminated [21]. Erosion of the core housing material can also expose the core to contaminant [21].

2.2.4 Electrical Punctures

This failure mode is analogous to that caused by erosion due to discharges with some remarkable differences in the process. They usually exist as a result of steep-fronted electrical pulses, which arise from external actions such as lightning and switching instead of the normal operating voltage of the system. The strength of the insulating material reaches the limit before the enclosed air can get ionized enough to form a flashover. This breakdown of the insulating material can lead to the formation of a channel in the material that can result in irregular line faults which are not easily located. This type of faults can also be called nuisance tripping [21].

2.2.5 Ultraviolent Ageing

Tracking and erosion are worsened by ultraviolet (UV) radiation which in turn results into insulator flashover and failure. Chalking or cracking of the interface of an insulator can be formed due to UV radiation and this can accelerate the process of erosion and lead to failure [25]. UV stabilizers are present in some materials such as silicone to avoid this type of failure mode [21].

Shed splitting has been observed in some insulator materials used for composite insulators such as EPDM due to a combination of electrical stresses, UV radiation and mechanical hoop stresses [21]. This affects the insulator performance.

2.2.6 Bonding Material Failure

Substances such as resins and cement are commonly used as bonding different insulator materials together during the manufacturing of insulators. The structural integrity of an insulator can be compromised when these bonding substances fail and this can results in mechanical failure, increased tracking and erosion which ultimately lead to flashover and electrical failure of the insulator [21].

A usual example of this type of failure occurs in porcelain insulators where cement is being utilized to join the fittings and insulator material together. Proper selection of the cement must be carried out in line with the anticipated service conditions so as to avoid the separation at the junction between the two materials which might enfeeble the connection and results into a mechanical failure of the insulator [21].

Composite insulators are also vulnerable to this type of failure mode as a result of their form of geometry with a sizeable number of parts and surfaces. Issues occur when insulator sheds and core are not joined together properly. Materials used as fillers such as silicone grease can begin to exude out and the resulting gap can be filled with contaminants. Finally, the sheds begin to move along the axis of the core resulting into an exposure of the core and eventually lessen the mechanical strength of the insulator [23].

2.3 Factors responsible for insulator material degradation

Insulator degradation or ageing is the gradual breakdown of insulator material impelled by stresses from external sources, which begins at the surface of the insulator and then continues far down into the material or the whole insulator length. This degradation of insulator reduces the performance of the insulator electrically and mechanically to the extent of insulator failure. Some major factors liable for this insulator deterioration are discussed in this section. Even though some

of these components do not actively lead to the material degradation, they can cause electrical discharge as a result of conductivity which can lead to the destruction of the insulation materials.

2.3.1 Pollution

Pollution can also be referred to as contamination. It is a term that is being used to describe the accumulation of any substances or contaminants at the interface of the insulator. They can be categorized into two classes [21]: pre-deposited and instantaneous contamination. The time frame at which contaminants accumulate on the insulator surface in the pre-deposited type of contamination is very long and it can be active, which is a formation of a wet conductive electrolyte. It can also be inert contamination, which does not form electrolyte but are non-soluble substances that act as binding material during the active type of contamination and they can increase the pathway required for leakage current to flow [21].

Instantaneous contamination takes place when the interface of the insulator becomes enveloped in a highly conductive contaminant [21]. Contamination can be found from different sources such as agricultural, marine and industrial sources [21].

2.3.2 Rain and Humidity

A specific level of humidity is generally required for the contamination layer on the interface of the insulator to transform into an electrolyte. Once this level is reached, current tends to flow along the insulator interface. This leads to the emergence of areas of dry bands and in turn discharges which can destroy the insulation material [25]. Humidity can be derived from the air enclosing the insulator or from fog and rain. Fog can also contain conductive particles (salts or acid) mixed in the water. This can result in instantaneous contamination and rapid flashover [21].

The level of conductivity of the contamination layer can also be increased by acid rain. Acid rain can equally interact with the insulation material which can result in erosion and a change in the chemical composition of the material [21].

2.3.3 Solar Radiation

Various forms of radiation with distinctive wavelengths and energy levels exist in the radiation from the sun. Some of these radiation types such as ultra-violent photons with high energy can result in the degradation of some materials used in the manufacturing of insulators such as polymers [9].

2.3.4 Bird faeces and Streamers

A huge quantity of nitrogen is present in bird faeces. The mixture of this nitrogen with water results in the production of nitric acids which causes deterioration of the insulator material [9]. The level of conductivity present in nitric acid is also high which can result in an increase in the

leakage current and in turn increases electrical discharges. Examples of such cases are bird streamers. They are very long strings of bird faeces which pose a huge level of conductivity that can result in the rapid breakdown of the insulator [9].

2.3.5 Destruction by Animals and Vandalism

Though the destruction of insulator material through vandalism or by animals such as rodents and birds do not actively cause material degradation. They form areas on the insulator interface which degrades at a faster rate than the materials that are not affected by vandalism or animals. This ultimately stimulates insulator ageing [21]. Damages done by animals are usually associated with composite insulators.

Glass and porcelain types of insulators are usually associated with the damages through vandalism simply because the materials tend to shatter under high impact [23]. Destruction of ceramic insulator glaze and non-ceramic insulator housing can allow contaminants and acid to get to the core materials and this fosters the degradation of insulator material.

The effect of all these factors responsible for insulator material degradation become more pronounced on high voltage insulators operating under HVDC when compared to those operating under AC transmission systems. This can be linked to the static electric field resulting from the effect of space charges which are usually associated with DC voltage [40].

2.4 Silicone Rubber Hydrophobic Characteristics

Hydrophobicity, from the chemical point of view, is simply the physical characteristics of a molecule whose affinity for water is very low. It can also be defined as the physical property of a material surface that impedes the formation of a continuous water layer [9]. These hydrophobic materials are non-polarized while water is a polarized molecule. Formation of a hydrogen bond is easier with water molecules while hydrophobic molecules cannot form hydrogen bonds [27]. As a result of these differences in the chemical properties, the contact surface between the hydrophobic material and water has been detected to be very low.

Hydrophilic as an opposite of hydrophobic molecules is the physical characteristics of a molecule that bonds with water easily through a hydrogen bond. They are polar and they can dissolve easily in various polar solvent [27]. The formation of a continuous water film or layer will not be impeded by hydrophilic surface. Due to high affinity for water which some hydrophilic materials possess, water molecules can easily be attracted to them from the environment or even penetrate through the material surface such as in the case of hygroscopic materials [9].

Hydrophobic materials are suitable and desirable for use in the manufacturing of high voltage insulators. Water layers will be restrained from bridging the gap between the live and dead end of the insulator. This ultimately prevents the formation of any conductive layer and inhibits electrical discharge which could destroy the insulator interface [28]. Hydrophobicity is also a varying characteristic that can either be lost or gained depending on the environmental factors and the surface of the insulation material [28]. This regaining ability of hydrophobic material has led to the reason why silicone rubber has been an important material for high voltage insulators.

2.4.1 Chemical Structure of Silicone Rubbers (SiR)

Silicone rubber material is made up of a polymer fused together with a filler material through a technique named vulcanization [29]. The backbone of oxygen and silicone are generally the main constituent of the polymer which bonds together in a pattern occurring in turn repeatedly to produce either a long chain of molecules or cyclic molecules if the molecules at both ends are bonded to one another [28]. Also to the silicone molecules, organic methyl groups which are carbon based are attached. These organic groups determine the chemical and physical characteristics of the final product [30]. Figure 2.1 describes the chemical structure of a silicone rubber molecule with the *R* representing the organic group.

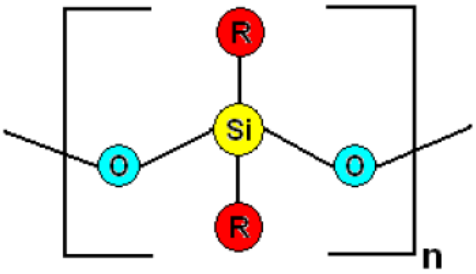

Figure 2.1: Chemical Structure of a Silicone Rubber Material.

The utilization of silicone and oxygen as base molecules proffers many merits such as thermal stability of the final product that is being formed over a broad range of temperature as a result of the strong bond between silicone and oxygen [29]. It is in opposition to natural, chemical and fire attacks [30]. It is not a harmful substance. In comparison to other polymers, the spreading ability of silicone rubber is very good and this makes it viable as an excellent coating material. Silicone rubber can tolerate UV radiation and high temperature. It can offer a high resistance to a large number of different external influence.

The cross-linked intermolecular bonds that take place in between the independent chain molecules in a silicone rubber material are usually of a very weak strength even though this allows the flexibility of the elastomers but provides a lower mechanical strength [28]. To enhance this mechanical strength of silicone rubber materials, a filler such as kaolin, silica, mica or alumina

trihydrate (ATH) can be added [31]. These fillers have a notable effect on the characteristics of the end product of the silicone rubber. They affect characteristics such as the degree of water absorption, the thermal conductivity of the final product, the hydrophobic nature, formation of leakage current and the resistance of the end product to erosion and tracking [26, 30].

At a separate degree of temperature, the process of vulcanization used in the manufacturing of silicone rubber produces a diverse number of silicone rubber types. A very good example is the high temperature vulcanized silicone rubber (HTV) produced at a high temperature of 200^{o}C, with excellent dielectric characteristics such as high mechanical strength and its resistance to ageing. These characteristics make HTV an excellent material that can be well utilized in the production of high voltage insulators [29]. Another type is the room temperature vulcanized silicone rubber (RTV) which is formed at room temperature with its curing either taking place on contact with humidity or upon the merger of two different fabricated elements of the same polymer material [30]. The dielectric characteristics of RTV products are the same as the HTV materials but its exceptional characteristics of good adhesion and low viscosity made it useful in the manufacturing of high voltage hardware [30]. Other types of silicone rubber products are the liquid silicone rubbers and the low temperature vulcanized (LTV). They are not usually used in the manufacturing of high voltage insulator.

2.4.2 Mechanism of Hydrophobicity

Strong hydrophobic nature of silicone rubber has approved its use in the manufacturing of high voltage insulators since the early 1970's. This hydrophobic nature is as a result of two factors which are the diffusion of the molecules or compounds of LMW and the positioning of the organic methyl group bonded to the polymer molecules [28].

2.4.2.1 Diffusion of LMW Compounds

LMW compounds are elements present in a polymer material with a molecular weight of less than 1000 as against that of HTV molecules with a weight of $5x10^5$ [31]. As a result of their small weight and size, LMW compounds can migrate without any restrictions all through the bulk of the material and cumulate at the surface of the polymer material.

In the presence of a contamination layer at the silicone rubber surface, LMW compounds diffuse into the contamination layer and envelop the contaminant [28]. LMW compounds are hydrophobic in nature and this makes the contamination layer hydrophobic, thereby suppressing the leakage current flow. This is one of the merits of silicone rubber. A special case of this process takes place when the contamination layer is made up of a uniform salt layer [28].

During rainy season or maintenance, the contamination layer is washed off resulting in loss of these LMW compounds. This can be called an indirect loss of LMW compounds [27].

Hydrophobic nature of the material surface is also lost to some extent. After some time, LMW components tend to diffuse from the bulk of the silicone rubber to the surface and eventually the hydrophobic nature of the material surface is recovered. Two sources of LMW compounds exist within the polymeric material:

- A huge accumulation of LMW generated in the course of the vulcanization process [27].
- LMW generated through scission of long molecular chains. This can also be called regeneration of LMW. It is a natural process which can speed up through discharges at the surface and various types of radiation. Even though the amount of LMW produced through this process is lower than the one already existing in the material [32].

One of the main factors causing the ageing of silicone rubber material is the steady loss of LMW compounds. The reason for these losses can be as a result of electrical discharge at the surface and leaching through interaction with water and through chemical reactions [28]. These are the direct losses of LMW compounds.

2.4.2.2 Positioning of Methyl Groups

Several organic compounds which are carbon-based can be bonded to the backbone bond of the silicone and oxygen through several chemical processes. The group which is usually utilized most is the methyl (CH_3). This gives rise to the term polydimethylsiloxanes materials (PDMS) which are usually used for silicone rubbers. The methyl groups are at liberty to move around the backbone bond of silicone and oxygen [30]. At the material interface, the molecules orient themselves in a fashion such that silicone oxide molecules points towards the inside while the methyl compounds face outwards. Methyl groups and the molecules of water repel one another simply because of water being a polar solvent while methyl a non-polar. Hence, the methyl group layers produce the hydrophobicity properties of the material. This can be seen in Figure 2.2.

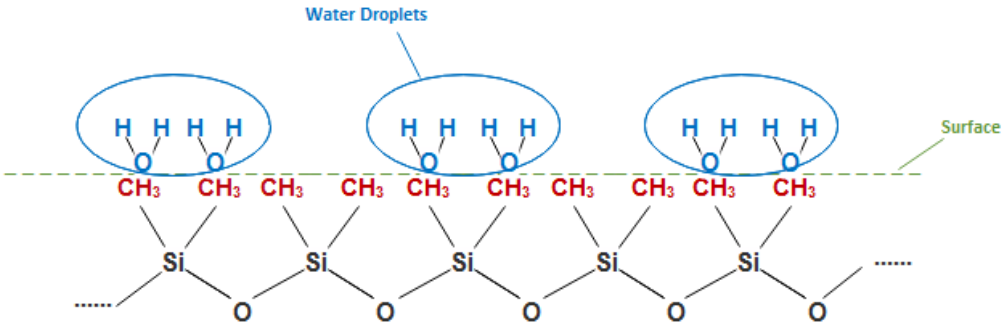

Figure 2.2: Mechanism of Hydrophobicity on Silicone Rubber Interface.

Sometimes, the polymer compounds in the silicone rubber material can also move around the axis such that the methyl group now points towards the inside while the silicone oxide faces outwards

to form the layers at the surface [32]. However, since water and oxygen compounds are polar in nature, they will be attracted together and this results in a change in the hydrophobic characteristics of the material surface to a hydrophilic surface. Water layers can then form easily on the surface, which if contaminants are present can result in the production of an electrolytic solvent which will cause an increased leakage current to flow. Repositioning of the molecular chains in a way that the methyl group points in the outward direction can lead to the recovery of hydrophobic characteristics of the insulating material.

2.4.3 Basis for Loss of Hydrophobicity

Many external factors affect hydrophobicity loss in polymeric materials. Electrical discharges in form of corona or dry arcing are one of such factors [28]. The energy released during the discharge give rise to a disintegration of polymer chains present in the material, particularly in smaller molecules such as low molecular weight molecules (LMW). The fragments that result from the disintegration can evaporate directly or form a bond with water and leach from the material [31]. Discharge activity in a secondary development can lead to the production of acids from water and air, leading to the deterioration of the material surface. Surface degradation causes a reduction in hydrophobicity which in turn aggravates the surface discharges [27].

Water is also a major factor in the hydrophobicity loss. Apart from the loss of smaller molecules, particularly LMW molecules through leaching, the existence of water on the interface can lead to a restructuring of the organic methyl groups in the chain structure which will increase the hydrophilic property [28]. The existence of a soluble layer of contaminants on the insulator surface can pave way for excess water to produce a conductive layer across the insulator. This conductive layer forms dry bands after drying locally and results in increased surface discharges. The electric field of the insulator can also be significantly altered by water droplets, resulting in an increased field strength that can be so high at the borders of the droplets. Water drop corona can thus be generated, intensifying the activities of electrical discharge along the insulator surface and stimulating hydrophobicity loss [32].

Temperature has a twofold effect on the hydrophobicity of polymer surfaces. Temperatures greater than 400 ^{0}C caused by arcing increases surface erosion. There is an exponential relationship between temperature and erosion mass that causes a decreased surface hydrophobicity [33]. The diffusion of LMW molecular and chain scission increases with elevated temperatures to further decrease hydrophobicity [28]. Furthermore, a high mobility of LMW indicates that the rate at which molecules diffuse to the material surface is high and this eventually enhances the hydrophobicity recovery [31].

The choice of materials is also another factor that affects hydrophobicity. The different processes of vulcanization can result in the presence of LMW molecules of varying amounts in the polymer. An example of this is HTV silicone rubbers that have 3% LMW mass whereas RTV silicone rubbers have 5% LMW mass [34]. The higher the amount of LMW, the higher the hydrophobicity in the material. Also, thick layers of polymer material recover hydrophobicity faster than thin layers because the transfer of hydrophobicity is not a surface phenomenon but a phenomenon aided by the bulkiness of material [28].

Filler contents present in polymers can also have an effect on its hydrophobicity. Higher filler contents can lead to lower levels of hydrophobicity. They also restrict surface degradation by repressing the development of leakage current [27]. While some previous studies have proved that high levels of filler content reduce the recovery process of surface hydrophobicity [34], others have proved the opposite to be the case [27].

It is noteworthy to mention that though the loss of hydrophobicity can be temporal, it is rarely lost totally in silicone rubber polymers. The LMW reservoirs of the molecules have been discovered to be large and are also replenished due to scission of the molecule chains by electrical discharges. These reservoirs cannot be easily depleted as LMW diffuses into and compresses the contamination layers in minimal amounts. According to studies on this, there is no significant depletion of the LMW reservoir [31].

2.5 Leakage Current

Any current flowing from the transmission line or live-end of the insulator to earth or the dead-end of the insulator over the insulator surface can be called the insulator leakage current [35]. In the design and construction of transmission lines, leakage current becomes a very crucial factor to take into consideration. Reason being that the capability of an insulator is extremely influenced by the degree of leakage current. This leakage current cannot penetrate through the insulator material but it passes through the surface of the insulator. This insulator surface has a low resistance pathway than the air enclosing the insulator. Figure 2.3 shows this scenario.

The degree of leakage current can be utilized as an excellent measure of the insulator capability to operate under high voltage stress. For example, a high degree of leakage current across the insulator surface depicts a poor insulator performance and this may lead to an electrical breakdown or a degradation of the insulator material such as silicone rubber in the case of polymeric insulators. Studies have shown that the leakage current around high voltage insulators can provide information about the surface condition of insulators and indeed a promising technique to study the performance of the insulators. Leakage current can be measured by making

use of current transformers, magnetic field sensors or resistive shunts [12]. A resistive shunt was used for this research investigation, it operates on the fundamental principles of Ohm's law. It is an intrusive method with a good measure of accuracy [12].

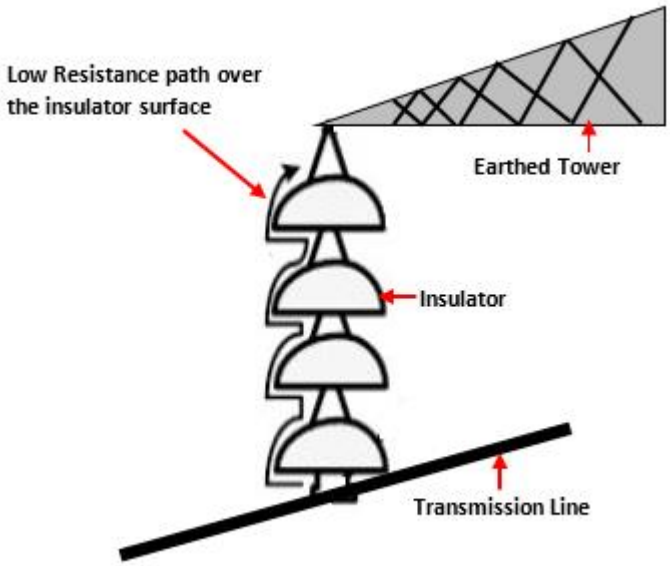

Figure 2.3: Leakage Current Flow along the Insulator.

In the research conducted by Krzma et al. [36] the comparative performance of polymeric insulators was investigated. Standard artificial contamination tests were used in the investigation which considered two types of silicone rubber insulators designs: textured and a non-textured surface. The insulators were energized with a positive DC and AC voltage types to compare their leakage current. The leakage current signals were computed through a data acquisition system. The insulator shed surfaces were also continuously monitored through an infrared camera to detect the development and location of dry bands and to assess the distribution of temperature along the insulator surface. The results of their investigation showed that the leakage current for DC, in the case of both insulator design, were higher than the AC with the non-textured having the highest. It was concluded that surface degradation was more severe on the non-textured designed insulators and that positive DC excitation was more severe than the rms AC.

In the investigations undertaken by Sorquist and Vlastos [13], long-term exposure of polymeric insulators to HVDC was studied. The insulators were energized with DC voltage for a long period while considering the leakage current, hydrophobicity and the surface condition of the insulator material which were studied by utilizing electron spectroscopy for chemical analysis (ESCA) and ATR-FTIR spectroscopy. Their results showed a strong interrelationship between leakage current

and the condition of the material surface. Investigations on the ageing of polymeric insulators were also carried out by Sorquist and Vlastos [37]. In their research, the leakage current of AC and HVDC energized silicone rubber insulators were monitored with the hydrophobicity and macroscopic conditions of the insulator interface. The morphology of the surface and the composition of the insulator material were studied by utilizing Scanning Electron Microscopy (SEM), Attenuated Total Reflection Fourier Transform Infrared Spectroscopy (ATR-FTIR) and X-ray Photo-electron Spectroscopy (XPS). Their results showed that the ageing of the insulator surfaces was moderate but the changes in chemical composition were noticeably greater in the case of HVDC. Also under clean fog conditions, it was discovered that the high degree of hydrophobicity level of the insulator materials considered were retained with different leakage currents and it was concluded that the leakage current, a determining factor of the surface resistance, depends on the environment under which the insulators are being subjected and on the interaction between humidity and the material particles present on the surface layers. It was finally concluded that the degree of hydrophobicity may not be a good indicator to evaluate the surface resistance of polymeric insulators.

The interaction between the insulators and the environment were investigated by Vosloo and Holzhausen [38]. The investigation was carried out by comparing three types of insulators: glass cap-and-pin, silicone rubber and EPDM rubber in a pollution test, considering the leakage current and weather data. The results showed notable differences in the leakage current characteristics of the insulators: EPDM exhibited the highest degree of leakage current, silicone rubber showed little leakage current while glass insulators displayed no significant value of leakage current until after very long hours (18 hours) of subjection to high humidity. It was concluded that material and profile of the insulator are key factors affecting the leakage current.

It has also been established that the flow of leakage current is as a result of the flow of charges on the insulator surface [39]. Hence the need to understand the mechanism of space charge accumulation on the insulator surface.

2.6 Mechanism of Charge Accumulation

Outdoor insulators operating under DC high voltage transmission experience a static electric field distribution as against the time-varying electric field experience under AC high voltage. This is as a result of the accumulation of space charges in the air-solid interface along DC insulators; these charges are called surface charges. Charges move down the field lines through air, solid or across the insulator interface and accumulate as a result of the conductivities of the insulating

media. The impact of surface charges causes increased leakage current to flow which may lead to a noteworthy reduction of the dielectric strength and this contributes greatly to the breakdown of DC insulators [40, 41].

Charge accumulation on the surface of the solid DC insulator is an issue which has been studied by various researchers, but due to newly emerging applications of polymeric insulators at extra-high DC voltages, a more extensive investigation into the associated physical processes of their breakdown is required. Influence of various parameters on charge accumulation and distribution along the interface of polymeric insulators have been clarified [42, 43]. These parameters include applied DC voltage polarity and amplitude, the shape of the electrode configuration, the geometry of the insulating system and time span of the DC voltage. In addition to these parameters are the environmental factors (such as pressure, humidity and temperature).

The characteristics of both phases at the interface of a gas (air)-solid insulating system also affects the deposition and accumulation of charge along the interface. These characteristics include electrical permittivities and conductivities of the solid insulating medium coupled with the parameters corresponding to the gas medium enclosing the solid insulator, such as conduction due to free ions, electric field distribution and rate of ion pair generation due to natural radiation [7]. The mechanisms involved in the accumulation process includes [42]:

- Electrical conduction within the gas volume
- Electrical conduction through the insulator volume
- Electrical conduction along the insulator surface

Charging the surface of high voltage insulators can be attained or accomplished in several ways such as contact charging, corona charging, utilization of an electron beam, exposure of insulation materials to high voltages, polarization, triple junction imperfections, partial discharges in the gas (air) medium enclosing the insulator, etc. [43]. Amid these sources, corona charging is the most common in practical applications and they are frequently utilized for research purposes because they produce a huge amount of free charge species, simplicity, the deposition process can be controlled and repeatability of results [40, 43]. Corona charging is being utilized in the experimental investigation presented in this dissertation.

2.7 Corona Charging

In a uniform electric field, exceeding the dielectric strength of the surrounding media usually leads to a complete electric breakdown [23]. If the electric field is non-uniform in its distribution between two electrodes, such as in coaxial cylinders, sphere-plane or point-plane geometries,

electrical discharges are noticed first before the total breakdown happens, this is usually the case in reality. These electrical discharges can also be called partial discharges and generally known as corona. Corona is therefore a self-sustained, non-disruptive electrical discharge occurring in the gas medium that can be triggered and actuated by electrodes which have a property of small surface curvature. These electrodes are connected to a very high voltage source [43]. High voltage insulators placed in between a corona electrode and the ground electrode will experience a deposition and accumulation of charges ions on its surface.

Furthermore, corona is related with some physical processes leading to charge generation and loss, which are of great importance in air. These processes include various types of ionization (due to electron impact, photo-ionization), attachment of electrons to neutral molecules, detachment of electrons from negative ions, recombination between opposite charges, emission from electrode surfaces and secondary emission from the cathode [40].

2.7.1 Charge Generation Mechanisms

At normal temperature and pressure, air performs as a perfect dielectric having an electrical conductivity in the range of 10^{-12} – 10^{-13} S/m [23]. Background ionization occurs due to the generation of free charged ions and electrons by cosmic radiation and radioactivity in the atmosphere and earth, it is characterized by a rate R_o which is influenced by the enclosed environment. Thus, at equilibrium, electron-ion pair occurrence in air medium whose concentration level of radon is normal and has an $R_o \approx$ 1-10 ion pairs cm^{-3} s^{-1}, coupled with an equivalent ion pair concentration $n_o \approx 10^3$-10^4 cm^{-3} [44]. If no external electrical field is applied, the ionization processes are counterbalanced by the decay processes, which are also taking place in the same air medium, hence equilibrium is continued without interruption.

Upon the application of an external field on a gas medium, electrons are accelerated resulting in non-elastic collisions between these electrons and neutral molecules at certain electric field intensity. If the electron energy, which an electron gains from the field as it moves between two collisions, is greater than the ionization energy of the gas, new charge species (electrons and positive ions) are produced. This mechanism is called electron impact ionization and it is the most crucial charge production process in gas discharge process [45]. The intensity of this mechanism is characterized by Townsend's ionization coefficient, α, which depicts the number of ionization events created by a single electron on a unit length of path. The ionization coefficient α is a quantity that is dependent on the electric field.

Electron detachment is another mechanism that takes place when negative ions are present in the gas medium. It is a process that involves the interaction of a negative ion with an atom, resulting in a free electron and an additional molecule [23].

Excited charged species can also recuperate from the excited state, this will lead to a radiation of energy called photon (*hv*). This recovery time is in the range of 10^{-7} – 10^{-10} sec. Ionization takes place when this radiated photon collides with another atom whose ionization energy is the same as or lower than the photon energy [23]. This process is called photoionization.

2.7.2 Charge Loss Mechanisms

Electron attachment is a very important charge elimination mechanism in gas discharge process. It takes place in electronegative gases. These gases are deficient in the number of valence electrons, thus they are always eager to attract free electrons so as to be able to form stable ions. Oxygen is a very good example of such type of a gas, it has a deficiency of two electrons in its valence shell. Electron attachment can take place in different ways [23]: radiative and dissociative. The former is the opposite of photo-detachment. Dissociative attachment is presented as the strongest in molecular gases. It uses the surplus energy of the electron to divide the molecule into a negative ion and a complete neutral particle. The strength of electron attachment is characterized by attachment coefficient η, which is the amount of attaching phenomenon taking place on a unit length moved by an electric field directed electron [44].

The process of recombination is another mechanism which takes place mostly in gases with a lot of ionized species and it is of two types. The first is called electron-ion recombination which can be explained as the coalescing of a positive ion with an electron to form neutral particles [23]. Another type of recombination process that takes place in gases is ion-ion recombination. This involves the merging of the positive and negative ions and it may occur as either collision between two species or between three species. In the collision between two species, one of the ions involved in the collision sucks up the surplus internal energy while the excess internal energy that exists in the collision between three bodies is eliminated by the third species involved in the collision [46].

2.7.3 Charge Transport Mechanisms

When a gas composed of charged species is being energized by an external electric field, charged particles tend to move either in the same or opposed the route of the external field depending on the polarity of the charge and this is in addition to their stochastic motion. This field governing the movement of charged particles is termed drift and its velocity, termed as drift velocity, depends on the applied electric field, pressure, charge species involved, etc. The ratio of the drift velocity to field gives the mobility, which is utilized to depict charge transport owing to drift. For most gases, mobility is influenced by the field. Also in a gas volume, the spatially non-uniform concentration of the charged species in motion leads to charge movement from areas of high concentration to areas of low concentration so as to reduce the concentration gradient [23]. Transport of charged particles owing to this process is called diffusion.

2.8 Flashover or breakdown Criterion

The flashover or breakdown scenario exists in both AC and HVDC transmissions, but more predominant with HVDC where space charges accumulate. Breakdown across an insulator is a progressive process from partial to complete. It occurs in the presence of a high electric field which is brought about by a high applied voltage. It is imperative that the phenomena leading to complete breakdown should be briefly empathised.

2.8.1 Electron Avalanche

When a high voltage is applied across a gap distance in an electrode system, it creates an electric field across the gap. Upon the application of voltage, V_1, free electrons which may be produced near the positively charge cathode by a natural ionization process or be illuminated by ultraviolet light are accelerated into the gap by the electric field toward the anode to create an initial current, i_o as shown in Figure 2.4.

Townsend's first ionization co-efficient, α was introduced by Townsend to describe the exponential current increase after the application of a voltage, V_2 stating that once electrons are accelerated sufficiently they are able to cause ionization on impact. An equation governing the amount of electrons over the distance *d*, can be given by equation (1) [23].

$$n_c = n_o e^{\alpha d} \tag{1}$$

Where n_o is the initial amount of electrons found at the cathode and n_c is the total amount of electrons produced by other electrons in the direction of the electric field. The exponential term, $e^{\alpha d}$ is called the electron avalanche that governs the number of electrons a moving electron will create when moving across the electric field.

However, the presence of electronegative gas components such as oxygen and nitrogen in an airgap results in loss of charge species as explained in *section 2.7.2*, yielding an attachment co-efficient, η, and thus the effective ionization co-efficient becomes $(\alpha-\eta)$. Thus, the new expression becomes [23]:

$$n_c = n_o e^{(\alpha-\eta)d} \tag{2}$$

The exponential rise in current can therefore be obtained as [23]:

$$i = i_o e^{(\alpha-\eta)d} \tag{3}$$

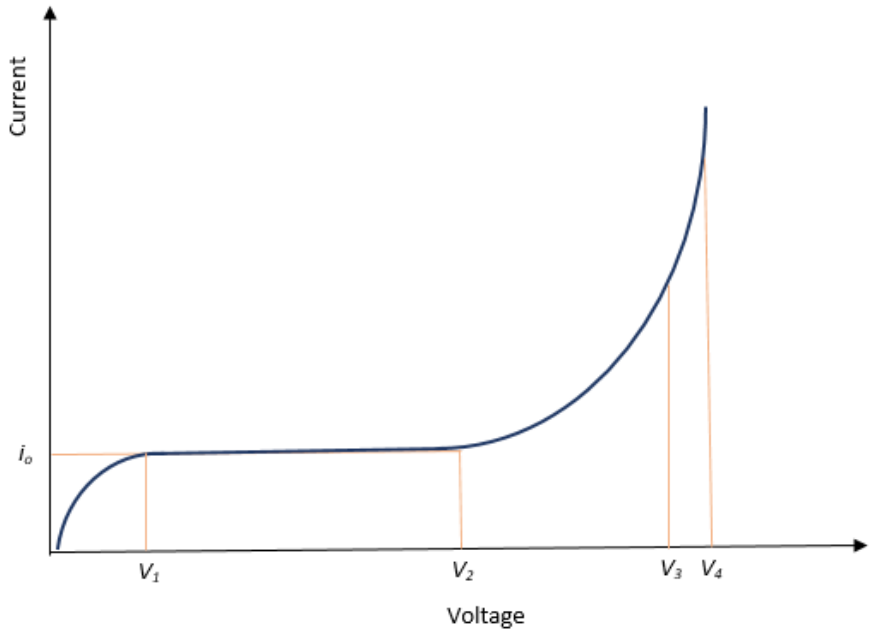

Figure 2.4: Voltage Current Relationship as seen in [23].

2.8.2 Streamer Development

The $e^{\alpha d}$ term is only valid as long as the space charge created by the electrons and ions can be neglected compared to the originally applied electric field, E_o [23]. In a uniform field, streamer development occurs when the concentration of charges within the head of the avalanche (active region) equals to a critical value of 10^8, the current rises exponentially as a result of a distortion of the original field by the space charge created by the electron avalanche. This can be represented by equation (4) and Figure 2.5 [23].

$$n_c = n_o e^{(\alpha-\eta)d} = 10^8 \tag{4}$$

The condition that the field created by the space charge assumes a similar value to that of the external field creates the first criterion required for an avalanche transition into a streamer. Once the avalanche has crossed the gap, *d*, the streamer mechanism will breakdown the gap. The development of streamers are generally found in smaller, shorter gaps. In the case of larger gaps, streamers are usually accompanied by the formation of leaders.

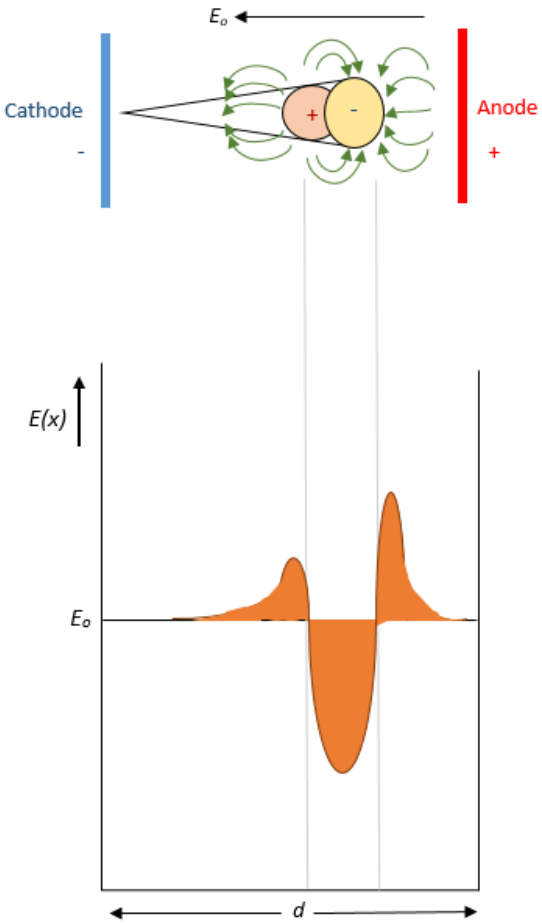

Figure 2.5: Uniform Field Distortion Caused by Space Charge as seen in [23].

In non-uniform field, the field strength and hence the effective ionization coefficient, *(α-η)* vary across the gap [46]. For a streamer to be initiated at the high-voltage electrode and for it to bridge the gap two conditions have to be satisfied; one for the streamer inception and the other for the streamer propagation.

The inception criterion for discharge can be represented by equation (5) [23].

$$exp \int_0^{x_c \leq d} (\alpha - \eta) dx = N_{cr} \tag{5}$$

Where N_{cr} is the critical electron concentration in an avalanche giving rise to initiation of a streamer, x_c is the length of the active region. Mathematically, this condition in equation (5) can be evaluated by integrating the effective ionization coefficient in the active region along its length, as shown in equation (6) [23].

$$K = \int_0^{x_c} (\alpha - \eta) dx \tag{6}$$

Where $K = ln\, N_{cr}$.

Once the integral *K* reaches the value (18-20 [23], 9.15-18 [47]) corresponding to a critical number of electrons, streamer initiation takes place. Equation (6) is applicable for computing the breakdown or discharge inception voltage depending on whether direct breakdown or only corona occurs.

Once the streamer is created the background electric field must be able to sustain the propagation of the streamer. For the streamer to reach the earth, this background field along the active region must be greater than ~0.5 MV/m for positive (cathode directed) streamers and at least 0.8 MV/m for negative streamers [41].

2.9 Effect of Surface Charges on Breakdown Voltage

Numerous findings have been stated on the effect of magnitudes, polarity and positions of charges pre-deposited by corona discharges on the flashover characteristics of polymeric insulators operating under impulse voltages, with different results for different insulating materials. EPDM and silicone rubber samples with different chemical composition were exposed to standard lightning impulse flashover voltages (FOV) in combination with pre-deposited surface charges of both positive and negative polarity in the investigation carried out by Blennow and Sörqvist [48]. Their results revealed that there was a reduction in the FOV from charges of the same polarity as the applied impulse in contrast to the case of both charges and applied impulse being of different polarity. Montano et al. [49] calculated the flashover voltages using a numerical model. The results obtained were compared with the experimental observations obtained in [48] and results revealed that the numerical model has a maximum of 11% deviation from the experimental observations.

An attempt was made by Kumara [40] to analyse the effect of the magnitude and location of deposited charges on the flashover performance of polymeric insulators through numerical simulations. The result showed a linear increase of the impulse FOV for positive polarity as a result of an increase in the magnitude of negative deposited charges. A non-linear behaviour was observed when the charges and the applied impulse voltages were both positive. The report also showed the position of the charged spot on the surfaces of the positive and negative charges in relation to positive applied impulse voltages. The electric field for each set-up determined the effects of the magnitude and location of deposited charges. Negative charges had an increase in the impulse FOV with increasing distance of the charge spot from the live electrode while positive charges had a decrease in the impulse flashover voltage with the charge spot closer to the earthed electrode and an increase in the FOV when the charge spot was in the middle of the insulating surface or closer to the live electrode.

In [50], the dielectric insulation properties of different silicone rubber materials, employable to 500 kV DC voltage insulators, were investigated by Seo et al. under AC and DC stress. Two silicone samples were prepared in several ways by selecting octamethylcyclotetrasiloxane and dimethylcyclosiloxane as separate base materials and adding to each materials different content ratio of ATH (aluminumtrihydroxide) fillers. These prepared materials were subjected to DC voltage stress to evaluate their breakdown characteristics and also energized under AC voltage stress for comparison. Their results showed that for all the material samples, the DC breakdown strength was higher than the breakdown strength under AC stress.

Experimental investigations were undertaken by Hammam et al. [51] to analyse the influence of accumulated charge on polymer surfaces under lightning impulse voltage, in three separate environmental conditions: under dry conditions, immediately after the upper shed and the body of the insulator are immersed in saline water and immediately the insulator is completely immersed in saline water. In [52], the influence surface charge has on impulse breakdown voltage was studied by Jun and Chalmers. Metallic particles were used as contaminants on the insulators which were clamped in between two parallel plane electrodes. Breakdown tests were also conducted by Semere [53] on cylindrical polymeric insulators comprising of polydimethylsiloxane by including a discharge system that works on the principles of DC corona which will deposit the surface charges. All these authors found the breakdown voltage to be highly influenced by surface charges. They presumed that negative charges increase the flashover voltage while positive charges reduce the characteristics of the flashover voltage.

The effect of surface charges was investigated by Qi et al. [54] on the characteristics of surface flashover for high voltage insulators operating under DC and AC voltage. Their results showed that under both DC and AC voltage applications, a higher quality of charge accumulation on the surface of the insulator resulted in a lower surface flashover voltage for the insulators. The surface flashover voltage was reduced by 23% for the DC while that of the AC voltage was reduced by 10.2%. The study by Kato et al. [55] altered the location and magnitude of surface charges accumulating on insulators under impulse voltage. It was observed from their results that positive charges resulted in a lower flashover voltage while negative charges increased the flashover voltage at points of proximity to the cathode electrode. For surface charges found at the discharge path, the positive and negative charges had no reducing effect on the flashover voltage.

According to the investigation undertaken by Wang et al. [42], it was posited that a decrease in the magnitude of the electric field in regions of high field abound when a negatively surface charged insulator is energized by a negative DC voltage and this results in an increased flashover voltages, while the existence of positive charges on the insulator surface increases the electric field magnitude near high field regions and this results in a lower flashover voltages. According

to the investigations conducted by Kumara et al. [41], where the effect of surface charges on DC flashover characteristics of a composite polymeric insulator was studied. In their experiments, the insulator surface was charged by an external corona source and different charging levels were realized by varying its intensity. A series of disruptive discharge tests were carried out on the charged insulator under negative DC voltages. Their results revealed that negative deposited surface charges led to an enhancement of the flashover performance while the positive ones reduced the flashover voltage level. Presumptions were also brought to spotlight that there was a linear variation between the breakdown voltages and the concentration of positive and negative charges. Further analysis of the electric field alongside effective ionization coefficient on the insulator surface by these authors showed that the observed variations which were detected in the DC breakdown voltages occurred as a result of alteration of the electric field in the cathode area.

Previous studies have also focussed on the pollution flashover characteristics to study the insulator breakdown phenomenon. Insulator discharge during the rainy season is a crucial factor influencing the performance of high voltage transmission insulation [56]. The insulator surface gets wet as a result of light rain and results in an increase in the quantity of leakage current flowing across its surface. Water droplets also alter the electric field intensity in certain locations on the insulator surface, creating an electrical stress on the insulator surface. This initiates partial discharges like corona which is an expected phenomenon for arc formation in high fields; the arc bridges the insulator sheds to cause a complete flashover or breakdown [57, 58]. In contaminated areas, increased leakage current heat the insulator surface to form dry band areas that pave way for electrical discharges and finally leads to flashovers.

According to previous research investigations [59-65] on insulator behaviour under wet conditions, the effects of characteristics such as contaminants effects, insulator material types, leakage distance, shed dimensions and water resistivity on the breakdown voltage have been the focus. The AC and DC flashover performance of insulators with different shed configurations were investigated by Baker et al. [59]. Their results showed that an increase in the leakage distance raised the flashover voltage for a minimum shed spacing. The flashover characteristics of contaminated flat insulator model under applied DC voltage were carried out by Wen-xia et al. [60] Their results showed that an increase in the degree of the contaminants lead to a maximum for the positive DC breakdown voltage and a minimum for the negative DC breakdown voltage.

In [61], field tests carried out at Sylmar Converter Station of the Pacific Intertie HVDC system to determine the process and factors influencing the contamination flashovers of HVDC ceramic insulators were presented by Cheng and Wu. The field tests spans a period of two years, the contaminants were identified and the rates of accumulation were determined. It was reported that the insulator flashovers were more severe on the DC than on comparable AC transmission system

in a similar environment. This severity was attributed to the electrostatic field in DC which allow more contaminants to accumulate on DC insulators, the absence of current and voltage zeros in DC transmission which aggravates the flashover problem. An investigation conducted by Farouk [62] focused on the effect of water resistivity and rain intensity on the AC breakdown voltage. The results showed that water resistivity causes a significant influence on the breakdown voltage especially during the wet test while the rain intensity had a slight effect on the breakdown voltage.

The investigation into the breakdown mechanism of silicone rubber insulators was undertaken by Karady et al. [63]. The authors considered the build-up of pollutants, wetting of the surface, migration of low molecular weight chains of the polymer, the field enhancement caused by the discharge, conductive areas and filaments generated. The investigation was carried out by employing a 3D X-Ray Microscopy (XRM) technique and it was concluded that pollutants from sea and industries create a uniform pollution layer on the insulator, the wetting creates a resistive surface layer covered by conductive droplets and the recovery of the material surface creates a thin intermittent silicone layer on the material interface which allows the movement of water to the pollutants and the salt from the pollutants to the droplets.

In [64], the influence of impulse polarity on the breakdown voltage of both clean and contaminated glass cap-and-pin insulator were investigated by Chrzan et al. Two types of glass cap-and-pin insulators were considered: standard and aerodynamic. They were energized with negative and the positive impulse polarities under clean, uniform and non-uniform contaminated conditions. Their results showed that under clean and uniform contaminated conditions, the negative impulse breakdown voltages were higher than the positive for the standard glass cap-and-pin insulators while the reverse was the case for aerodynamic type and in non-uniform environmental conditions. Also in [65], the breakdown characteristic of air-gaps and insulator strings under lightning and switching impulse voltages were investigated by Paris and Cortina. In their research, different electrode shapes (rod-rod, rod-plane, conductor-rod, conductor-cross arm) and configurations with and without insulators were considered and it was discovered that the electrode shapes had great influence on the breakdown voltages.

2.10 Electric field stress

In the design of insulators that will perform better in high voltage transmissions, understanding the intensity of the electric field is essential. The stresses exerted upon an insulator by the electric field generated as a result of the electric potential on the insulator is called electric stress. The intensity of the field can be used to deduce the magnitude of the electric stress on the insulator. The performance of insulators operating under high voltage depends largely on the electric field

distribution and stress. The field intensity or strength can be defined by equation (7) as the electrostatic force, *F*, per unit elementary charge, *q*, located at a specific point, *p*, on insulators [66].

$$F = qE \tag{7}$$

In Figure 2.6, the potential difference, U_{ab}, that exists between the two specific location *a* and *b* with scalar voltage potential $\emptyset_a$ and $\emptyset_b$ in a field, $\vec{E}$, can be defined as the work done by an external source in moving a unit charge from point *b* to point *a*.

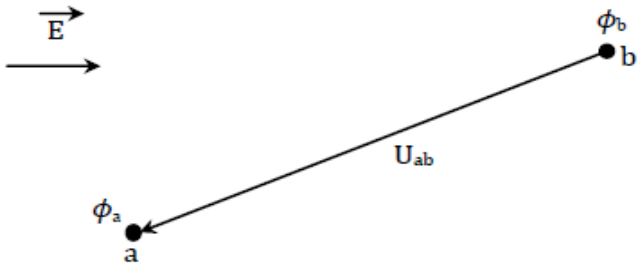

Figure 2.6: Electric Field Illustration.

This can also be described by equation (8) [66],

$$U_{ab} = -\int_b^a |\vec{E}| dx = (\emptyset_a - \emptyset_b) \tag{8}$$

The rate of change of the potential with corresponding distance gives the magnitude of the electric field strength. Hence the maximum electric field strength can be derived when the direction of the electric field is in opposite direction to the direction of the maximum potential.

$$\frac{dU_{ab}}{dx}\Big|_{max} = -|\vec{E}|_{max} \tag{9}$$

Equation (9) [66] above gives a physical explanation of deriving the electric field strength from the scalar potential, $\emptyset$. The operator on the scalar potential that will enable us to obtain the electric field is called gradient and the relationship can be written as shown in equation (10).

$$\vec{E} = -\nabla\emptyset \tag{10}$$

Using Maxwell's equation,

$$\nabla\vec{E} = \frac{\rho}{\varepsilon} \qquad (\varepsilon = \varepsilon_o\varepsilon_r) \tag{11}$$

Where ε depicts the permittivity of insulating material, ρ represents the density of the volume charge.

The electric field intensity at the insulator surface can be influenced by the electric potential at the surface of the insulator. Therefore, the substitution of equation (11) into equation (10) gives the Poisson's equation in equation (12) which illustrates the relationship between the charge density and the electric potential.

$$\nabla^2 \emptyset = -\frac{\rho}{\varepsilon} \tag{12}$$

When the value of the space charge ρ=0, the Laplace's equation can be derived as shown in equation (13).

$$\nabla^2 \emptyset = 0 \tag{13}$$

2.11 Finite Element Method (FEM)

According to [8], various methods of numerical analysis can be used for the evaluation of electric field strength or distribution along high voltage insulators. These methods are boundary element method (BEM), charge simulation method (CSM), finite element method (FEM), and finite difference method (FDM). Among these methods, FEM approach stands out to be the best in solving problems with complicated geometry and small close bounded problems. Very large problems require numerous finite elements which will result in complicated calculations [8].

This method is a numerical system with solutions to Maxwell's equations in a differential form. FEM utilizes a process known as meshing to part the problem space and its surrounding area into numerous non-separated sub-regions that do not overlap [8]. These sub-regions, referred to as finite elements, can come in different shapes though triangles are used for two-dimensional analysis while three-dimensional analysis requires tetrahedrons. Polynomials are used to express the geometry of each element and nodal values for coefficients. For each element the potential present is a linear interpose of electric potentials at different points. The partial differential equations are solved into a simple, positive, and regular definite matrix equation with the weighted residual approach [8].

The fundamental basis of FEM is the conversion and approximation of differential equations in integral modes [8]. The equations are transformed with the aid of function which minimizes an energy integral. The electric field distribution can easily be calculated by first calculating the potential distribution, thereafter deducting the gradient of potential distribution from the calculated electric potential distribution [70].

2.12 Factors Affecting the Electric Field Stress on Insulators

According to previous research [72-76], factors other than leakage distance may be responsible for the long-term and otherwise efficiency of insulators. A short analysis of these factors that influence the field on the insulator is given in this section.

2.12.1 The Insulator Shape

The shape of the insulator has a major influence on the field stress exerted on the insulator. A properly shaped insulator is expected to provide an electrical field stress lower than the ionization inception. The profile of the weather shed and the designs of the end fitting are important determinants of the electric field stress on an insulator.

Chakravorti and Steinbigler [72] investigated into the correlation between a porcelain-shaped post-type insulator and the limit of electric field strength that surrounds the insulator in the presence and absence of pollutants, the maximum electric field strength was located around the area of the triple junction. Their research which studied variables such as the insulator axial height, core radius, radius of the electrodes, radius and slope angle of the weather shed; revealed that:

- The insulator axial height was inversely proportional to the peak electric field intensity.
- The extent of core radius has a minimal effect on the reduction of the maximum field intensity.
- An increase in the slope angle has an insignificant effect on the field intensity.
- An increase in the extent of the shed radius by as little as 6cm resulted in a significant reduction of the electric field intensity.
- An increase in the radius of the electrodes will increase the field intensity for an insulator in a pollutant-free environment and reduce the field intensity once insulator surface is polluted.

The end-fitting design has also been found to significantly influence the field around the live end. In [73], three different types of insulator fittings were modelled and simulated in the absence of a corona ring by Phillips et al. Their results revealed that end fittings whose edges are rounded were synonymous with a reduction of the highest magnitude of the field intensity near the end fitting. The end fitting with a larger diameter was also observed to have a more desirable field distribution in the area near the fitting.

2.12.2 Corona Ring

The presence of a corona ring serves to reduce the effect of voltage stress on the insulator near the live end and this results in the grading or dispersion of the gradient of the electric field. It is

attached to the composite insulator directly or indirectly with the hardware as a Corona Shield. Corona ring inhibits the action of corona on the hardware.

The effect of the application of a corona ring on the field and electric potential distribution along a 22 kV glass cap-and-pin insulator were studied by Ilhan and Özdemir [74]. Their results showed a considerable reduction in the voltage of insulators at the bottom (live end) and a slight increase in the voltage shared among the uppermost insulators. This implies that the use of a corona ring will ensure evenness in potential distribution and a reduction in the electric field intensity at the live end, depending on its design parameters and the tube settings of the corona ring. The upper limit of the electric field was found to be on the ring's outer radius while the lower limit of the electric field was discovered in the ring's inner radius.

Zhao and Comber [75] carried out an investigation on the electric field and potential distribution along non-ceramic insulators using Coulomb electric field analysis software package, considering the transmission lines, tower and the insulator. Their results revealed that the conductor length created a shielding effect on the high voltage insulators, that is an increase in the length of the conductor resulted in a reduction in the field intensity while the tower structure in the vicinity of the insulator and the grading ring diameter and positioning are factors that influence the field intensity along an insulator.

2.12.3 Insulating Material Permittivity

The permittivity (ε) of an insulating material defines how much electric field, or better still, fluxes, is generated per unit charge. It defines how a dielectric medium influences and is influenced by an electric field. Permittivity is proportionally correlated to electric susceptibility, which gauges the ease of a dielectric polarization in relation to an electric field. As a result of polarization effects, a dielectric medium which poses huge amount of permittivity will have less fluxes.

The field and electric potential distribution for a post-type insulator shed were estimated by Kaana-Nkusi et al. [76]. Criteria such as potential discrepancy, tangential field intensity discrepancies, normal electric flux density and potential error were applied to assess the quality of the results obtained from the system that was modelled using 146 ring charges; 30 charges per electrode. Their results revealed that an increase in the field intensity close to the surface of the insulator was as a result of a high degree of dielectric permittivity for the insulating material. Their results also indicated that a decrease in the shed's radius of curvature increased the normal and tangential elements that make up the electric field intensity.

2.12.4 Applied Voltage

The field stress experienced by an insulator can also be influenced by the voltage applied or potential difference across the insulator. Using equation (7) described earlier, the electric field

can be described as the force experienced by the charged particles per unit charge while the applied voltage can be described as the energy per unit charge. The voltage difference that exists between any given points is the effort put in to move a unit test charge from one point to another and it can be represented by ΔV. Therefore the correlation between the voltage difference and field can be described as:

$$\vec{E} = -\frac{\Delta V}{\Delta d} \tag{14}$$

Where Δd indicates the distance moved by the charge as a result of the applied voltage and the negative sign is an indication of a decrease in potential in the field direction.

2.12.5 Surface Charges

The geometry and permittivity of insulation materials in an AC system play a crucial role in the electric field. The field distribution under this AC system is said to be capacitive [67]. The electric field under HVDC system is complicated owing to the charges accumulated at the interface of the insulators, this made the field shift from being capacitive to resistive. According to Hering et al. [67], the electric field is being influenced by temperature-dependent conductivities of the dielectric materials being used in the insulation system. This was proved by the authors by building a computational fluid model to evaluate the distribution of temperature at various temperature of the electrodes under DC voltage. They concluded that charge accumulation at the interface contributes to the transition of the electric field from capacitive to resistive.

The field distribution along the interface between the dielectric materials (gas-solid) in an HVDC insulation system was evaluated by Winter and Kindersberger [4]. The authors built a simulation model taking into consideration the physical processes involved in gas: generation, motion and recombination of the charges as a result of the drift and diffusion and the dielectric characteristics of epoxy resin insulator. The field distribution along the insulator was investigated and it was discovered that the transition of the field (capacitive to resistive) is directly interconnected with the charges accumulated on the surface of the insulator. According to Qin et al. [68], the degree of distortion in a field under HVDC insulating system increases with an increase in the volume conductivity of the insulating material. This was confirmed by the authors by developing a surface charge accumulation model of an insulation system operating under HVDC to study the distribution and intensity of the electric field by changing the volume conductivity of the material.

Finite element models were also developed for glass cap-and-pin insulators considering the effect of accumulated surface charge on the voltage and electric field distribution [39, 69]. It was concluded in [69] that surface charges affected the field distribution by enhancing the field strength and lowering the breakdown voltage. In [39], the simulation results were compared to

the experimental results and they were in good agreement, it was concluded that the voltage and electric field distribution are linked closely with the charge distribution on the insulator surface. Finite element models have also been developed for polluted composite insulators considering the effect of contaminants [70] and corona ring [71] on the electric field distribution of silicone rubber insulators. In [70], it was concluded that the contaminants distorted the field and reduced the degree of field uniformity. In [71], it was confirmed that corona ring reduced the probability of insulator breakdown in polluted conditions.

CHAPTER 3
METHODOLOGY

This section presents the experimental setups and procedures as well as the finite element models used for the research. The experiments were carried out as far as reasonable possible in compliance with IEC 60060-1 [77] standard requirements at the University of KwaZulu-Natal (UKZN) High Voltage (Howard Campus) and HVDC (Westville Campus) laboratories. FEMM 4.2 software package [78] was used for the modelling of the insulators to further understand the electric field distribution along the surface and around the high voltage insulators.

3.1 High Voltage Generation

The High Voltage laboratory at Howard College was used for the AC and impulse breakdown test. The lightning impulse voltage was supplied by a seven-stage Marx impulse generator. The lightning impulse voltage used had a front time of 1.2 µs and a time to half-value of 50 µs which could be described as a standard 1.2/50 µs impulse. The Marx was configured with a positive and negative polarity, where the polarity of the impulse was dependent on the polarity of the charged stage capacitors or on the direction of the rectifying diode. The measurement circuit consist of a calibrated damped capacitive voltage divider with a dividing ratio of 856 coupled with an impulse peak measurement system. The impulse peak measurement system had a further dividing ratio and could be attenuated at the point of measurement in steps of 2, 4 or 6 in order to safely read measured values from the laboratory. Figure 3.1 provides the Marx generator circuit diagram.

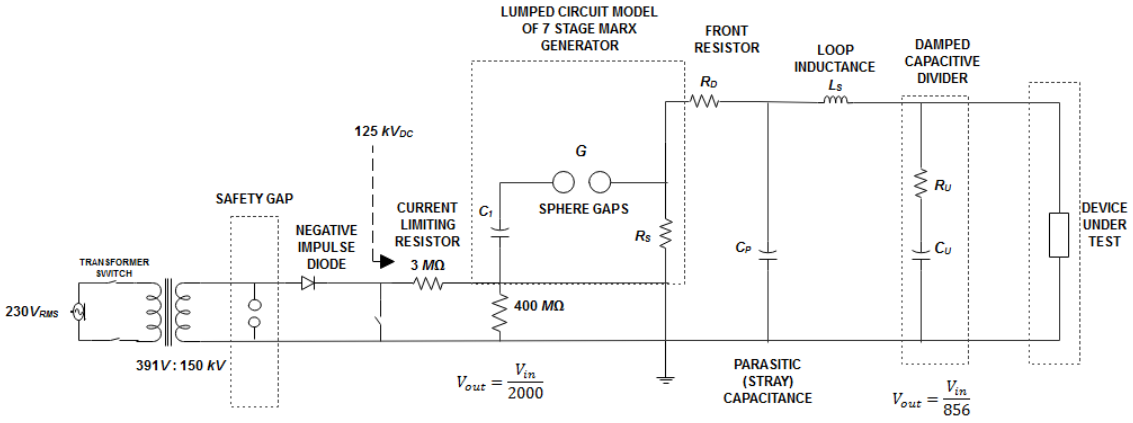

Figure 3.1: Schematic of the Marx Generator and Experimental Circuit.

The AC breakdown tests were carried out by making use of a 240 kV, 150 kVA, 50 Hz cascaded transformer set with a voltage regulator. The AC power was directed to the insulator under test through a water resistor, while a capacitive voltage divider (Hipotronics CVD4000) with ratio

1:4000 was used for the peak breakdown voltage measurements and recorded via a digital oscilloscope (Rigol D51052E 50 MHz 1 GSa/s) this can be seen in the circuit diagram shown in Figure 3.2.

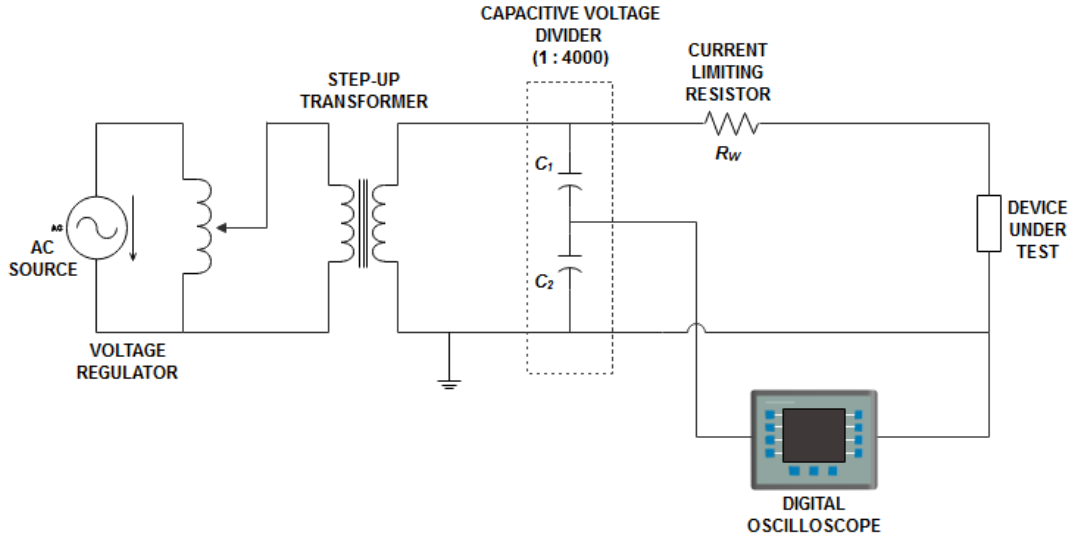

Figure 3.2: Schematic of the AC Generator and Experimental Circuit.

The DC voltage was supplied by a two-stage Cockcroft-Walton generator at UKZN HVDC laboratory, the generator has a rated output voltage of +500 kV and -540 kV, with a current of 7.5 mA. The peak voltage achievable in the laboratory is ±300 kV, this was as a result of height restrictions in the laboratory. At maximum load current, the ripple factor is lower than 3% and the voltage drop was lower than 10% [77, 79]. Figure 3.3 [79] describes the circuit diagram of the generator and the circuit parameters are shown in *Appendix B*. The AC generator supplies power to the step-up transformer of 100 kV, 5 kVA through a voltage regulator, which regulates the input voltage between 0 kV and 100 kV and the Cockcroft-Walton test circuit converts the AC to HVDC. The step-up transformer has a maximum current capability of 50 mA. During flashover, the current could temporarily surge to magnitudes higher than the rating of the transformer. As an additional precaution to protect the transformer, a series connected current limiting resistor was used as shown in Figure 3.3. The resistance of the resistor was 10 MΩ and during a flashover event at 300 kV, the surge current would be approximately 30 mA, which is within the safe operating limits of the transformer and diodes. The applied voltage was measured using a digital multimeter connected to a resistive potential divider.

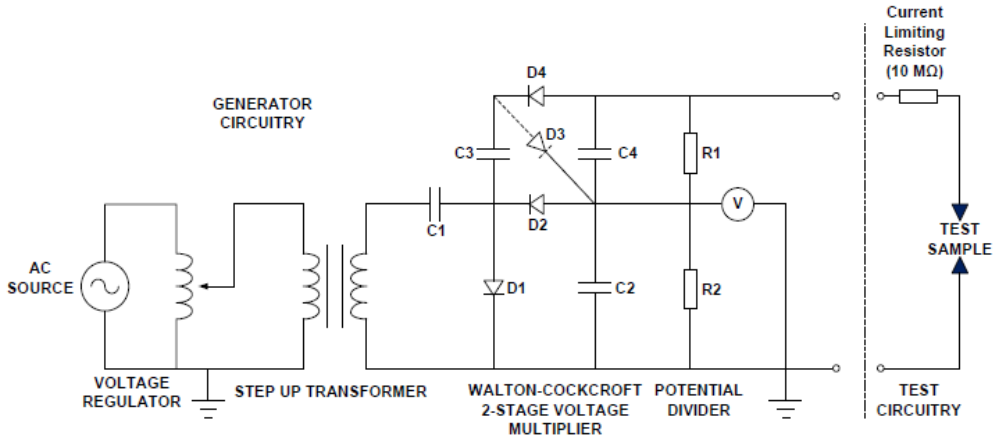

NOTE: C_2=100,000 pF; $C_2 = C_3 = C_4$ =50,000 pF; $R_1 = R_2$ = 600 MΩ

Figure 3.3: Schematic of the Cockcroft-Walton Generator and Experimental Circuit.

3.2 Leakage Current Measurement System

The leakage current was recorded by making use of a shunt resistor, where the voltage drop across a shunt resistor is measured using a digital multimeter and this voltage measurement, combined with the known value of the shunt resistor (5.6 kΩ), gives the current. The value of the resistor (5.6 kΩ) was chosen so as to make the digital multimeter more sensitive to the voltage measurement. A protective device was also used: gas discharge tube (GDT) of 90 V with a maximum surge current rating of 10 kA across shunt resistor. A value of 90 V was below the common maximum input voltage of 600 V of digital multimeters.

Figure 3.4 shows the schematic of the leakage current monitoring system. The measurement system has negligible influence on the applied voltage across the insulator.

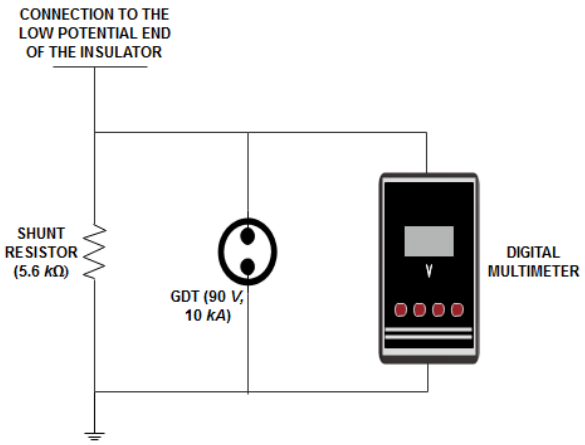

Figure 3.4: Leakage Current Monitoring System Circuit Diagram.

3.3 Test Samples

The insulator samples used in the breakdown tests were 22 kV silicone rubber insulator and a 22 kV glass cap-and-pin insulator. The technical dimensions and profile of these two types of insulators used can be found in Table 3.1 and Table 3.2. Figure 3.5 and Figure 3.6 shows these insulator samples: silicone rubber and glass cap-and-pin insulators respectively. The insulators were well cleaned and void of contaminants before subjecting them to any of the breakdown tests.

A simulated transmission line conductor which is made up of a 1.6 cm diameter aluminium tube was attached through a bracket to the live-end of the insulators as shown in the experimental set-ups.

Table 3.1: Technical Dimensions and Profile of 22 kV Silicone Rubber Insulator.

Insulator Geometry	**Dimension**
Number of sheds	8
Arcing distance	0.28 m
Leakage distance	0.807 m
Shed diameter	0.066 m
Sheath diameter	0.02 m
Service voltage	22 kV

Table 3.2: Technical Dimensions and Profile of 22 kV Glass Cap-and-Pin Insulator.

Insulator Geometry	**Dimension**
Number of sheds	2
Total Arcing distance	0.315 m
Total Leakage distance	0.760 m
Shed diameter	0.255 m
Service voltage	22 kV

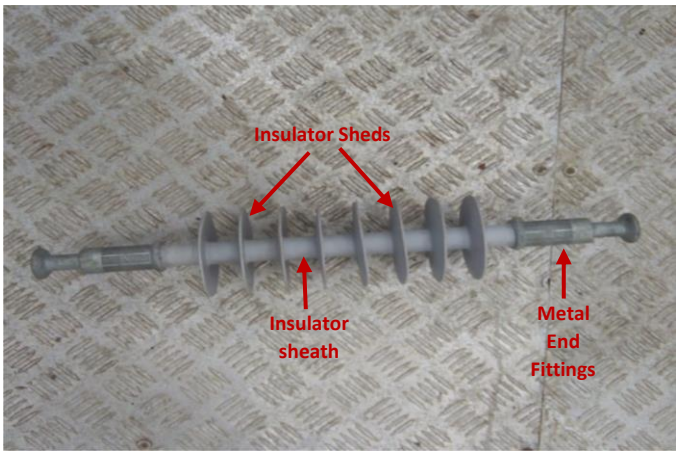

Figure 3.5: 22 kV Silicone Rubber Insulator.

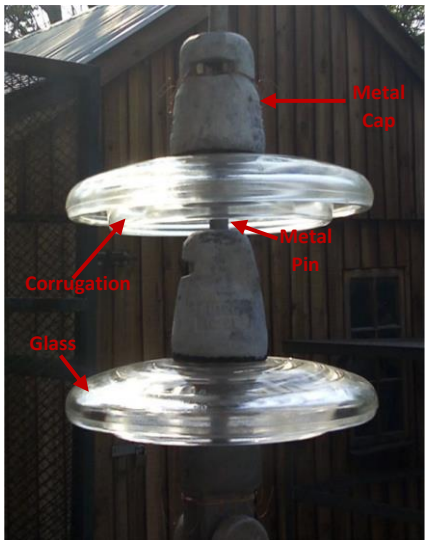

Figure 3.6: 22 kV Glass cap-and-pin Insulator.

3.4 Experimental Set-up

3.4.1 Breakdown Voltage under AC, Standard Lightning Impulse and HVDC

For this experiment, different types of applied voltage were used to examine whether the breakdown under DC conditions differs from that of AC and impulse. The experiment was done for both dry and wet environmental conditions.

The 22 kV silicone rubber insulator was used during the breakdown tests for these tests. For the dry AC test and the dry and wet impulse tests the insulator was setup as illustrated in Figure 3.7.

Figure 3.7: Experimental Set-up for the Dry AC and Dry and Wet Impulse Test.

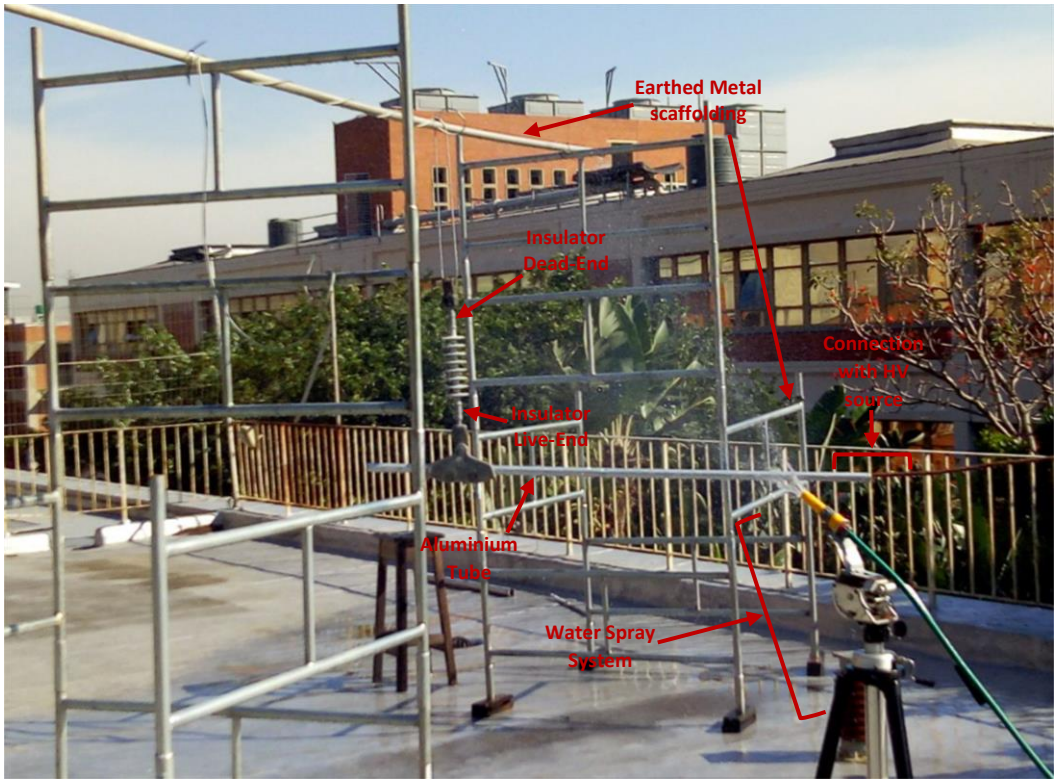

Figure 3.8: Experimental Set-up for the AC Wet test.

For the wet AC test, the insulator was suspended through a metal pole scaffolding assembly as shown in Figure 3.8. The scaffolding assembly was earthed, this made the upper part of the insulator earthed while the live-end was at the lower part. In the case of the DC and impulse breakdown tests, the insulator was energized with both positive and negative polarities of the applied voltages. To avoid flashovers with external structures, the clearance of the conductor to all external structures was not less than 1.5 times the length of the insulator dry arcing distance.

For the dry and wet DC tests the insulator was set up as illustrated in Figure 3.9.

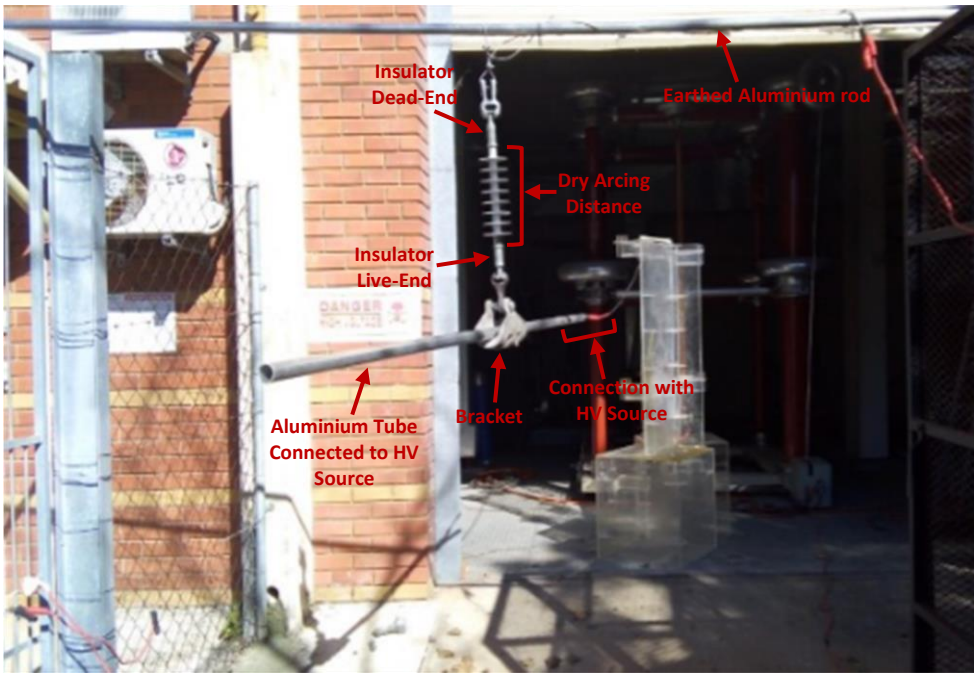

Figure 3.9: Experimental Set-up for the DC Dry and Wet test.

3.4.2 Breakdown Voltage and Current under HVDC

This experiment focussed on the effect of current and space charges on the breakdown voltage. The leakage current performance of the insulators under negative and positive polarity DC voltage with additional corona sources (space charge generating sources). Two types of 22 kV high voltage insulators were considered: the silicone rubber insulator and glass disc cap-and-pin insulator. Additional breakdown voltage tests were carried out under AC voltage to compare their leakage current characteristics.

The breakdown tests, under DC voltage, on each insulator types were broken down into two areas namely:

1. Insulator breakdown test in the absence of additional charges on the insulator surface.
2. Insulator breakdown tests in the presence of additional charges on the insulator surface.

The effect of space charges usually associated with HVDC systems were emulated during the experiment. The additional charges were generated through a corona source, which was created by small pieces of sharp copper wires of diameter 0.5 mm each. These copper wires were wound around the insulator end fittings, eight pieces in number, with the sharp end of the wires point towards the insulator. These corona sources were outside of the dry arcing distance of the insulator. Different configurations were considered for the corona source including at the low voltage end (dead-end) fittings only, high voltage end (live-end) fittings only and at both end fittings.

These additional charges generated through the corona sources were then quantified by measuring the related leakage current along the insulator surface with the use of the current monitoring system, which was connected between the low voltage end (dead-end) of the insulator and the HVDC laboratory earth.

Figure 3.10: Experimental Set-up for Silicone Rubber Insulator under DC Voltage.

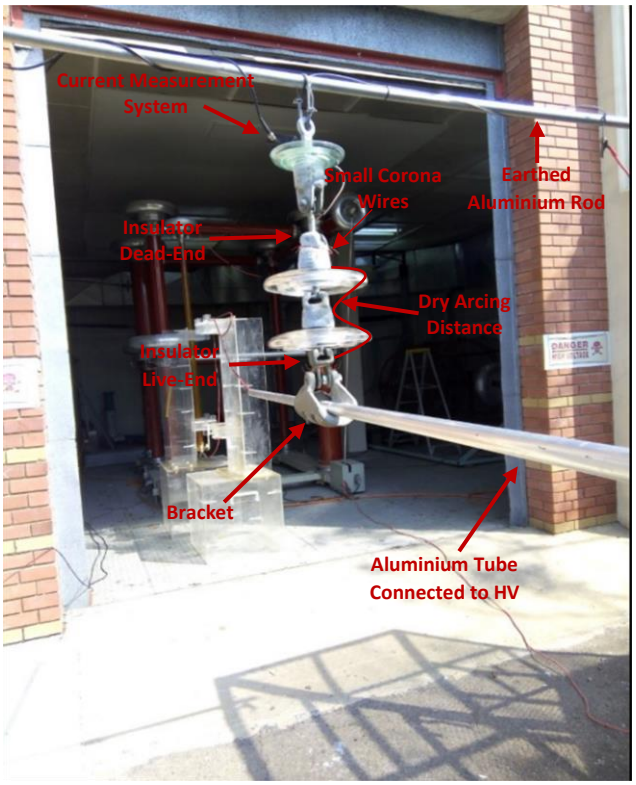

Figure 3.11: Experimental Set-up for Glass Cap-and-Pin Insulator under DC Voltage.

A similar set-up as described in *section 3.4.1* was used for the leakage current performance test under AC voltage with the inclusion of the current monitoring system. The current monitoring system was connected in between the low voltage end (dead-end) of the insulator and the high voltage laboratory earth.

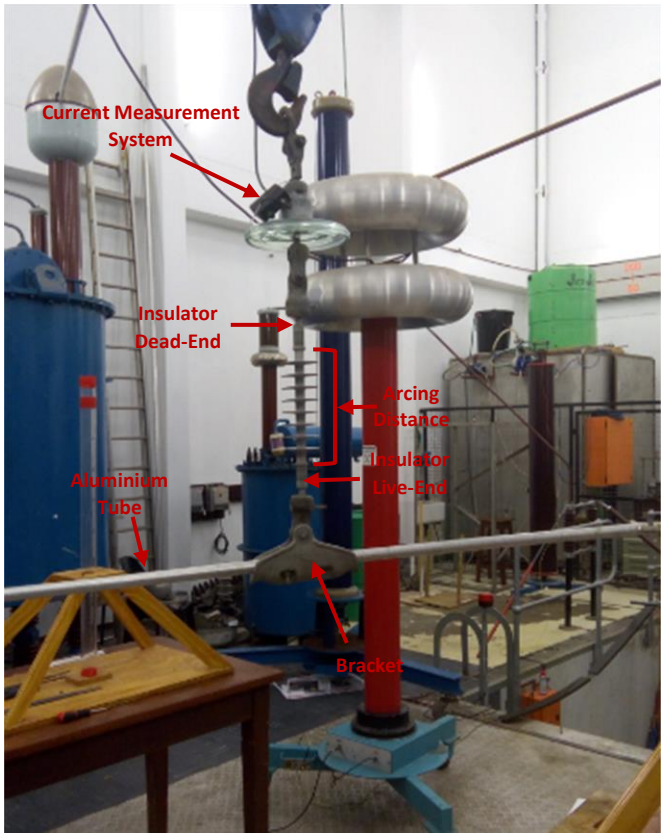

Figure 3.12: Experimental Set-up for Silicone Rubber Insulator under AC Voltage.

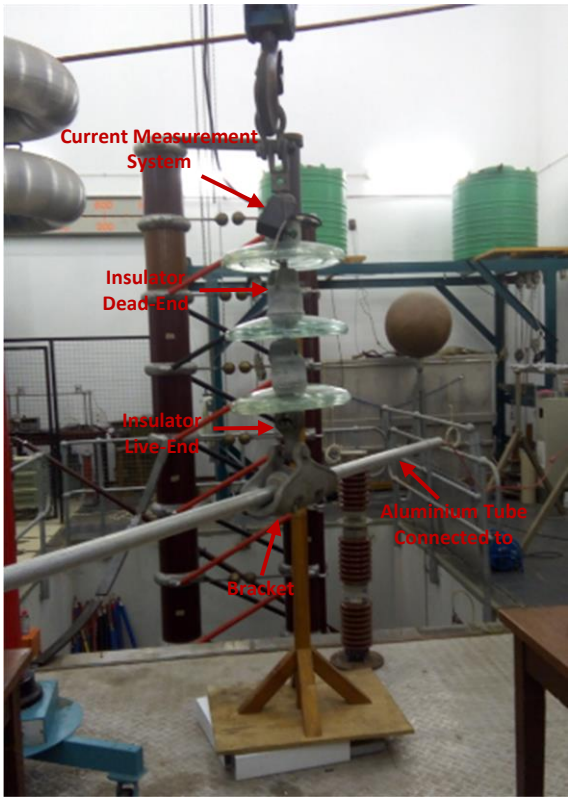

Figure 3.13: Experimental Set-up for Glass Cap-and-Pin Insulator under AC Voltage.

3.5 Experimental Procedures

3.5.1 Breakdown Voltage under AC, Standard Lightning Impulse and HVDC

The breakdown voltages were taken at recorded atmospheric conditions and corrected to the standard atmospheric conditions using the atmospheric correction factors as specified in IEC 60060-1 [77]. Also, during the experiments, a 4 in 1 professional measuring instrument (Lutron LM-8000): Anemometer, Hygrometer, Thermometer, and Light meter, was used for the relative humidity and temperature measurements. A handheld Altimeter, Oregon scientific Altimeter (RA 123), with barometer was also used for measuring the atmospheric pressure.

The AC voltage was applied and continuously raised until a flashover occurred across the insulator. The DC voltage was applied and raised in continuous steps until a flashover occurred across the insulator. The last test voltage measured just before the instance of the disruptive discharge was recorded as the breakdown voltage. This same procedure was repeated five times and averaged, the average breakdown voltages for the AC test is given by [77]:

$$U_{ave} = \frac{1}{N}\sum_{i=1}^{N} U_i \tag{15}$$

Where U_i represents the measured breakdown voltages each time the tests were performed, U_{ave} the average breakdown voltage and N the number of repeated test time.

For the wet test, the artificial rain was applied to the insulator through a nozzle system, details of the precipitation conditions used according to [77] are given in *Appendix B*. Under this condition, the insulator was pre-wetted at the outset for at least 15 minutes before the test.

The up-and-down method was used to calculate the 50% breakdown or flashover voltage (U_{50}) during the lightning impulse test, where a total number of 20 impulse shots were used, with a starting voltage level V_i. For each breakdown voltage that occurred, the voltage level used for the succeeding shot was reduced, i.e. a voltage level of V_{i-1} was utilized. Each occurrence of withstand results into an increase of the voltage level applied, i.e. a voltage level of V_{i+1} was used for the succeeding shot. At the end of the tests, the total number of flashovers and withstands were added and the U_{50} voltage was derived using equation (16) [77].

$$U_{50} = \frac{\delta \times k \times \frac{\sum n \times V_i}{P} \times z \times r}{1000} \tag{16}$$

Where z represents the scale factor of the impulse measurement circuit, r the divider ratio, U_{50} the 50% breakdown voltage, k the humidity correction factor, δ the air density correction factor and P the number of shots.

For the lightning impulse wet test, the insulator was sprayed thoroughly with a water bottle before the start of the test. Moreover, the humidity correction factor was not applied to the wet test under all the applied voltage types. Also, due to the short distance of the insulator arcing distance which was less than 0.5 m as specified in IEC 60060-1 [77], the humidity correction factor was also not applied to the dry test under all the applied voltage types.

3.5.2 Breakdown Voltage and Current under HVDC

The effect of charging time on the rate of accumulation of surface charges on a model cylindrical polymeric insulator consisting of a glass fibre reinforced epoxy core covered with a layer of silicone rubber was carried out in [40]. A corona belt was used for the charging under both DC polarities and the surface charges were quantified by measuring the surface potential distribution. Their results showed that an increase in charging time from one to three minutes does not significantly affect the resulting surface charge distributions for both negative and positive DC polarities.

In this research investigation, the DC and AC voltages were applied to the live end of the insulator and continuously raised in steps at every two minutes until a flashover occurred along the insulator, the breakdown voltages and the measured current were recorded. This procedure was repeated five times and averaged for each experimental configuration. The breakdown voltages were corrected to the standard atmospheric conditions using the atmospheric correction factors specified in IEC 60060-1 standards [77].

3.6 Finite Element Model

This section presents the modelling of the two types of insulator used for the analysis of the electric field and current. The simulation was carried out with the use of FEMM 4.2 software package [78] by first building the insulator model in air and then setting up the test conditions to replicate the real experimental set-up. An axisymmetric two-dimensional (2D) current flow problem was used. The procedures followed are highlighted below:

- The models were created as shown in Figure 3.14 and Figure 3.15. The insulator dimensions used in the model were based on the actual geometrical measurements of the insulators as specified in Table 3.1 and Table 3.2. (It should be noted that conductors, supporting structures and other accessories were not considered in the model.)
- The materials involved in the insulation system were then added.

- A string of two glass cap-and-pin insulators were modelled as shown in Figure 3.14. *A* representing cast iron as the metal cap, *B* represents the glass sheds, *C* represents cast iron as metal pin, *D* depicts the surrounding air and *E* represents the cement grout.
- For the silicone rubber type of insulator model shown in Figure 3.15, four major parts were modelled: *F* represents the surrounding air, *G* depicts silicone rubber (SiR) as a sheath on the rod, *H* is the fibre reinforced polymer (FRP) core, *I* represents silicone rubber as weather sheds, and *J* represents cast iron as the metal end fittings.
- Table 3.3 shows the material properties used for the various parts of the insulators in the model.

- The boundary conditions (BC) were defined for the insulation model. The fixed voltage was used, where the high voltage side (live-end), a fixed voltage of 22 kV was used and a fixed voltage of 0 V was set on the low voltage side (dead-end).
- The triangular meshes were generated for the problems as shown in yellow colour in Figure 3.14 and Figure 3.15. Based on the method of finite element, the partial differential equations for the insulation system as represented in equation (12) and (13) were then solved by the software to evaluate the electric field.
- To account for the different type of voltages: AC and DC voltage types, the frequencies were altered on the software's problem definition option. In the case of the AC, 50 Hz was used and a frequency of zero was set for the DC.
- In the case of the DC, a small layer (0.0008 m) with a relative permittivity of 1.0 was included on the surface of the insulator models to account for the surface charges.

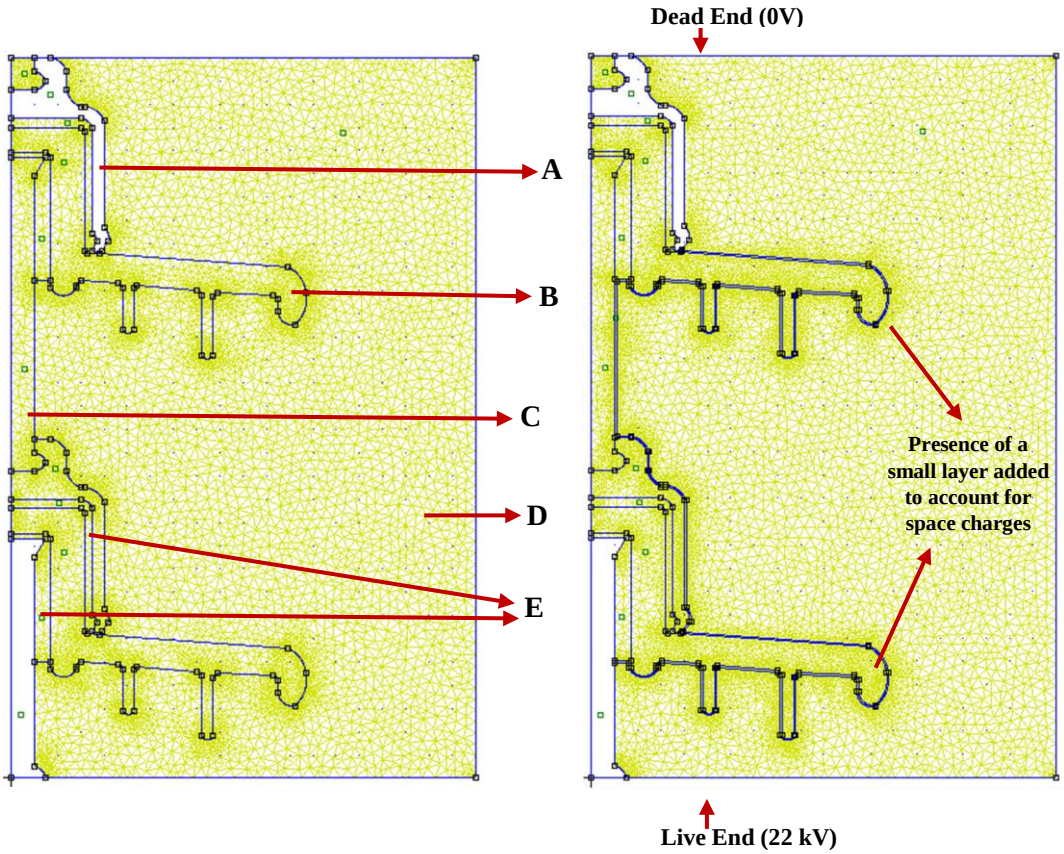

Figure 3.14: Glass Cap-and-Pin Insulator Model.

Table 3.3: Material Properties [39, 70].

Insulation Part	Relative Permittivity	Conductivity (S/m)
SIR	4.3	10^{-12}
FRP Core	7.2	10^{-12}
Air	1.0	10^{-13}
Glass	4.2	5×10^{-9}
Cement Grout	15.0	10^{-4}
Cast Iron	1.0	10300000

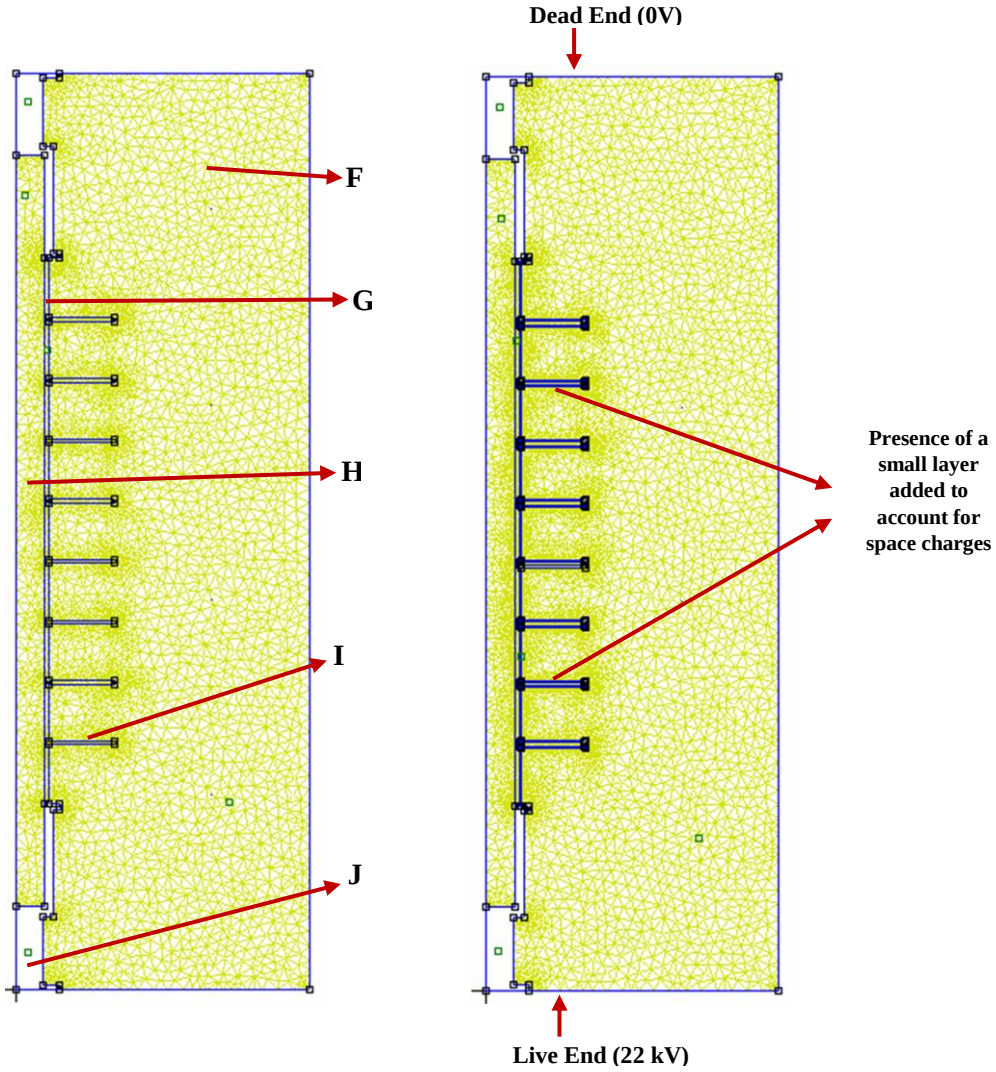

Figure 3.15: Silicone Rubber Insulator Model.

Two scenarios were simulated to match with the experimental work

1. The differences in the electric field distribution between AC and DC voltage. This was carried out only on the silicone rubber insulator model, where the model had been energized separately with AC and DC voltage at the live-end fittings and earthed at the dead-end fittings of the insulator.
2. Understanding the differences in the electric field distribution under DC voltage in the presence and absence of surface charges. This was carried out on both the silicone rubber and glass cap-and-pin insulator model.

3.7 Determination of the Effective Ionization Coefficient

Once the electric field distribution was obtained, the effective ionization coefficients in the active region were computed. Townsend's ionization coefficient, α and the attachment coefficient, η for dry air which are dependent on the electric field were adopted from [80] and were used for calculating the effective ionization coefficient (α – η).

Figure 3.16 shows the variation of the ionization and attachment coefficients with the electric field strength within the range of $25 \leq \frac{E}{p} \leq 60$ V/cm.torr for dry air at atmospheric pressure 760 torr (0.1 MPa) and temperature of 25 ^{0}C. This can also be empirically expressed as [80]:

$$\frac{\alpha}{p} = 4.7786e^{-221p/E} \tag{17}$$

$$\frac{\eta}{p} = 0.013 - 0.54 * 10^{-3}\frac{E}{p} + 0.87 * 10^{-5}\left(\frac{E}{p}\right)^2 \tag{18}$$

The integration of the effective ionization coefficient along the length of the active region in equation (6) was performed by using trapezoidal numerical method of integration.

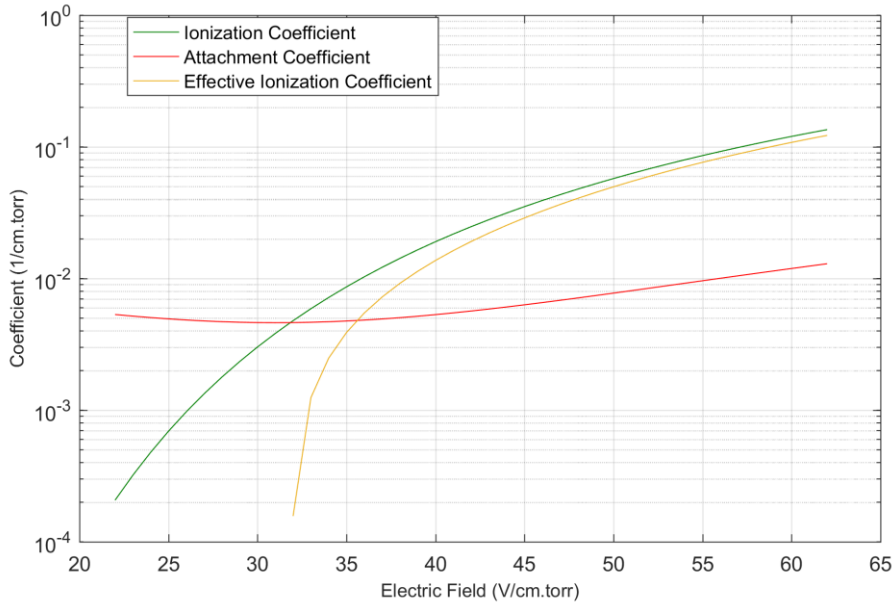

Figure 3.16: Ionization, Attachment and Effective Ionization Coefficients for Dry Air [80].

CHAPTER 4
RESULTS AND DISCUSSION

The results of all the breakdown tests of the two types of insulator used in this research investigation are presented in this chapter. These results were analyzed and compared to other available research studies.

The electric field results derived from the simulation are presented with relevance to the difference in its distribution under different voltage and insulator types. The simulation proved to be very important in understanding the experimental results.

4.1 Breakdown Voltage under AC, Impulse and HVDC

The results obtained from the breakdown tests carried out on the 22 kV silicone rubber insulator under AC, impulse and DC voltage types in dry and wet environmental conditions are shown in Figure 4.1 and Figure 4.2 respectively. Table 4.1 shows the atmospheric conditions at which these breakdown results were obtained before correcting them to standard atmospheric conditions.

Table 4.1: Experimental Atmospheric Conditions

	Dry			**Wet**		
Breakdown Tests	**Relative Humidity (%)**	**Pressure (mbar)**	**Temperature (^oC)**	**Relative Humidity (%)**	**Pressure (mbar)**	**Temperature (^oC)**
Standard Negative Impulse	66.9	998.9	28.1	63.2	996.0	27.3
Standard Positive Impulse	64.8	997.8	26.5	62.8	995.6	28.2
AC	68.9	996.3	26.0	29.3	990.8	32.5
Negative DC	37.7	1003.5	23.3	59.9	1002.1	21.2
Positive DC	64.5	996.9	23.0	60.0	990.1	24.5

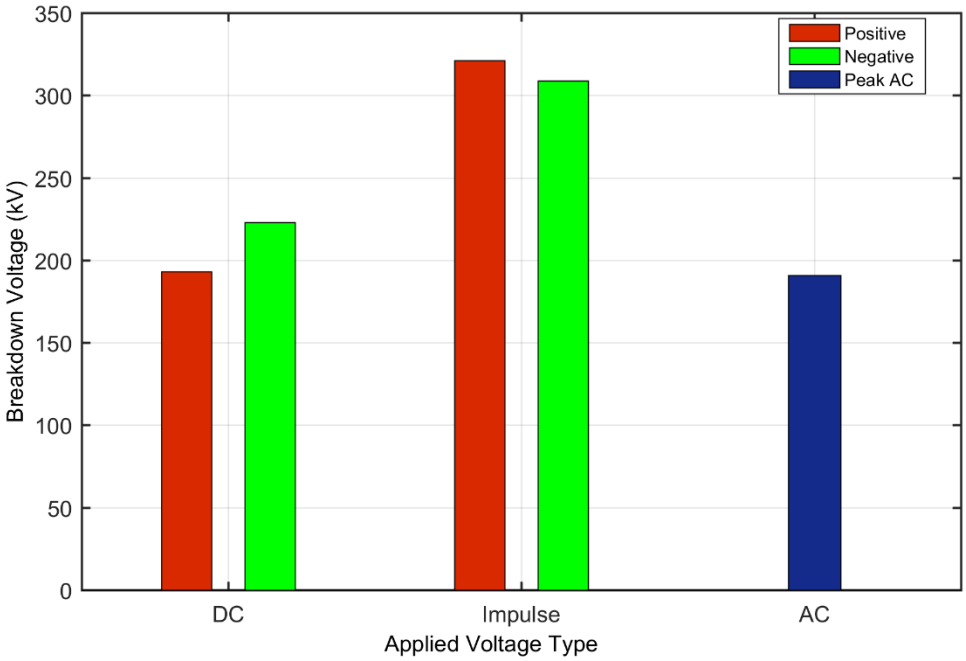

Figure 4.1: Breakdown Voltages for Dry Tests.

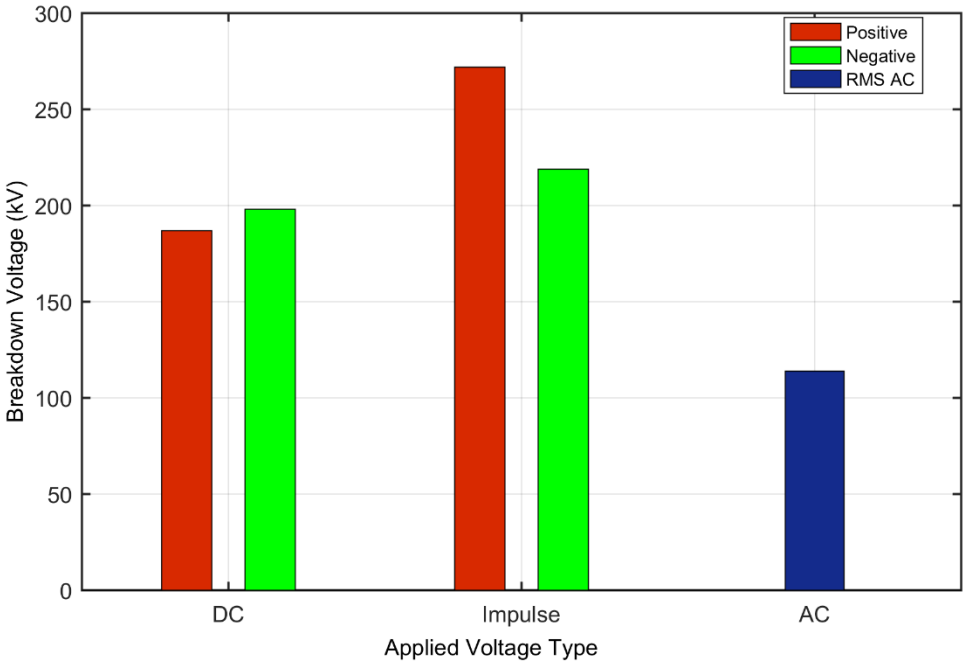

Figure 4.2: Breakdown Voltages for Wet Tests.

The wet breakdown voltage results for all the voltage types were expectedly lower than the dry breakdown voltage results. The silicone rubber insulator used was hydrophobic and any water droplet on the surface causes field enhancement [73]. For the impulse voltage, when the insulator

experienced wetting only before the start of the test, the lower breakdown voltage under wet conditions in comparison to dry conditions was due to the earlier development of the discharge.

The lower DC and AC breakdown voltages, when the insulator experienced continuous wetting during the experiment, were due to the conduction path created by the water and the related change in the electric field. These results were in good agreement with the results obtained by [62, 63]. According to Karady et al. [63], a highly resistive layer exists around each conducting water droplets scattered on the silicone rubber insulator surface, with continuous wetting, the density of the droplets increases and the distance between the droplets reduces. The influence of the electric field on water droplets generates an oscillating force which coalesces droplets with a small distance between them to form random conducting filaments on the insulator surface. These filaments limits the length between the electrodes and this results in a high electric field between adjacent filaments. This high field intensity generates a randomly distributed spot discharge along the insulator surface which distorts the resistive layers around the droplets. This creates room for the filaments to join together to form wet regions, conductive paths, conducive for arc formation which finally leads to the breakdown of the insulator.

From the results obtained under both environmental conditions, the average breakdown voltages for negative polarity DC were higher than the positive DC; this was attributed to the generation and distribution of charges. These observations were in agreement with that of [23, 41]. According to Kumara et al. [41], when the insulator is energized with positive DC, ionization by electron collision occurs in the high field region close to the high voltage electrode (anode). Electrons with their high mobility move towards the anode, leaving the positive ions behind. The space charge reduces the field strength close to the anode and simultaneously increases the field strength away from it. With the high field region eventually moving further into the gap and increasing the areas of ionization, a cathode directed streamer may be initiated due to the high electric field strength which is at the head of the space charge. This would eventually lead to breakdown.

When negative DC is applied to the insulator, the fast-moving electrons are repulsed to the low field region while the positive ions are attracted to the cathode and remain in the space between the cathode and the electrons. Close to the cathode, the field is greatly increased but the ionization region is reduced and once ionization is terminated, the applied electric field clears away the charges from the vicinity of the cathode and the cycle starts again. This slowing action of the ions can only be overcome by a very high voltage. This was evident as the negative breakdown voltage was higher than the positive breakdown voltage.

As explained in *section 3.5.1*, the humidity correction factor was ignored. However, during the dry DC breakdown experiments, some irregularities were observed in the measured relative

humidity as shown in Table 4.1. The negative dry DC test was carried out on a low humidity day while the positive dry DC test was carried out on a high humidity day. The humidity was significantly different during these experimental days. Therefore, it is unclear from this research investigation whether these differences in the humidity influences the dry DC results.

According to some previous studies [61, 81-82], the average breakdown voltage for insulators operating under DC voltage is lower than that of the peak AC breakdown voltage. In [81], AC and DC flashover tests were carried out by Shu et al. on ice-covered porcelain, glass and composite insulators under the conditions of low air pressure and pollution. Their results showed that air pressure had a greater influence on the AC breakdown voltage than that of DC whereas the influence of pollution on both AC and DC breakdown voltages were almost the same. This higher AC breakdown was attributed to the zero passage of current when AC is applied which makes arc periodically repeat the process of establishment, development and extinguishment. When DC was applied, the arc ignites steadily because of the non-existence of zero passage. In [82], Jiang et al. investigated the flashover performance of polluted insulators, considering composite and ceramic insulators, using two different test methods: average flashover voltage obtained by even-raising the voltage and the 50% breakdown voltage obtained by the up-and-down method. The influence of these methods on the flashover voltages were considered and it was considered significant with the average flashover voltage being 6.2% to 10% higher than the 50% breakdown voltage. Both AC and DC pollution flashover voltages of the insulators were found to have decreased with an increase in pollution. In [61], field tests carried out at Sylmar Converter Station of the Pacific Intertie HVDC system to determine the process and factors influencing the contamination flashovers of HVDC ceramic insulators were presented by Cheng and Wu. The field tests spans a period of two years, the contaminants were identified and the rates of accumulation were determined. It was reported that the insulator flashovers were more severe on the DC than on comparable AC transmission system in a similar environment. This severity was attributed to the electrostatic field in DC which allow more contaminants to accumulate on DC insulators, the absence of current and voltage zeros in DC transmission which aggravates the flashover problem.

The results from the experiment indicate that the average breakdown voltage for the peak AC was less than both polarities of DC under both dry and wet conditions. The reason for this deviation experienced in this research investigation could be attributed to the difference in experiment set-up. Higher DC breakdown voltages than AC breakdown voltage were also reported by [50, 83]. In [50], the dielectric insulation properties of different silicone rubber materials, employable to 500 kV DC voltage insulators, were investigated under AC and DC stress by Seo et al. Two silicone samples were prepared in several ways by selecting octamethylcyclotetrasiloxane and

dimethylcyclosiloxane as separate base materials and adding to each materials different content ratio of ATH (aluminumtrihydroxide) fillers. These prepared materials were subjected to DC voltage stress to evaluate their breakdown characteristics and also energized under AC voltage stress for comparison. The difference between DC and AC was attributed to the different mechanism of breakdown: partial discharge for AC and under DC stress, space charge accumulation and distribution. Alles et al. [83] carried out an investigation on the breakdown performance of different types of glass insulators in dry conditions, under AC, DC, lightning impulse voltages considering the shed diameter and arcing distance. Their results showed that the arcing distance is the main parameter affecting the breakdown voltage, the relationship between flashover voltage and arcing distance for DC was discovered to be more linear than that of AC. Also the differences between the AC and the DC breakdown voltage was attributed to dust particles and air current which affects the distribution of the charges and the electric field in DC.

It can be observed from the results that the negative impulse U_{50} were lower than the positive polarities U_{50} under both dry and wet conditions. Similar results were observed by [64, 65] and it was attributed to a reversal polarity phenomenon which is experienced with non-uniform field air gaps. This phenomenon may be caused by the non-uniformity of the electric field, electrode shape and configuration.

The lightning impulse voltages results were observed to be higher than DC under both polarities as well as AC. This was expected and was attributed to the duration of the applied voltage and the availability of an electron to initiate the breakdown process. For DC, the space charge additionally has enough time to build up and thus distort the field while for the impulse voltage; the space charge cannot accumulate [23].

4.2 Breakdown Voltage and Current under HVDC

This section presents the results obtained from the charging and breakdown tests carried out on a 22 kV silicone rubber and glass cap-and-pin insulators under AC and DC voltage types. In the case of DC, the space charges were altered as discussed in *section 3.4.2*. The rms value of the AC current was used for comparison with the DC current in this section, this is simply because rms AC current or voltage would produce the same amount of heat energy dissipation as the DC through an equal resistance [84].

Figure 4.3 shows the relationship between the measured leakage current and applied voltage for silicone rubber and glass cap-and-pin insulator under AC voltage. Both the current and voltage are in their rms values. It can be observed from this result presented in Figure 4.3 that the leakage current for silicone rubber insulator was lower than that of the glass cap-and-pin insulator, an

indication that silicone rubber may perform better than glass under AC voltage. The higher current shown in the glass cap-and-pin insulator can be attributed to the high self-capacitance in each disc unit of the glass insulator.

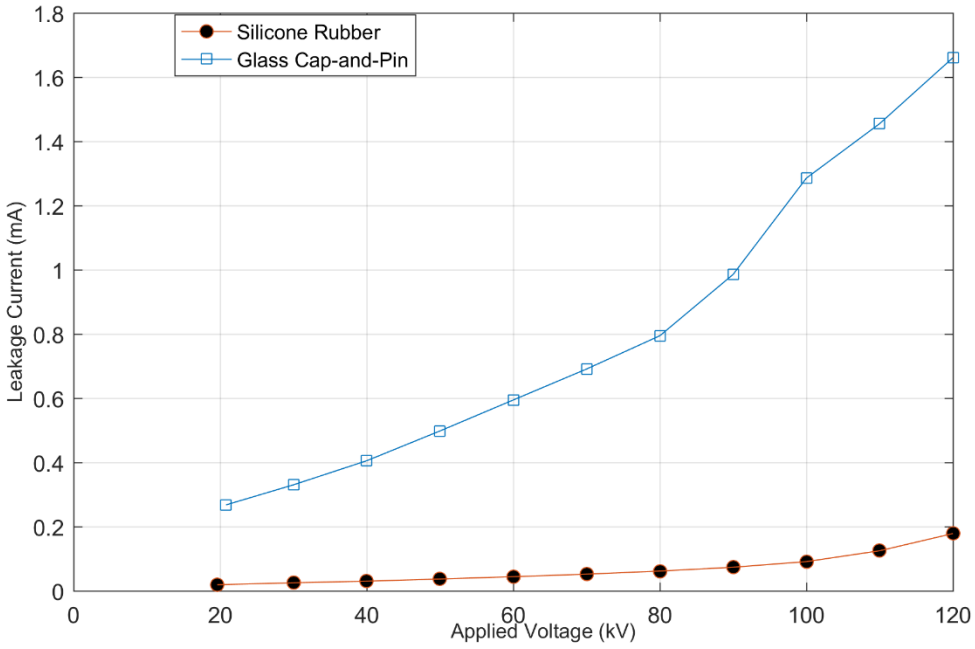

Figure 4.3: Leakage Current of Silicone Rubber and Glass Cap-and-Pin Insulator under AC Voltage.

Figure 4.4 and Figure 4.5 shows the relationship between the measured leakage current and applied voltage for silicone rubber and glass cap-and-pin insulator under negative DC voltage respectively. Also in the case of positive DC, Figure 4.6 and Figure 4.7 presents the relationship between the measured leakage current and the applied voltage for both insulator types.

Comparing these AC and DC results, it can be observed that the AC currents were higher (in the mA range) than the DC currents (in the µA range) for both types of insulator considered in this investigation. This can be attributed to the combination of both resistive and capacitive current components that exist in AC as against DC where only the resistive current component exists.

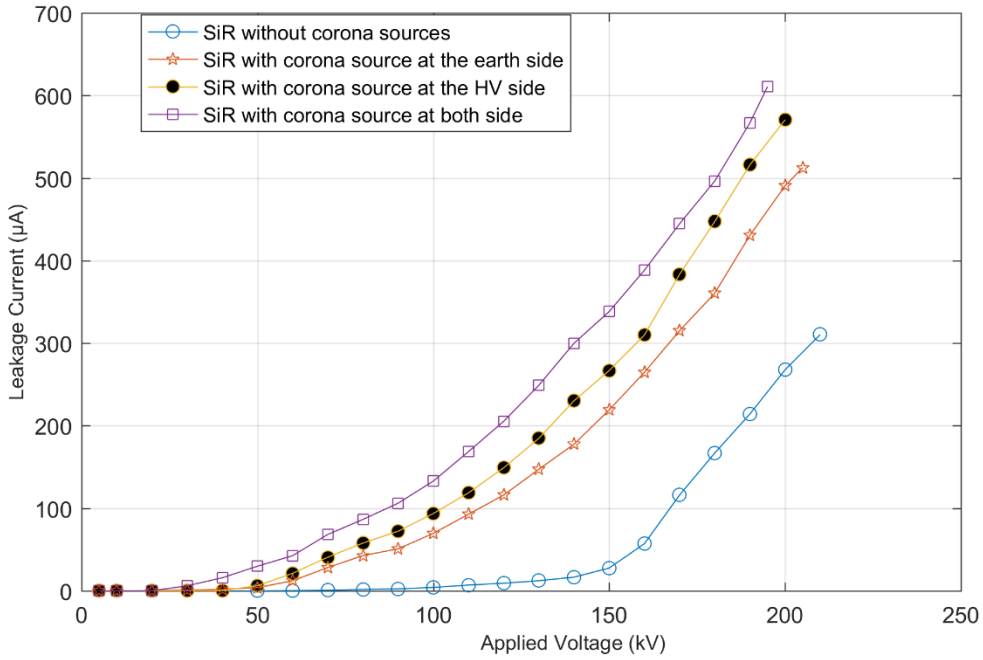

Figure 4.4: Leakage Current Characteristics of Silicone Rubber Insulator under Negative DC voltage.

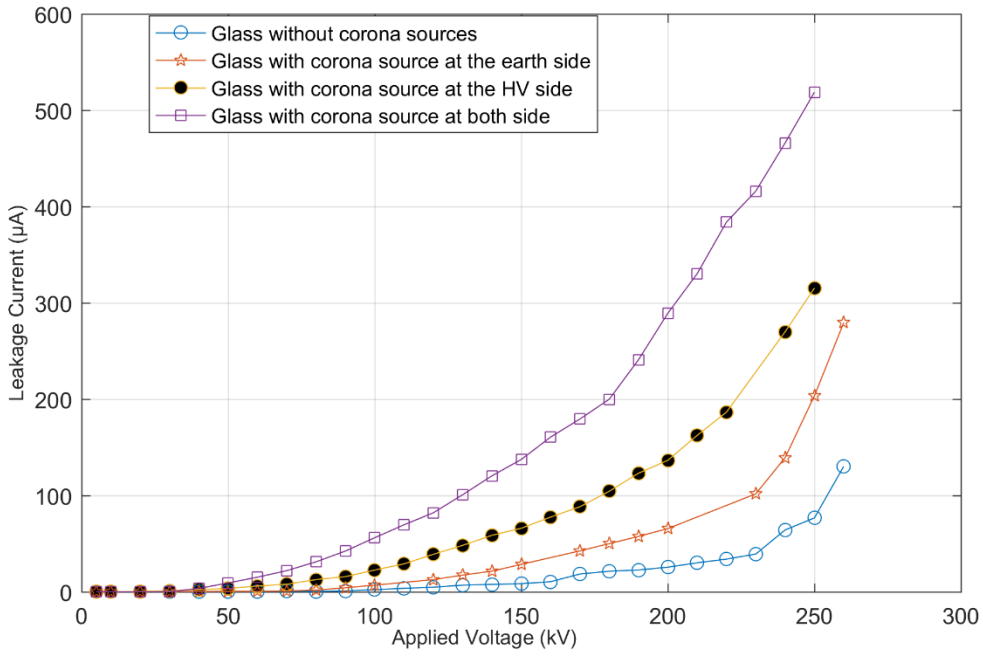

Figure 4.5: Leakage Current Characteristics of Glass cap-and-pin Insulator under Negative DC voltage.

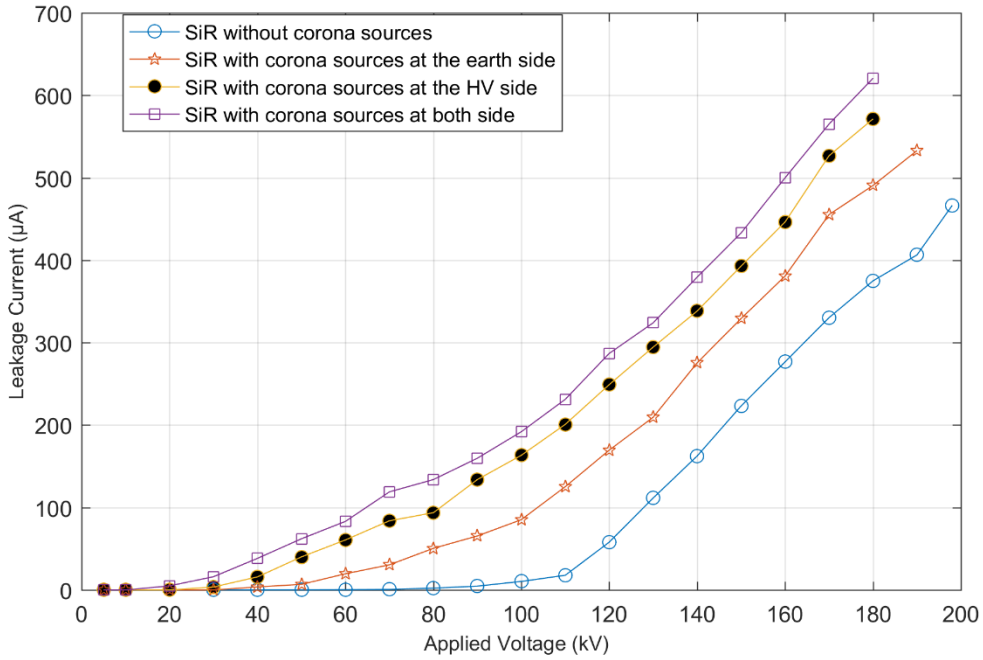

Figure 4.6: Leakage Current Characteristics of Silicone Rubber Insulator under Positive DC voltage.

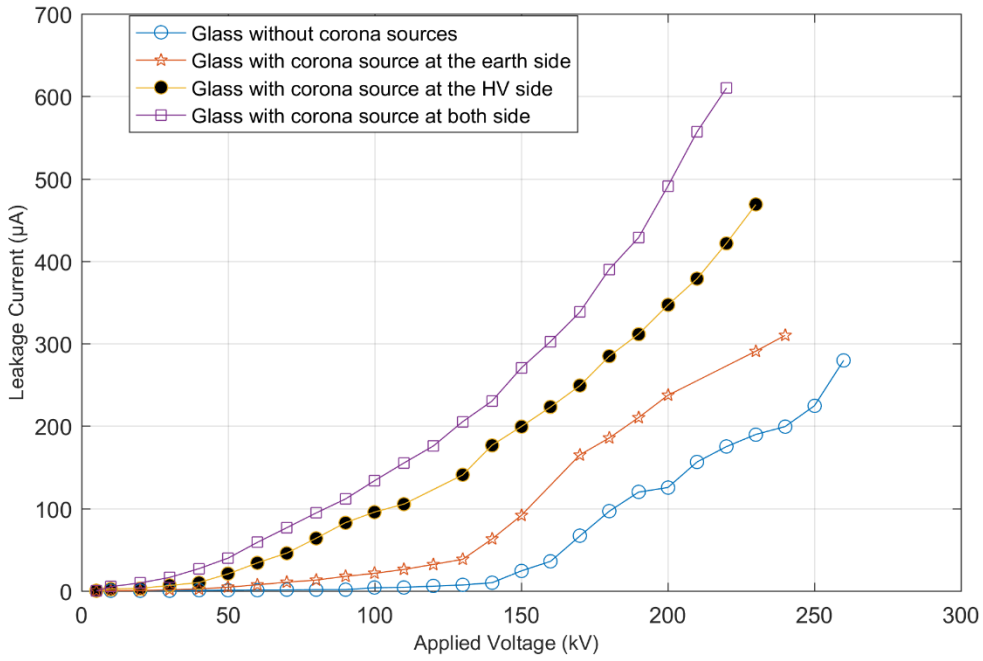

Figure 4.7: Leakage Current Characteristics of Glass cap-and-pin Insulator under Positive DC voltage.

According to Waluyo et al. [85], high voltage insulators can simply be modelled as a combination of a capacitor (C) and resistor (R) in a parallel connection as show in Figure 4.8, where C is the dielectric capacity and R is the surface leakage resistance of the insulator. During the application of an AC voltage, the total current would consist of a capacitive current that flows and a small current. The capacitive current decays exponentially to zero a few seconds after the DC voltage is applied due to the non-varying nature of the voltage leaving only a small resistive current as the total current that flows during the application of a DC voltage.

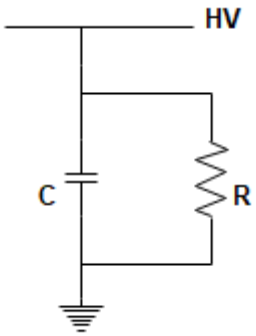

Figure 4.8: High Voltage Insulator Model.

This capacitive current can be termed as a displacement current which exist as a result of the time-varying electric field and geometric capacitance of the system [40]. The resistive current can also be termed conduction current that exists as a result of the drift and diffusion of charge carriers (electrons and ions).The capacitive component of the current appears to be more dominant over the resistive component and this corroborates the fact that the higher the capacitance of the insulator under test, the higher the magnitude of the capacitive current which contributes greatly to the total current flow along the insulator [85]. This can also be observed in Figure 4.3 where the glass with a higher capacitance exhibited a higher current flow.

Considering Figure 4.4 which shows the relationship between the leakage current and applied voltage for silicone rubber insulator under negative DC, the leakage current in the presence of the corona source where higher than when they were absent. It can be observed that different configurations of the corona source accounted for different quantity of space charges: the corona source at both ends having the highest quantity of space charges and the least quantity of charges were observed in the absence of corona sources. This was observed for both insulator types under both DC polarities as shown in Figure 4.5 to Figure 4.7. The results shows that the more the number of corona sources, the more the amount of charges created at the insulator surface. Thus, the higher the leakage current, which is an indication of the presence of a resistive leakage current. Similar results were reported in [13, 36] as explained in *section 2.5* and their results shows that

the leakage current increases in the case of a DC voltage. This is as a result of the charges accumulated on the insulator surface.

It can be observed from the result in Figure 4.4 that the leakage current increased linearly until it attained a certain voltage where it exponentially increased with the applied voltage. The voltage at which this exponential increase began is termed a 'knee point'. It can be noticed that in the absence of the corona sources (low charge generation resulting in low current) the knee point occurred at a higher voltage while in the presence of the corona sources (high charge generation resulting in high current) the knee point occurred at a lower voltage. This indicates that the voltage at this knee point may have been a corona starting point and this was further investigated with the FEM models in *section 4.3.2*. These observations were noticed on both insulator types considered under both DC polarities as shown in Figure 4.5 to Figure 4.7.

It can also be noticed from the results, Figure 4.4 to Figure 4.7, that the pattern of variation of leakage current under the different conditions (with and without charges) along the silicone rubber and glass insulator, looks similar with the silicone rubber exhibiting a higher current than the glass insulator under both DC polarities. This might be as a result of the different material types involved: silicone rubber, an organic material as discussed in *section 2.4* and glass, an inorganic material. Similar high degree of current for silicone rubber insulators was obtained in [36, 37] and it was attributed to the changes in chemical composition of silicone rubber material surface due to the attack by corona discharge. These changes were discovered to be more pronounced with silicone rubber insulators exhibiting high currents under HVDC stress in [37].

Similar results of low current exhibited by the glass cap-and-pin insulators were obtained by Vosloo and Holzhausen [38], where the glass displays a significant value of leakage currents flow after a very long duration (18 hours) of subjection to high levels of humidity and in corroboration to [35], it was attributed to the insulator's protected under-rib design of its shed, which increases the leakage distance resulting in an increase in the surface leakage resistance. The surface resistance is directly related to the leakage distance of the insulator, the increase in leakage resistance results in a decrease in the leakage current.

The polarity effects can also be observed from the DC results, positive DC had a higher current than negative DC for all cases of corona source configuration. The breakdown voltages for positive DC were also lower than that of negative DC. These results were expected and attributed to the physics relating to the development and movement of the electron avalanche in both positively and negatively energized systems as explained in *section 4.1*. The breakdown voltages for both negative and positive polarities under the different charging conditions are shown in Figure 4.9 and Figure 4.10 respectively.

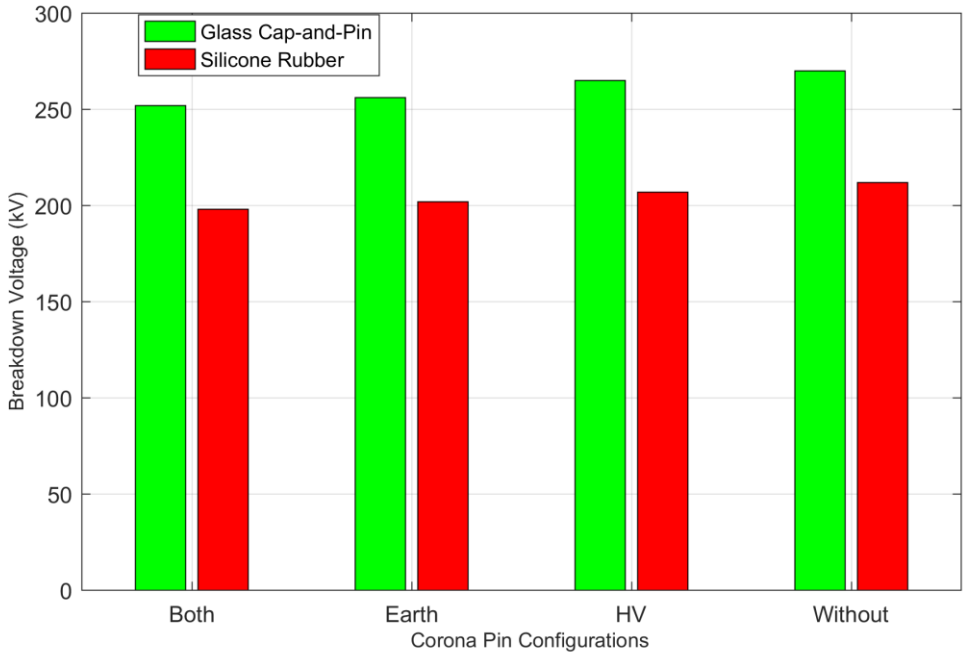

Figure 4.9: Insulator Breakdown Voltage with Different Charging Configurations under Negative DC Voltage.

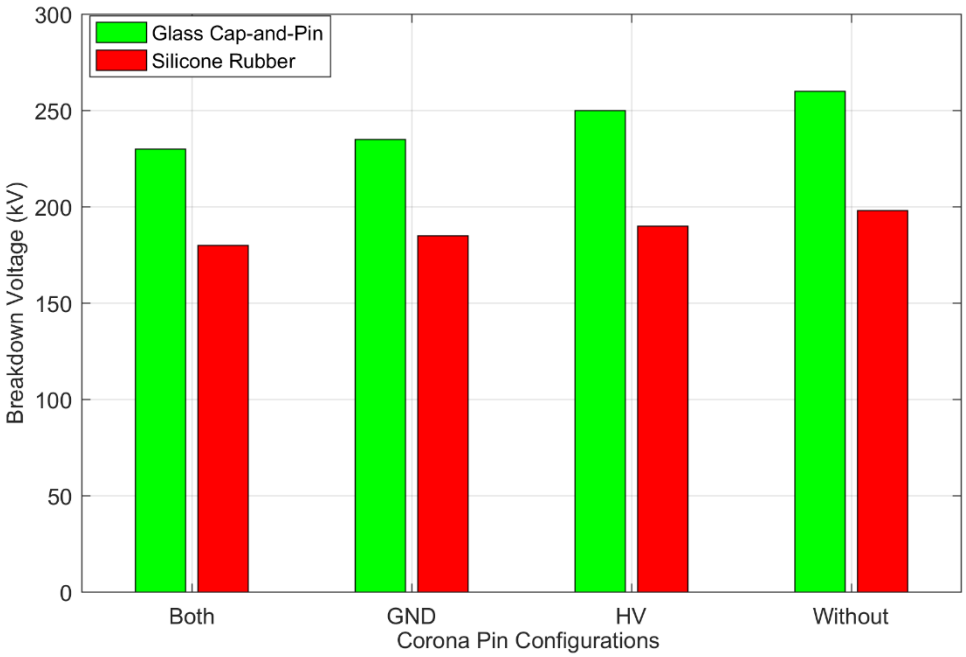

Figure 4.10: Insulator Breakdown Voltage with Different Charging Configurations under Positive DC Voltage.

The electric field becomes resistive under DC voltage as against the capacitive field under AC, this is as a result of space charges accumulating on the insulator surfaces [4]. These accumulated surface charges distort the field and reduced the breakdown voltage. This was confirmed by the

breakdown result obtained during the experimental tests as shown in Figure 4.9 and Figure 4.10 for both negative and positive polarities respectively where the breakdown voltages for both insulator types were reduced in the presence of surface charges.

Space charge accumulation on the insulator surface leads to leakage current along the insulator which can affect the breakdown strength of the insulator. This leakage current can also provide more information about the surface condition of DC insulator. It has been established that leakage current flow is as a result of charge flow. According to Othman et al. [39], insulators with similar shapes and material operating under the same environmental conditions are expected to possess the same degree of negative and positive charges in other to have a zero net charge. However, a charge imbalance exists on the insulator surface in the presence of space charges which results in static electric effects. These electric effects migrate from one surface of the insulator to another and lead to an electrostatic discharge. The electrostatic field formed on the insulator surface will result in electrical pathways that may allow relatively under-rated voltages to flow across the surface of the insulator and ultimately lead to breakdown [39].

Similar results of breakdown voltages characteristics were also obtained in [86, 87]. In [86], Sumathi and Jeeri performed a leakage current measurement and flashover studies on polluted 11 kV porcelain pin and suspension insulators under healthy and different scenarios. The different scenario conditions are urea pollution, sea salt pollution and wet conditions. The highest leakage current and lowest flashover voltage was measured under the urea pollution condition while the lowest leakage current and highest flashover voltage was measured under the healthy condition. It was concluded that the higher the conductivity of the insulator surface, the lower the breakdown voltage. Samimi et al. [87] evaluated the effect of pollution on the leakage current performance of silicone rubber insulators under dry and wet conditions. It was reported during the wet condition that the thermal energy dissipated as a result of the flow of the leakage current evaporates the moisture on the insulator interface, this led to the emergence of dry band areas. The electric field intensity of these dry band areas is higher than that of air and this paves way for the occurrence of partial arcs across these dry band areas. This partial arc propagates further and eventually leads to insulator breakdown.

An indication of the dielectric strength characteristics of the insulator can also be provided by the applied electric stress needed to cause electric breakdown of the insulator. This quantity can be represented by the ratio of the measured breakdown voltage to the measured arcing distance or creepage distance. The arcing and creepage distance of both insulator types are provided in Table 3.1 and Table 3.2. This average applied electric stress needed to cause breakdown were calculated and shown in Table 4.2 and Table 4.3 for both AC and DC voltages. It can be observed that the average electric stress for the DC were slightly higher than that of the AC. Also the average

applied electric stress for the glass were higher than that of the silicone rubber insulator. This indicates the role of arcing and creepage distance in specifying DC insulators as the dielectric strength of the insulators seems to be a function of the arcing and creepage distance.

Table 4.2: Average Electric Stress by Arcing Distance.

Insulator Types	**Negative DC (kV/m)**				**Positive DC (kV/m)**				**AC (kV/m)**
	No Corona Source	**Corona Source at Dead-End**	**Corona Source at Live-End**	**Corona Source at Both End**	**No Corona Source**	**Corona Source at Dead-End**	**Corona Source at Live-End**	**Corona Source at Both End**	
SiR	7.6	7.4	7.2	7.1	7.1	7.0	6.8	6.6	6.8
Glass	8.6	8.4	8.1	8.0	8.4	7.9	7.4	7.2	6.3

Table 4.3: Average Electric Stress by Creepage Distance.

Insulator Types	**Negative DC (kV/m)**				**Positive DC (kV/m)**				**AC (kV/m)**
	No Corona Source	**Corona Source at Dead-End**	**Corona Source at Live-End**	**Corona Source at Both End**	**No Corona Source**	**Corona Source at Dead-End**	**Corona Source at Live-End**	**Corona Source at Both End**	
SiR	2.627	2.565	2.503	2.454	2.454	2.416	2.354	2.292	2.367
Glass	3.553	3.487	3.368	3.316	3.474	3.289	3.092	3.000	2.618

4.3 FEM Analysis of Electric Field

This section presents the simulation studies that were carried out to understand the differences in electric field distribution.

4.3.1 Scenario 1

Two case studies were considered to understand the difference in the electric field between AC and DC under this study. The silicone rubber insulator was energized at the live-end with 22 kV and earthed at the dead-end. Table 4.4 provides the currents obtained while Figures 4.11 shows the relationship between the electric field and the leakage distance of the insulator which was also obtained from the simulation results for the two cases of applied voltage considered. It was observed from the simulation results in Table 4.4 that the current was significantly higher for the AC case; which was due to the capacitive component. The resistive components were similar for AC and DC. This was in good agreement with the experimental results explained in *section 4.2*.

Table 4.4: Case Studies.

Case	Conductivity (S/m)	Current (nA)
AC	10^{-13}	0.45+j*16.60e3
DC1	10^{-13}	0.45
DC2	10^{-12}	0.46
DC3	10^{-10}	1
DC4	10^{-8}	36

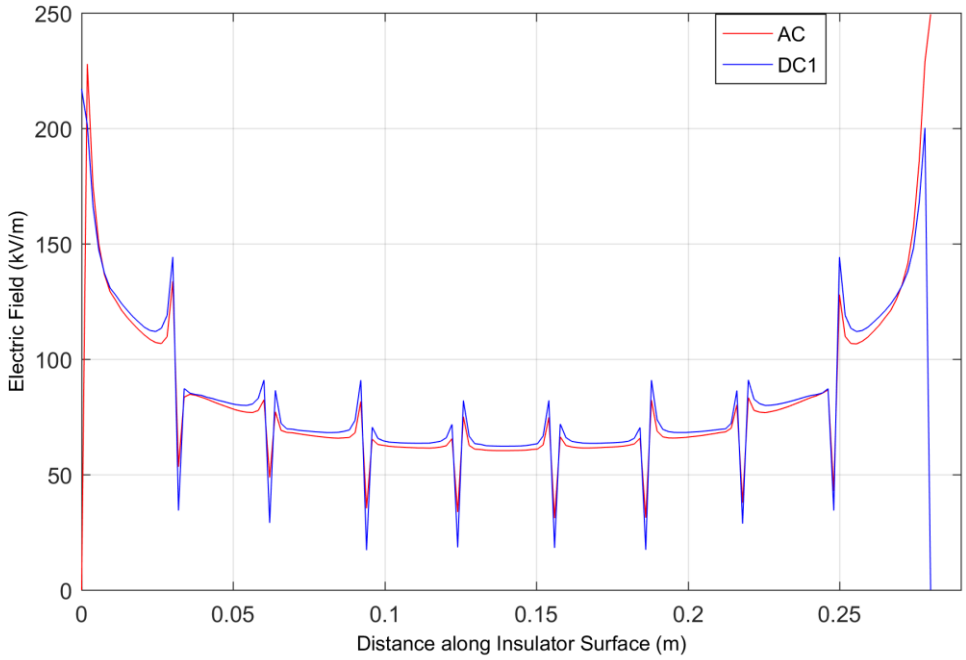

Figure 4.11: Electric field for cases AC and DC1.

The electric field distribution for the two cases, AC and DC1, were similar. The field distribution is non-uniform: having areas of high and low fields. The electric fields for the models were most intense at both end fittings under both AC and DC voltages. This was due to the localized geometric field enhancement caused when insulators of two different permittivities meet at an electrode i.e. where the air and silicone rubber meet the end fitting [72]. These high field areas give an indication of where corona discharges are likely to occur [71].

To account for the influence of space charge along the surface of the insulator in the case of the DC, the conductivity of the surface was changed and it was shown that an increase in surface conductivity or the amount of surface charge resulted in an increase in current. This can be seen in Table 4.4 and was in good agreement with the experimental results of leakage current with different positioning of the corona source explained in *section 4.2.*

Scenario 2 gives more insight into the influence of surface charges on the electric field considering two types of DC insulators.

4.3.2 Scenario 2

Silicone rubber and glass cap-and-pin insulators were energized by a DC voltage in these simulation studies to interpret the experimental results and understand the influence of the surface charges on the electric field.

To account for the surface charges developed during the experimental testing in the laboratory, the conductivity was altered to ascertain the effect of the space charge on the electric field. This was achieved by making use of the measured current at 190 kV for both insulators during the experimental testing in the model for the calculations of the electric field, as the breakdown voltage for silicone rubber in the presence of surface charges under negative polarity was 198 kV. Table 4.5 provides the conductivities used to generate the experimentally measured currents while Figures 4.12 and Figure 4.13 shows the electric field distribution for both insulator types under DC voltage.

Table 4.5: Conductivities at 190 kV.

Insulator Type	**Conductivity (S/m)**	**Current (µA)**
Glass	0.000019	241
SiR	0.000143	567

Figure 4.12 presents the electric field distribution for the glass cap-and-pin insulators in the absence and presence of surface charges respectively.

The electric field strength inside the glass material was intense in the absence of charges, this is as a result of the effect of the self-capacitance of the insulator and it becomes more intense in the presence of surface charges. This indicates that the presence of surface charges on glass insulator will increase the field strength inside the glass. It can also be seen that the equipotential lines appear to be distributed evenly from the pin to the cap along the shed of the insulator in the presence of the charges than in the absence.

The electric field distribution for silicone rubber insulator is shown in Figures 4.13. The presence of surface charges results in the modification of the electric field, most especially along the sheds. It can also be seen that the equipotential lines follow a different path.

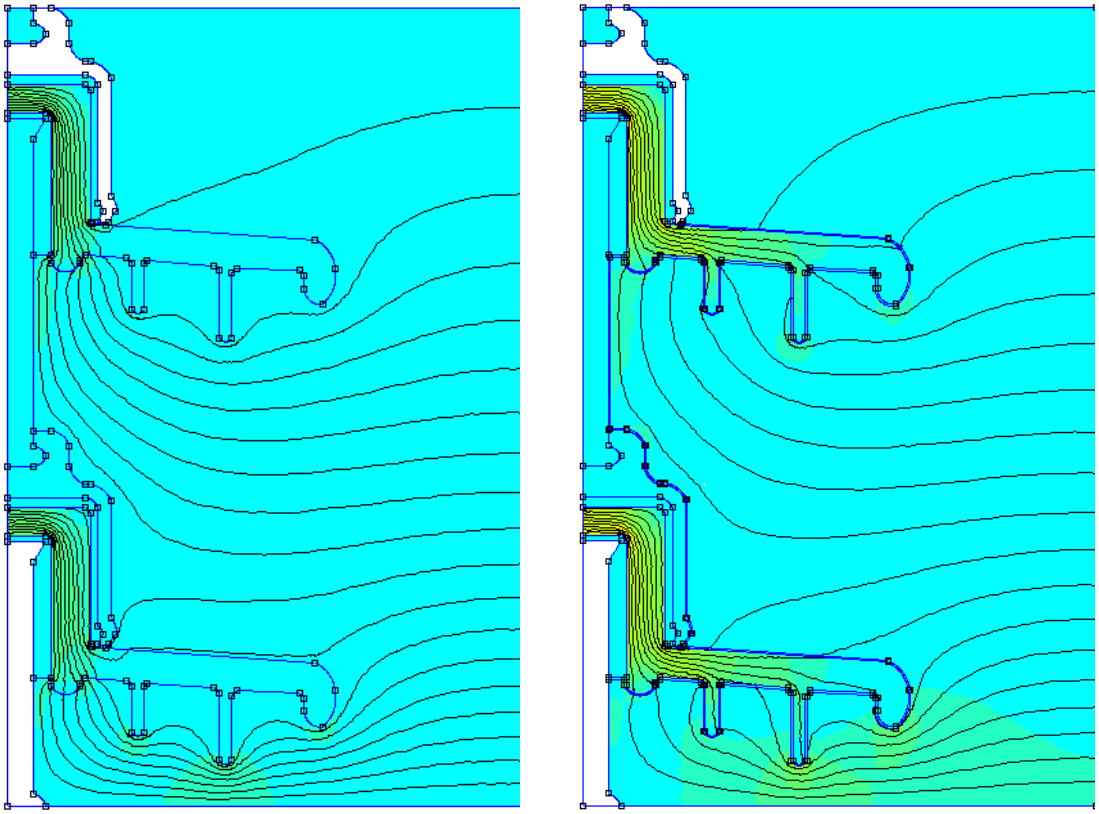

(a) (b)

Figure 4.12: Model of Glass cap-and-pin Insulator in the absence of charges (a) and in the presence of charges (b).

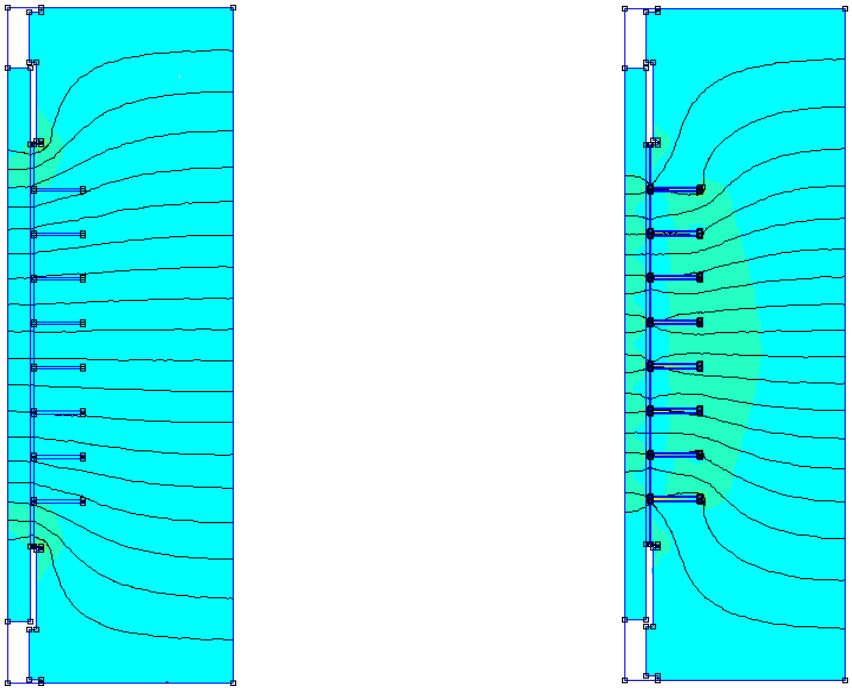

(a) (b)

Figure 4.13: Model of Silicone Rubber Insulator in the absence of charges (a) and in the presence of charges (b).

In [88], Chakravorti and Mukherjee carried out a detailed study on electric field distribution around a porcelain post-type insulator without as well as with surface pollution under power frequency as well as impulse voltages. Different severities of surface pollution were considered using the charge simulation method. They reported that the field modification might be due to the space charges in the air existing around the insulator surface which may be pulled to the insulator surface by the normal component of the electric field while the tangential component of the electric field moves the charges along the insulator surface. Additional charges could also be generated around the insulator surface because of the high electric field. This would lead to a high surface leakage current that is being experienced in a resistive field. Hence, the higher leakage current experienced at the surface of the insulator in a resistive field will increase the probability of flashover at the insulator surface and reduce the breakdown voltage [71]. This can also be confirmed by the differences in the breakdown voltages measured during the laboratory testing as shown in Figure 4.9 and Figure 4.10, where the silicone rubber insulator which exhibits the highest flow of leakage current has the lowest breakdown voltage.

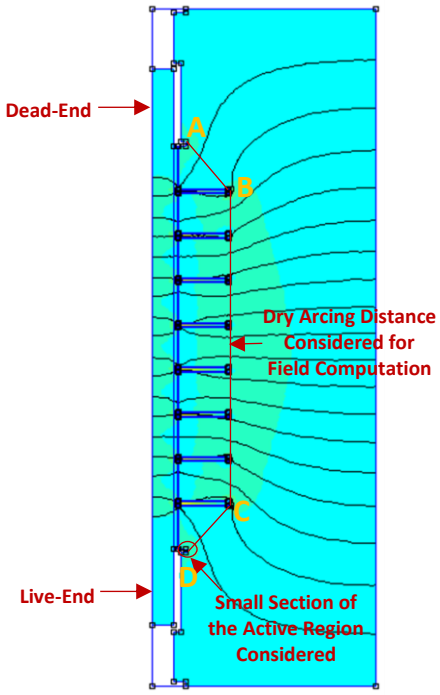

Figure 4.14: Annotated Model of Silicone Rubber Insulator.

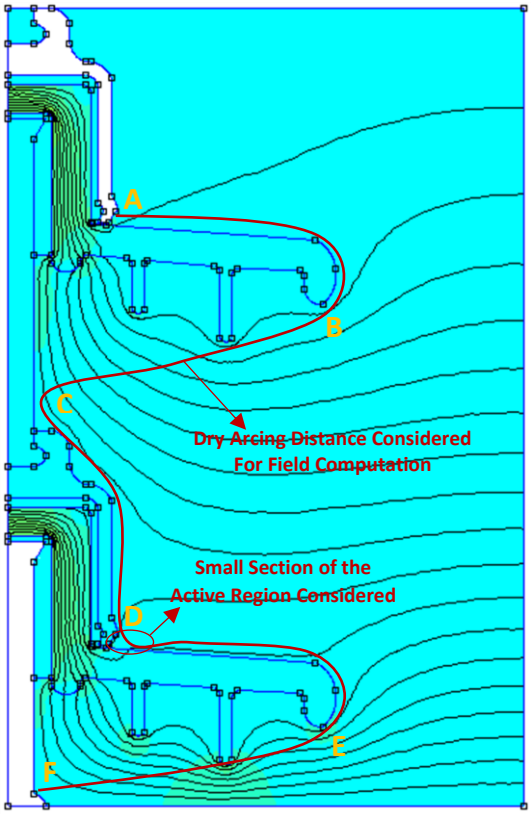

Figure 4.15: Annotated Model of Glass Cap-and-Pin Insulator.

Considering Figure 4.4 and Figure 4.5, which depicts the leakage current characteristics for silicone rubber and glass cap-and-pin insulators respectively under negative DC voltage. A knee point was observed as explained in the experimental results in *section 4.2*. The electric field distribution for both silicone rubber and glass insulator at the voltage at which the knee point occurred in the absence of corona source were taken and are shown in Figure 4.16 and Figure 4.17 respectively. For both insulator types, the field distribution were taken along the dry arcing distance as annotated in Figure 4.14 and Figure 4.15 and as expected, they were discovered to be non-uniform. Dry arcing distance is the shortest distance in air along the surface of the insulator sheds. Areas with low magnitude of field strength are lower than the ionization level while areas with high magnitude field strength are said to be the ionization region, where free electrons exist [40]. These high field regions can also be called active regions.

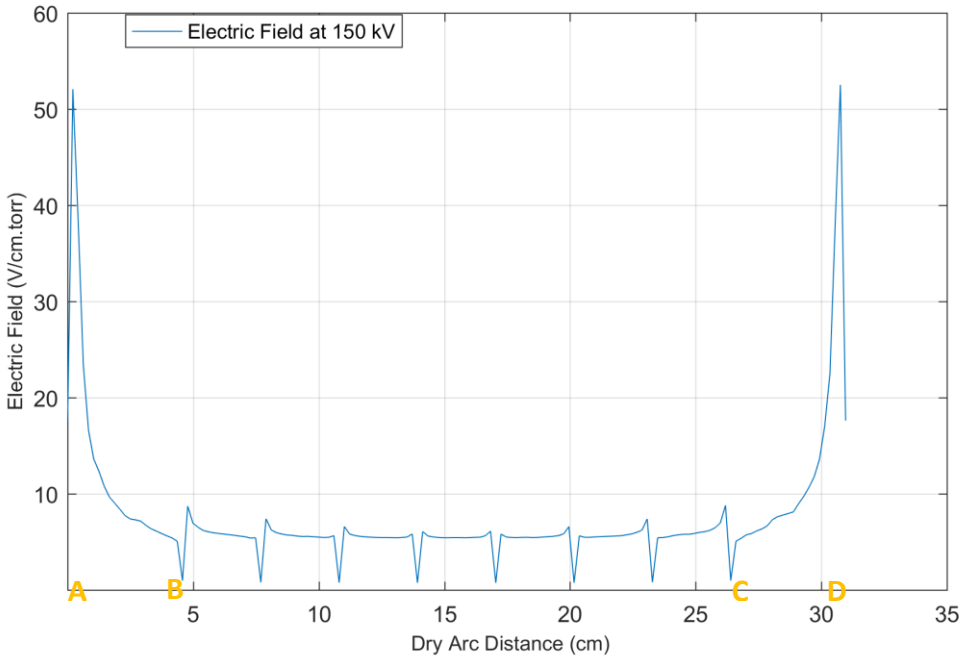

Figure 4.16: Electric Field Distribution along the Dry Arcing Distance for Silicone Rubber Insulator at 150 kV (Knee Point).

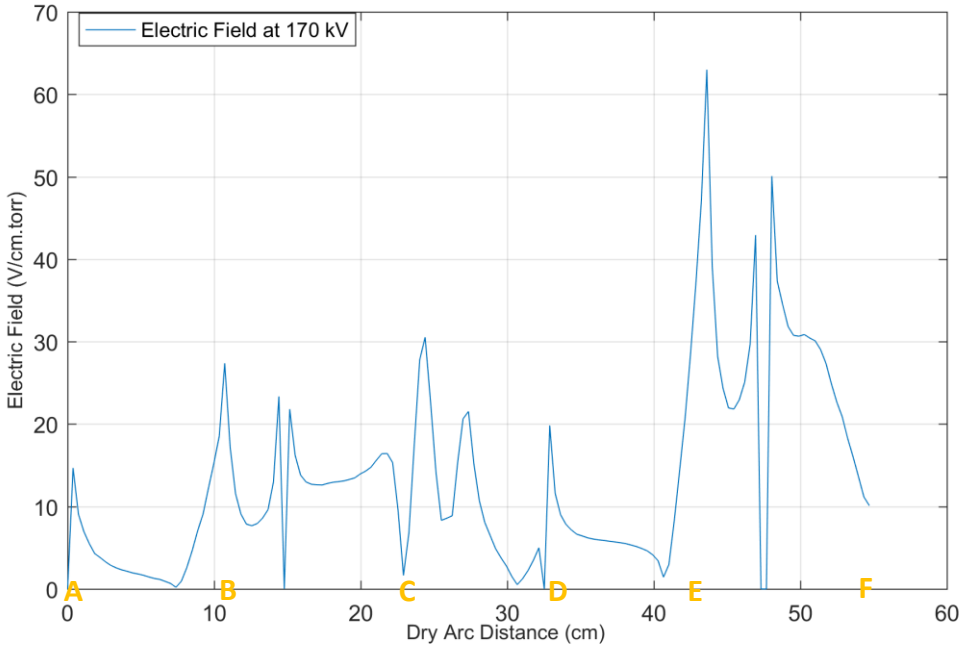

Figure 4.17: Electric Field Distribution along the Dry Arcing Distance for Glass cap-and-pin Insulator at 170 kV (Knee Point).

The effective ionization coefficient, $(\alpha - \eta)$, at this knee point voltages were computed from the electric field distribution obtained from the simulation for both insulator types as discussed in

section 3.5. The process of direct ionization of molecules by electrons and dissociative electron attachment to oxygen molecules were considered in determining the effective ionization coefficient, all other processes involved in charge generation and elimination such as photoionization, detachment, etc., were not considered. Standard atmospheric temperature of 25 ^{0}C and pressure of 760 torr were also assumed.

As seen from the experimental results shown in Figure 4.4, the knee point occurred at 150 kV in the absence of corona sources for the silicone rubber insulator. A small section of the active region at the live-end of the insulator, as shown in Figure 4.14, was selected and considered, this is due to the non-uniformity of the electric field along the whole dry arcing distance. During the experiment, the dry arcing distance for the silicone rubber insulator was observed to be arcing along the shortest path in air along the insulator from *A* to *D* as shown in Figure 4.14. Also at the knee point voltage, the integration of the effective ionization coefficient along this small section of the active region was computed by using trapezoidal integration rule. The results of the effective ionization coefficients are shown in Figure 4.18 while Figure 4.19 shows the cumulative integration of the coefficients along the active region considered.

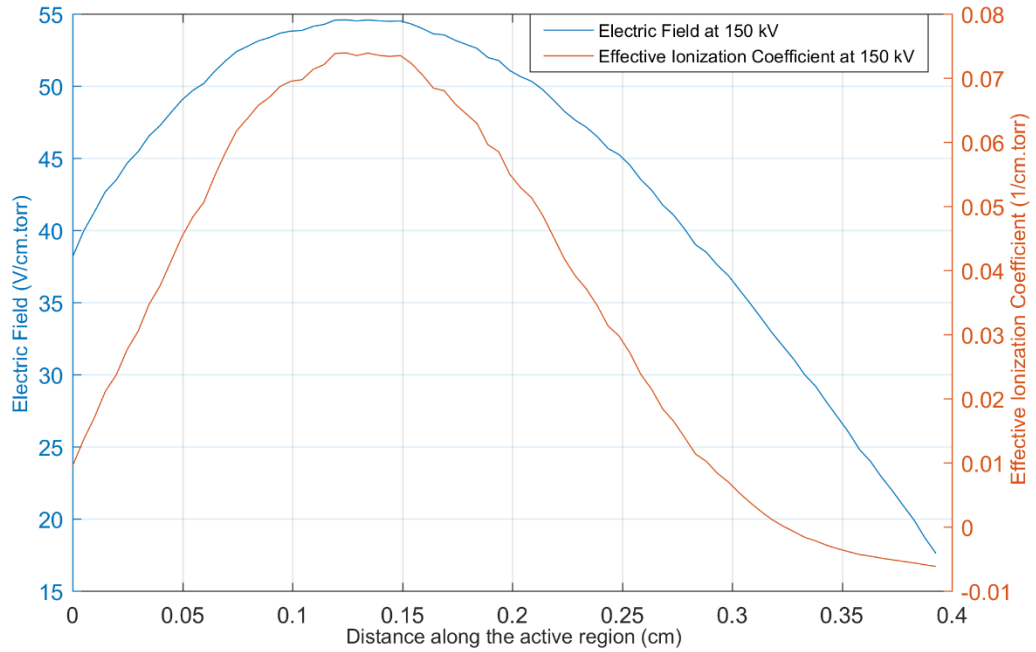

Figure 4.18: Effective Ionization Coefficient and Electric Field along the Active Region at 150 kV for Silicone Rubber Insulator.

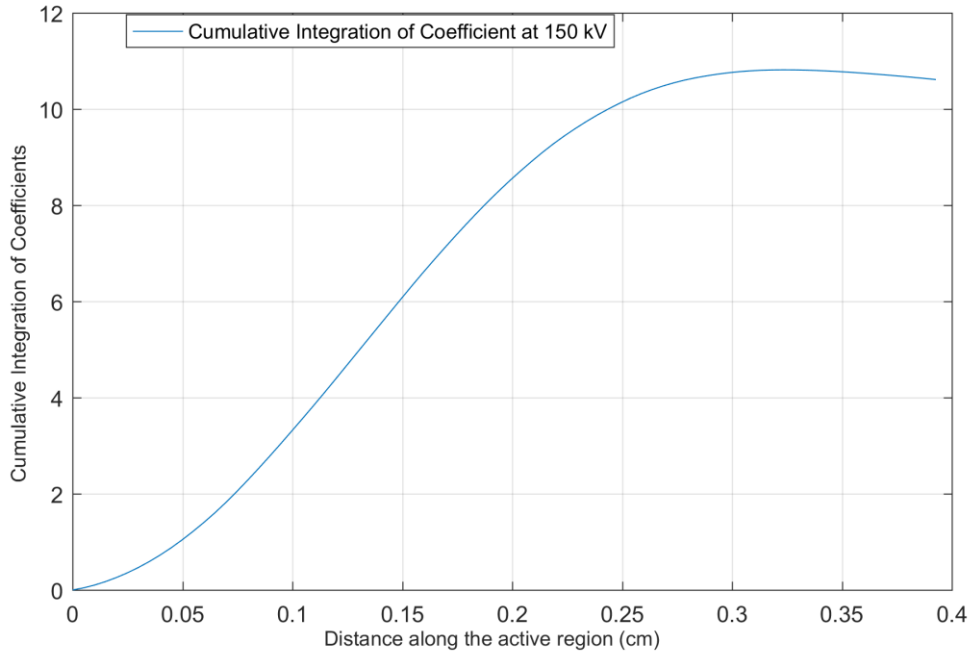

Figure 4.19: Effective Ionization Coefficient along the Active Region at 150 kV for Silicone Rubber Insulator.

It can be observed from the simulation results shown in Figure 4.16 that the electric field strength at both the dead-end and live-end of the insulator are symmetric, i.e. the field strengths are of the same magnitude and they exceed the ionization threshold of air, 30 kV/cm [41] which is equivalent to 39.5 V/cm.torr. This is an indication of ionization taking place at the knee point voltage. It can also be observed from Figure 4.18 that the effective ionization coefficient, $(\alpha - \eta)$, computed along the active region considered at this knee point voltage are in the positive region and this clearly indicates that the rate of ionization,α, which increases the number of electrons, is higher than the rate of attachment, η, which decreases the number of electrons. Increase in the number of electrons ultimately leads to an increase in electric current flow. Furthermore, it can be observed in Figure 4.19 that the cumulative integral of the rate of effective ionization coefficient is computed to be: K = 10.6 at the knee point voltage. This integration of coefficient as explained in *section 2.8.2* is applicable to the calculation of discharge inception voltage which can be linked to the knee point voltage and it was found to be within the typical range of discharge inception: 9.15-18, specified in [47].

In the case of the glass insulator, it was observed that the electric field distribution along the dry arc distance is not as symmetric as that of the silicone rubber insulator, this can be seen in Figure 4.17. The complexity of this field distribution made it difficult to interpret the same way as that of the silicone rubber. However, during the experimental tests, it was observed that the arcing distance included the surface of the two glass sheds. The dry arcing distance for the glass insulator was observed to be arcing along the shortest path from *A* to *C* and *D* to *F* as annotated in Figure

4.15. Some critical areas were also noticed on the glass insulators, such as areas around either the cap or the pin, these are areas where the arcing started before the breakdown as observed during the experimental test carried out at the laboratory. Thus, a small area around the cap of the glass disc close to the energized electrode, as shown in Figure 4.15, was selected and taken as the active region. As seen from the experimental result shown in Figure 4.5, the knee point voltage in the absence of corona sources was not clearly distinct as that of the silicone rubber, so the voltage was increased gradually during the simulation until ionization became greater than attachment along the chosen active region. This occurred at 170 kV, Figure 4.20 shows the electric field distribution along this active region which was obtained from the simulation results and used for the computation of the effective ionization coefficient. It can be observed from the result that the maximum electric field strength at this knee point voltage was discovered to be more than the ionization threshold of air. This clearly depicts ionization occurrence at this voltage.

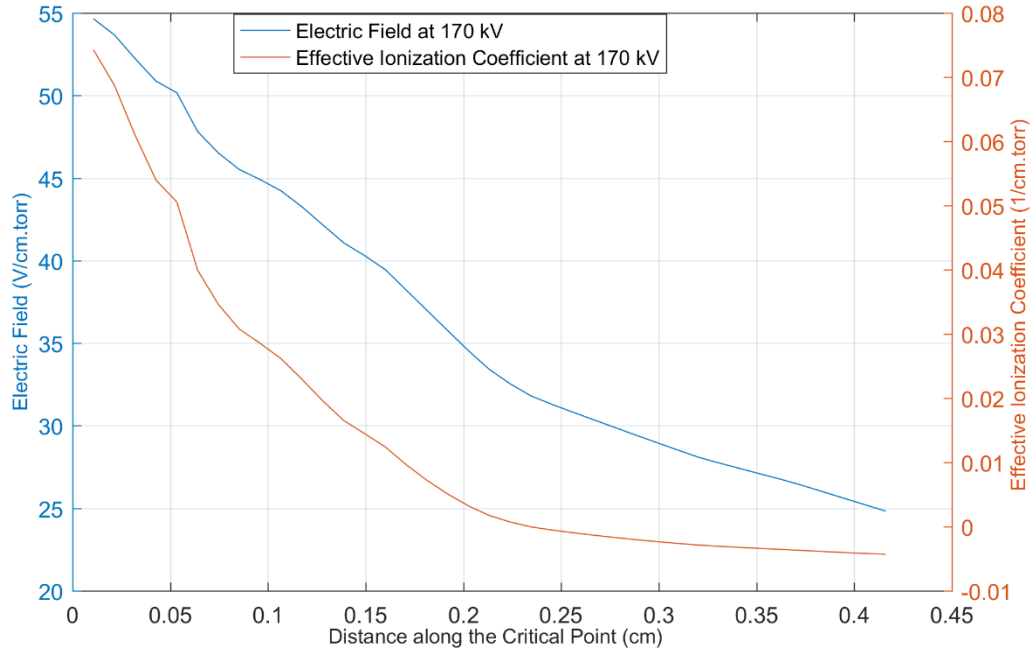

Figure 4.20: Calculated Effective Ionization Coefficient and Electric Field along the Active Region at 170 kV for Glass cap-and-pin Insulator.

It can be deduced that the rate at which electrons are generated at these knee point voltages for both insulator types are higher than the rate at which they are been eliminated, leading to an exponential growth of ions and electron concentration. This ultimately result to the exponential rate of current increase as seen in the experimental results. As the electric field increases due to an increase in applied voltage, electrons are accelerated more and more between collisions until they gain enough energy to cause ionization on collisions with air molecules or atoms. The voltage

at which this knee points occurred can be liken to be the starting point voltage at which ionization dominates to start-up the breakdown process.

As seen in the experimental results, the knee point voltage occurred at a lower voltage for cases of different configuration of the corona sources, this is because the presence of the corona sources have altered the conductivity of the air surrounding the insulator by adding more charge species which creates ionization quickly when the voltage is applied. The electrons ionize the neutral atoms and molecules on collision, producing more electrons. These additional electrons are accelerated to ionize even more atoms, producing even more free electrons in an avalanche build-up process. This led to the increased current in the presence of the corona source as against the low current in the absence of the corona source.

Presently there are no specific standards for DC insulators. The breakdown voltages obtained from this investigation for AC are higher than the standard minimum withstand voltages reported by IEC 60071[89]. The impulse basic insulation level (BIL) were calculated and shown in *Appendix A*, the calculated BIL was also higher than the standard minimum BIL reported by [88] which are shown in *Appendix B*. The results obtained from this research investigation have revealed that insulators operating under HVDC stress exhibit a high leakage current due to the presence of surface charges, hence the need to increase the surface resistance of HVDC insulators. It can be proposed from this research investigation that the creepage distance of insulators operating under DC high voltage can be increased more than their equivalent under AC, this will increase their surface resistance and reduce the leakage current. This will also reduce the electric field strength along the insulator surface, reduce the breakdown rate and ultimately lead to a higher withstand voltage for HVDC insulators. Finally, it can be proposed from this research investigations that with the present increase in the operating voltage of HVDC transmission system, it will be economical and safer to increase the creepage distance of silicone rubber insulators than that of glass cap-and-pin insulators due to their advantage of light-weight. The higher the operating transmission voltage, the bigger the number of glass units attached and this will make glass cap-and-pin insulators heavier for higher transmission line voltages.

CHAPTER 5
CONCLUSION

5.1 Conclusion

In this research investigation, both experimental work and mathematical simulations have been carried out to investigate the performance of insulators under AC, impulse and HVDC stress. More emphases have been placed on the insulator's performance under HVDC considering their leakage current and breakdown voltage characteristics due to the importance of DC voltage and the challenging space charge effect associated with it. This research investigation has resulted in the following conclusions:

1. The breakdown voltages under all voltage types were found to be affected by environmental conditions, being decreased during wet conditions.
2. The impulse breakdown voltages were higher than both AC and DC breakdown voltages, with AC having the lowest breakdown voltage.
3. The dielectric strength of the insulators was found to be higher under negative DC when compared to positive polarity as a result of charge distribution.
4. The breakdown voltages of the insulators under DC voltage was found to be affected by the presence of surface charges, which increases the leakage current along the insulator surface. Hence the need to increase the surface resistance of DC insulators through an increase in leakage distance.
5. The insulator material type plays a vital role in DC insulation system.
6. The electric field distribution was proved to be purely resistive and distorted due to the effect of space charges.
7. The experimental results, which was also validated by the simulation results of the electric field distribution, revealed the dependency of breakdown voltage on ionization process. Hence the reason for the increased leakage current in the presence of charges around the insulators under DC applied voltage.

In conclusion, an increase in conductivity not only results in an increase in current but also alters the electric field, as shown in the simulation results. As the breakdown of air is dependent on the electric field and it is important that the influence of the space and surface charges on both the breakdown voltage and electric field of the insulator be considered in specifying insulators for HVDC.

5.2 Recommendation for Future Work.

As a continuation of the work presented in this dissertation, improved experimental studies related to the effect of charges on the breakdown performance of insulators can be carried out. This can involve the development of a better charging method which would make charge deposition controllable, characterization of the dynamics of space charges on the surface of HVDC insulators and accurate quantification of surface charges. It has been proposed in this research investigation that the creepage distance of DC insulators need to be increased, silicone rubber insulators with different creepage distance can be considered for testing so as to know the extent of the increase. For comparison of the influence of insulator material composition on the results presented, dry and wet tests under the application of AC, DC and standard impulse voltages can also be carried out on another type of insulators. The type used under this section in this research investigation was the silicone rubber type of insulator.

Finally, the continuation of this work would assist in developing appropriate standards for testing HVDC insulators. It is believed that this research investigation would present a considerable reference point for its continuation.

REFERENCES

[1] R. Krishna, "Reactive power control in HVDC transmission system" [electrical stuffBlogspot], retrieved from http://electricala2z.blogspot.com/2011/06/reactive-power-control-inhvdc.html?m=1/. Last accessed November 25, 2015.

[2] N. Mahatho, N. Parus and T. Govender, "An Investigation into the effect of Shattered Glass Discs on Insulation Strength under HVDC Voltage Stress," *IEEE Transaction on Dielectrics and Electrical Insulation*, Vol. 23, No. 4, pp.2181-2188, August 2016.

[3] O. A. Lasabi, A. G. Swanson and I. E. Davidson, "Surface charge accumulation on DC insulators: an overview", *25th Southern African Universities Power Engineering Conference*, Vol. 1, pp. 38-43, January 2017.

[4] A. Winter and J. Kindersberger, "Stationary Resistive Field Distribution along Epoxy Resin Insulators in Air under DC Voltage," *IEEE Trans. Dielectr. And Electr. Insul.* , Vol. 19, No.5, pp. 1732-1739, 2012.

[5] "The Authoritative Dictionary of IEEE Standards Terms, Seventh Edition", *IEEE Std 100-2000*, pp. 1-1362, 2000.

[6] S. M. Gubanski, "Modern outdoor insulation - concerns and challenges", *IEEE Electrical Insulation Magazine*, vol. 21, pp. 5-11, 2005.

[7] B. Lutz and J. Kindersberger, "Surface charge accumulation on cylindrical polymeric model insulators in air: simulation and measurement", *IEEE Transactions on Dielectrics and Electrical Insulation*, vol. 18, No. 6, pp 2040-2048, 2011.

[8] Zhou P. B., Numerical Analysis of Electromagnetic Fields. Spinger-Verlag, Berlin, ISBN 0387547223, 1993.

[9] R. S. Gorur, E. A. Cherney and J. T. Burnham, Outdoor insulators, Ravi S. Gorur Inc, Phoenix, Arizona, USA, 1999.

[10] H. EI-Kishky and R. S. Gorur, "Electric potential and field computation along AC HV insulators", *IEEE Trans. Dielectrics and Electrical Insulation*, vol. 1, pp. 982-990, December 1994.

[11] H. EI-Kishky and R. S. Gorur, "Electric field computation on an insulating surface with discrete water droplets," *IEEE Trans. Dielectrics and Electrical Insulation*, vol. 3, pp. 450-456, June. 1996.

[12] M. Roman, R. R. van Zyl, N. Parus and N. Mahatho, "Insulator leakage current monitoring: Challenges for high voltage direct current transmission lines," *2014 International Conference on the Eleventh industrial and Commercial Use of Energy*, Cape Town, pp. 1-7, August 2014.

[13] T. Sorquist and A. E. Vlastos, “Outdoor polymeric insulators long-term exposed to HVDC,” *Proceedings of 1996 Transmission and Distribution Conference and Exposition, Los Angeles, CA*, 1996, pp. 135-142, September 1996.

[14] E. A. Cherney, “Nonceramic Insulators- A simple design that requires careful analysis”, *Electrical Insulation Magazine*, vol. 12, No.3, pp. 7-15, May/June 1996.

[15] E. A. Cherney, “Nonceramic insulator Technology for overhead lines- a state-of-the-art review”, EACH Engineering Inc. Report, 1995.

[16] L. A. Dissado and I. C. Fothergill, “Electrical degradation and breakdown in polymers”, Peregrinus Ltd, 1992.

[17] G. C. Montanari, “Bringing an insulation to failure: the role of space charge”, *IEEE Trans. Diel. Elec. Insul.*, vol. 18, no. 2, pp. 339-364, 2011.

[18] R. Hackam, “Outdoor high voltage polymeric insulators”, *Proc. IEEE Int. Symp. Elec. Insul.*, Toyohashi, pp. 1-6, 1998.

[19] A. Salama and M. Arief, “The performance of silicone rubber for HV insulators under natural tropical aging”, *IEEE Int. Conf. Solid, Diel.*, pp. 304-307, 2004.

[20] V. M. Moreno and R. S. Gorur, “Accelerated corona discharge performance of polymer compounds used in high voltage outdoor insulators”, *Annual Report IEEE Conf. Elec. Insul. Diel. Phenomena*, pp. 731-734, 1999.

[21] WL Vosloo, RE Macey, C de Tourreil, The Practical Guide to Outdoor High Voltage Insulators, Crown Publications CC., Johannesburg, 2004.

[22] Electra No.143, Guide for the identification of brittle fracture of composite insulator FRP rod, August 1992.

[23] E. Kuffel, W.S. Zaengl, and J. Kuffel, High Voltage Engineering: Fundamentals, Second Edition, Burlington, MA, Newsnes 2000.

[24] International Standard IEC 60587, Electrical insulating materials used under severe ambient conditions – Test methods for evaluating resistance to tracking and erosion, Third edition 2007.

[25] M Amin, and M Salman, Ageing of Polymeric Insulators (An Overview), *Reviews on Advanced Material Science*, Vol. 13, pp. 93-116, November 2006.

[26] R. S. Gorur, L. A. Johnson and H. C. Hervig, Contamination performance of Silicone Rubber Cable Terminations, *IEEE Transactions on Power Delivery*, Vol. 6, No. 4, page 1366 – 1370, 1991.

[27] S. H. Kim, E. A. Cherney and R. Hackman, The Loss and Recovery of Hydrophobicity of RTV Silicone Rubber Insulator Coatings, *IEEE Transactions on Power Delivery*, Vol. 5, No. 3, page 1491 – 1499, 1990.

[28] J. P. Reynders, I. R. Jandrell and S. M. Reynders, “Review of Aging and Recovery of Silicone Rubber Insulation for Outdoor Use”, *IEEE Trans.on DEI*, vol. 6, no. 5, pp. 620-631, 1999.

[29] J. Kindersberger, A. Schultz, H. C. Kärner and R. van de Huir, Service Performance, Material Design and Applications of Composite Insulators with Silicone Rubber Housings, *Cigré Session 1996*, page 33 – 303, 1996.

[30] A. Tomanek, Silicones & Industry: A compendium for practical use, instruction and reference, Wacker-Chemie GmbH, Munich, 1991.

[31] R. S. Gorur, G. G. Karady, A. Jagota, M. Shah and A. M. Yates, Ageing of Silicone Rubber used for Outdoor Insulation, *IEEE Transactions on Power Delivery*, Vol. 7, No. 2, page 525 – 538, 1992.

[32] R. Barsch, J. Lambrecht and H. J. Winter, On the Evaluation of Influences on the Hydrophobicity of Silicone Rubber Surfaces, *ISH Conference, 1997, Montréal*, pp 13 – 16, 1997.

[33] L.H. Meyer, S. H. Jayaram, E. A. Cherney, Correlation of Damage, Dry Band Arcing Energy, and Temperature in Inclined Plane Testing of Silicone Rubber for Outdoor Insulation, *IEEE Transactions on Dielectrics and Electrical Insulation*, Vol. 11, No.3, page 424 – 432, 2004.

[34] H. Janssen, A. Herden and H. C. Kärner, The Loss and Recovery of Hydrophobicity on Silicone Rubber Surfaces, *ISH Conference, 1997, Montreal*, page 145 – 148, 1997.

[35] M. Amin, M. Amin and M. Ali, “Monitoring of Leakage Current for Composite Insulators and Electrical Devices” *Rev. Adv. Material Science*, vol. 21, pp. 75-89. 2009.

[36] A. S. Krzma, M. Albano and A. Haddad, “Comparative performance of 11 kV silicone rubber insulators using artificial pollution tests,” *2015 50th International Universities Power Engineering Conference (UPEC), Stoke on Trent*, pp. 1-6. September 2015.

[37] T. Sorquist and A. E. Vlastos, “Outdoor Ageing of Silicone Rubber Based Polymeric Materials”, *IEEE International Conference on Conduction and Breakdown in Solid Dielectrics*, Sweden, pp. 401-405, June 1998.

[38] W. L. Vosloo and J. P. Holzhausen, “A comparison of glass cap-and-pin, silicone rubber and EPDM rubber insulators over a four day period at Koeberg Insulator Pollution Test Station,” *1999 IEEE Africon. 5th Africon Conference in Africa (Cat. No.99CH36342), Cape Town*, vol. 2, pp. 743-748, October 1999.

[39] N.A. Othman, M.A.M. Piah, Z. Adzis, H. Ahmad, N.A. Ahmad, H. Kamarden and A.A. Suleiman, “Characterization of charge distribution on the high voltage glass insulator string” *Journal of Electrostatics*, vol. 72, pp 315-321, June 2014.

[40] S. Kumara, “Electrical charges on polymeric insulator surfaces and their impact on withstand performance”, PhD thesis, Chalmers University of Technology, Gothenburg, Sweden, 2012.

[41] S. Kumara, S. Alam, I. R. Houqe, Y. V. Serdyuk and S. M. Gubanski, “DC Flashover Characteristics of a Polymeric Insulator in Presence of Surface Charges”, *IEEE Trans. Diel. Elec. Insul.*, vol. 19, no. 3, pp. 1084-1090, March 2012.

[42] F. Wang, Q. Zhang, Y. Qiu and E. Kuffel, “Insulator surface charge accumulation under DC voltage”, *Proc. IEEE Int. Symp. Elec. Insul.*, pp. 426 – 429, 2002.

[43] J. A. Giacometti, and O. N. Jr. Oliveira, “Corona charging of polymers”, *IEEE Trans. Elec. Insul.*, vol. 27, no. 5, pp. 924-943, 1992.

[44] Y. V. Serdyuk, “Numerical simulations of non-thermal electrical discharges in air, lightning electromagnetics”, *IET Power and Energy: The Institution of Engineering and Technology; 1st Edition*, pp. 87-138, 2012.

[45] Y. P. Raizer, “Gas Discharge physics”, Springer Verlag, 1997.

[46] J. M. Meek and J. D. Craggs, Electrical Breakdown of Gases, Wiley Series in Plasma Physics, John Wiley & Sons, Ltd, 1978.

[47] K. Petcharaks and W. S. Zaengl, “Numerical calculation of breakdown voltages of standard air gaps (IEC 52) based on streamer breakdown criteria,” *Proc. 9th Int. Symp. High Volt. Eng. (ISH 95)*, paper 2173, Graz, Austria, 1995.

[48] J. Blennow and T. Sörqvist, “Effect of Surface charge on the flashover voltage of polymeric material”, *Proc. of the 19th Nordic Insulation Symposium*, 2005.

[49] R. Montano, H. Sjostedt, Y. Serdyuk, and S. Gubanski, “Effect of surface charges on the flashover voltage characteristics of polymeric materials: comparison between theory and practice”, *Annual Report Conference on Electrical Insulation and Dielectric Phenomena*, pp. 368-371, 2007.

[50] I.J.Seo, J.Y.Koo, J.K.Seong, B.W.Lee, Y.J.Jeon and C.H.Lee, “Experimental Investigation on the DC Breakdown of Silicone Polymer Composites Employable to 500kV HVDC Insulator”, *1st International Conference on Electric Power Equipment and Switching Technology*, pp 697-700, 2011.

[51] M.S.A.A. Hammam, S. Ochiai and C. Burns: “Effect on 50% flashover voltage due to accumulated charges on the surface of polymer insulators”, *Prop and Appl. Diel. Materials*, pp. 981-984, July 1991.

[52] X. Jun and I. D. Chalmers: "The Influence of Surface Charge upon Flash-Over of Particle–Contaminated Insulators in SF6 under Impulse Voltage Conditions", *Journal of Physics: Applied Physics*, vol. 30, no 7, pp. 1055-1063, January 1999.

[53] M.M. Semere: Charges on polymeric insulators and their effect on flashover characteristics, Master Thesis, Chalmers University of Technology, SE-41296 Göteborg, Sweden, 2011.

[54] B. Qi, C. Gao, C. Li, L. Zhao and X. Sun: "Effect of surface charge accumulation on flashover voltage of GIS insulator in SF6 under DC and AC voltages", *In Electrical Insulation and Dielectric Phenomena (CEIDP), IEEE Conference on*, pp. 848-851, October 2015.

[55] K. Kato, H. Kato, T. Ishida, H. Okubo and K. Tsuchiya: "Influence of surface charges on impulse flashover characteristics of alumina dielectrics in vacuum." *IEEE Transactions on Dielectrics and Electrical Insulation*, vol. 16, no 6, pp.1710-1716, December 2009.

[56] W. McDermid and T. Black, "Experience with preventing external flashovers in HVDC converter stations", *IEEE Int'l. Sympos. Electr. Insul., Vancouver, BC, Canada*, pp. 81-84, 2008.

[57] J. Ndoumbe, A. Beronal and A.M. Imano, "Behavior of water droplets on insulator surfaces submitted to DC voltage-coalescence", *IEEE Conf. Electr. Insul. Dielectr. Phenomena, Montreal QC, CA*, pp. 725-728, 2012.

[58] I.J.S. Lopes, S.H. Jayaram and E.A. Cherney, "A study of partial discharges from water droplets on a silicone rubber insulating surface", *IEEE Trans. Dielectr. Electr. Insul.*, Vol. 8, No. 2, pp. 262-268, 2001.

[59] A.C. Baker, L.E. Zaffanella, L.D. Anaivino, H.M. Schneider and J.H. Moran, "A Comparison of HVAC and HVDC Contamination Performance of Station Post Insulators", *IEEE Power Eng. Review*, vol. 9, no.4, pp. 110-111, 1989.

[60] S. Wen-xia, M. A. Gao-quan and Y. Qing, "Flashover characteristics of flat model under DC voltage in wind-sand two-phase mixture", *International Conference on High Voltage Engineering and Application, Chongqing, China*, pp. 158-162, November 2008.

[61] T. C. Cheng and C. T. Wu, "Performance of HVDC insulators under contaminated conditions", *IEEE Transactions on Electrical Insulation*, vol. EI-15, no.3, June 1980.

[62] A. M. Farouk, "Mechanism of insulator flashover under artificial rain", *Proc. IEEE*, vol. 122, no. 4, pp 449-454, April 1975.

[63] I G. Karady, M. Shah and R. L. Brown, "Flashover mechanism of silicone rubber insulators used for outdoor insulation -I", *IEEE Transactions on Power Delivery*, vol.10. no. 4, pp. 1965-1971, October 1995.

[64] K. L. Chrzan, H. Schwarz, and H. Hausler, “Effect of impulse polarity on the flashover voltage of polluted cap-and-pin insulators”, *Proceedings on the 16th International Symposium on High Voltage Engineering*, pp 1-5, 2009.

[65] L. Paris and R. Cortina, “Switching and lightning impulse discharge characteristics of large air gaps and long Insulator Strings”, *IEEE Transactions on Power Apparatus and Systems*, vol. pas-87, no. 4, pp. 947-957, April 1968.

[66] C. Bayliss and B. Hardy, Transmission and Distribution Electrical Engineering 4th edition: Elsevier, ISBN 0080969135, 2011.

[67] M. Hering, T. Götz, J. Speck, S. Großmann and U. Riechert, “Influence of space charges on the field transition in gas-insulated DC systems”, *IEEE International Conference on Dielectrics (ICD)*, Vol. 1, pp. 38-41, July 2016.

[68] S. Qin, Y. Tu, C. Wang, F. Zhou, G. Ma and H. Zhou, “The influence of the insulator volume conductivity on charge accumulation in HVDC-GIL,” *In IEEE Electrical Insulation Conference (EIC)*, pp. 325-328, June 2016.

[69] J. h. Geng and B. y. Jia, “Research on the Influence of Surface Accumulation Charge on Flashover Voltage of Ceramic Insulator,” *2009 International Conference on Energy and Environment Technology, Guilin, Guangxi*, pp. 244-246, October 2009.

[70] C. Muniraj and S. Chandrasekar, “Finite Element Modeling For Electrical Field And Voltage Distribution Along The Polluted Polymeric Insulator”, *World Journal of Modelling and Simulation*, vol. 8, no. 4, pp. 310-320, March 2012.

[71] R. F. Kerendian, H.K Ziarani and J. Ebrahimi, “Effect of corona ring on potential distribution and electric field on silicone insulator in pollution condition”, *International Journal of Mechatronics, Electrical and Computer Technology*, vol. 4, no 12, pp. 1394-1403, July 2014.

[72] S. Chakravorti and H. Steinbigler, “Boundary-Element Studies on Insulator Shape and Electric Field around HV Insulators with or without Pollution”, *IEEE Transactions on Dielectrics and Electrical Insulation*, vol. 7, no. 2, pp. 169-176, April 2000.

[73] A. J. Phillips et al., “Electric Field on AC Composite Line Insulators”, *IEEE Transactions On Power Delivery*, vol. 23, no. 2, pp. 823-830, April 2008.

[74] S. Ilhan and A. Özdemir, “Effect of Corona Ring Design on Electric Field Intensity and Potential Distribution along an Insulator String,” *IEEE ELECO*, 2007.

[75] T. Zhao and M.G Comber, “Calculation of Electric Field and Potential Distribution Along Non-Ceramic Insulators Considering the Effects of Conductors and Transmission Towers,” *IEEE Transactions on Power Delivery*, vol. 15, no. 1, pp. 313-318, January 2000.

[76] S. Kaana-Nkusi, P.H. Alexander and R. Hackam, "Potential and Electric Field Distributions at a High Voltage Insulator Shed," *IEEE Transactions on Dielectrics and Electrical Insulation*, vol. 23, no. 2, pp. 307-318, April 1988.

[77] International Electro-technical Commission, High Voltage Test Techniques, Part 1: General Definitions and Test Requirements, IEC 60060-1.

[78] Finite Element Method Magnetics Version 4.2 User's Manual, October 2015.

[79] HVDC Test Set Instruction Manual, MWB India Limited, 2000.

[80] M. P. Sarma and W. Janischewskyj, "D.C. corona on smooth conductors in air. Steady-state analysis of the ionisation layer," *in Electrical Engineers, Proceedings of the Institution of*, vol. 116, no. 1, pp. 161-166, January 1969.

[81] L. Shu, Y. Shang, X. Jiang, Q. Hu, Q. Yuan, J. Hu, Z. Zhang, S. Zhang and T. Li, "Comparison Between AC and DC Flashover Performance and Discharge Process of Ice-Covered Insulators under the Conditions of Low Air Pressure and Pollution," *IET Gener. Transm. Distrib.*, vol. 6, no. 9, pp. 884–892, October 2012.

[82] X. Jiang, M. Bi, Z. Zhang, J. Hu and Y. Yuan, "Study on the Influence of Test Methods on AC and DC Pollution Flashover Performance of Different UHV Insulators," *Przeglad Elektrotechniczny*, vol. 89, no. 3, pp. 166-170, January 2013.

[83] J. Alles, A. Beroual, J. M. George and E. Brocard, "Evaluation of Electrical Performance on High Voltage Glass Suspended Insulators," *IEEE Electrical Insulation Conference (EIC), Baltimore, MD, USA*, pp. 252-255, June 2017.

[84] A. Waygood, An Introduction to Electrical Science, Taylor & Francis, 2013.

[85] W. Waluyo, P. M. Pakpahan and S. Suwarno, "Study on the Electrical Equivalent Circuit Models of Polluted Outdoor Insulators," *2006 IEEE 8th International Conference on Properties and Applications of Dielectric Materials, Bali*, pp. 546-549, June 2006.

[86] N. Sumathi and V. Jeeri, "Evaluation of Electrical Properties of 11 kV Pin and Suspension Insulator," *International Research Journal of Engineering and Technology (IRJET)*, vol. 2, no. 6, pp. 1052-1058, September 2015.

[87] M. H. Samimi, A. H. Mostajabi, I. Ahmadi-Joneidi, A. A. Shayegani-Akmal and H. Mohseni, "Performance Evaluation of Insulators Using Flashover Voltage and Leakage Current," *Electric Power Components and Systems*, vol. 41, no. 2, pp. 221-233, January 2013.

[88] S. Chakravorti and P.K. Mukherjee, "Power frequency and impulse field calculation around a HV insulator with uniform or non-uniform surface pollution", *IEEE Transactions on Electrical Insulation*, Vol. 28, No. 1, pp. 43–53, 1993.

[89] International Electro-technical Commission, Insulation Co-ordination — Part 1: Definitions, Principles and Rules, IEC 60071-1:2006.

APPENDIX A

Table A1: Average Breakdown Voltage Results.

TEST VOLTAGE	DRY (kV)		WET (kV)	
	POSITIVE	**NEGATIVE**	**POSITIVE**	**NEGATIVE**
DC	193	223	187	198
IMPULSE	321	309	272	219
AC (RMS)	135		114	
AC (PEAK)	191		161	

Table A2: Leakage Current Results for Both Insulators under AC Voltage.

Applied Voltage (kV)	Current for Glass (mA)	Applied Voltage (kV)	Current for SIR (mA)
20.8	0.267857	19.6	0.019161
30	0.330357	30	0.025232
40	0.405357	40	0.030304
50	0.498214	50	0.036982
60	0.594643	60	0.044161
70	0.691071	70	0.052179
80	0.794643	80	0.061661
90	0.985714	90	0.073643
100	1.285714	100	0.091161
110	1.455357	110	0.125
120	1.660714	120	0.178571

Table A3: Results of Silicone Rubber insulator Under Negative DC Voltage.

No corona source		**Corona source at dead-end**		**Corona source at live-end**		**Corona source at both ends**	
Applied Voltage (kV)	**Current (µA)**	**Applied Voltage (kV)**	**Current (µA)**	**Applied Voltage (kV)**	**Current (µA)**	**Applied Voltage (kV)**	**Current (µA)**
5	0.002054	5	0.000357	5	0.000893	5	0.001964
10	0.002054	10	0.002679	10	0.000893	10	0.001964
20	0.002054	20	0.169643	20	0.000893	20	0.125
30	0.0025	30	0.875	30	0.004464	30	6.160714
40	0.004643	40	1.901786	40	0.25	40	15.89286
50	0.010714	50	3.857143	50	6.25	50	29.91071
60	0.25	60	12.32143	60	21.33929	60	42.67857
70	0.669643	70	28.30357	70	40.80357	70	68.39286
80	1.785714	80	42.76786	80	57.94643	80	86.60714
90	2.410714	90	50.96429	90	72.32143	90	106.25
100	4.196429	100	69.71429	100	93.75	100	133.0357
110	7.053571	110	92.85714	110	118.75	110	168.75
120	9.285714	120	116.0714	120	149.1071	120	205.3571
130	12.32143	130	147.3214	130	184.8214	130	249.1071
140	16.60714	140	177.6786	140	230.3571	140	300
150	27.67857	150	219.2857	150	266.9643	150	338.3929
160	57.14286	160	264.6429	160	309.8214	160	388.3929
170	116.0714	170	315.1071	170	383.3929	170	444.6429
180	166.9643	180	360.5714	180	447.3214	180	496.4286
190	214.2857	190	430.7143	190	516.0714	190	566.9643
200	267.8571	200	490.6756	200	570.55	195	610.7143
210	310.567	205	512.6543	202	Flashover	198	Flashover
212	Flashover	207	Flashover				

Table A4: Results of Glass Cap-and-Pin insulator Under Negative DC Voltage.

No corona source		**Corona source at dead-end**		**Corona source at live-end**		**Corona source at both ends**	
Applied Voltage (kV)	**Current (µA)**	**Applied Voltage (kV)**	**Current (µA)**	**Applied Voltage (kV)**	**Current (µA)**	**Applied Voltage (kV)**	**Current (µA)**
5	0.017143	5	0.065893	5	0.048661	5	0.00875
10	0.031696	10	0.126429	10	0.119643	10	0.017768
20	0.066964	20	0.223214	20	0.348214	20	0.03125
30	0.104464	30	0.310714	30	1.035714	30	0.223214
40	0.116071	40	0.366071	40	2.321429	40	3.571429
50	0.182143	50	0.482143	50	3.571429	50	9.285714
60	0.232143	60	0.571429	60	6.071429	60	15.26786
70	0.271429	70	0.946429	70	7.946429	70	22.05357
80	0.401786	80	1.857143	80	12.76786	80	31.25
90	1.071429	90	4.294643	90	15.80357	90	42.41071
100	2.232143	100	6.964286	100	22.67857	100	56.25
110	3.75	120	12.76786	110	29.10714	110	69.64286
120	4.821429	130	17.41071	120	39.01786	120	82.14286
130	6.964286	140	21.51786	130	48.30357	130	100.8929
140	7.767857	150	28.57143	140	58.75	140	120.5357
150	8.571429	170	42.58929	150	66.07143	150	137.5
160	10.53571	180	50.08929	160	77.67857	160	160.7143
170	18.57143	190	57.58929	170	88.39286	170	179.4643
180	21.42857	200	65.71429	180	104.4643	180	200
190	22.76786	230	101.7857	190	123.2143	190	241.0714
200	25.625	240	139.2857	200	136.6071	200	289.2857
210	30.17857	250	203.5714	210	162.5	210	330.3571
220	34.01786	260	279.4643	220	186.6071	220	383.9286
230	39.28571	265	Flashover	240	270	230	416.0714
240	64.28571			250	315.3571	240	466.0714
250	76.78571			256	Flashover	250	518.75
260	130.3571					252	Flashover
270	Flashover						

Table A5: Results of Silicone Rubber insulator Under Positive DC Voltage.

No corona source		**Corona source at dead-end**		**Corona source at live-end**		**Corona source at both ends**	
Applied Voltage (kV)	**Current (µA)**	**Applied Voltage (kV)**	**Current (µA)**	**Applied Voltage (kV)**	**Current (µA)**	**Applied Voltage (kV)**	**Current (µA)**
5	0.000075	5	0.000089	5	0.000893	5	0.001071
10	0.000107	10	0.000125	10	0.00125	10	0.002143
20	0.000143	20	0.001071	20	0.001964	20	5.01875
30	0.000804	30	0.012411	30	3.633929	30	16.12
40	0.0025	40	3.741071	40	15.89286	40	38.39286
50	0.084286	50	6.839286	50	40.17857	50	62.14286
60	0.307768	60	19.67857	60	60.71429	60	83.21429
70	0.710714	70	30.53571	70	83.92857	70	119
80	2.258909	80	50.53571	80	93.75	80	133.9286
90	4.678571	90	65.53571	90	133.9286	90	159.8214
100	10.39286	100	85.28571	100	163.3929	100	191.9643
110	17.85714	110	125.2857	110	200.8929	110	231.25
120	58.03571	120	169.6429	120	249.1071	120	286.9643
130	111.6071	130	209.5357	130	294.6429	130	324.1071
140	162.5	140	275.5357	140	338.3929	140	379.4643
150	223.2143	150	329.2857	150	392.8571	150	433.0357
160	276.7857	160	380.8214	160	446.4286	160	500
170	330.3571	170	455.3571	170	526.7857	170	565.1786
180	375	180	490.6739	180	571.4286	180	620.7143
190	406.4286	190	532.9803	190	Flashover	185	Flashover
195	466.4286	195	Flashover				
198	Flashover						

Table A6: Results of Glass Cap-and-Pin insulator Under Positive DC Voltage

.

No corona source		Corona source at dead-end		Corona source at live-end		Corona source at both ends	
Applied Voltage (kV)	**Current (μA)**	**Applied Voltage (kV)**	**Current (μA)**	**Applied Voltage (kV)**	**Current (μA)**	**Applied Voltage (kV)**	**Current (μA)**
5	0.151786	5	0.178571	5	0.5	5	0.042857
10	0.348214	10	0.392857	10	2.5	10	5.292679
20	0.482143	20	0.625	20	3.232143	20	9.785714
30	0.607143	30	1.392857	30	6.642857	30	16.44643
40	0.75	40	2.410714	40	10.25	40	27.05357
50	1	50	4.642857	50	20.75	50	39.91071
60	1.232143	60	7.5	60	34.19643	60	59.05357
70	1.303571	70	10.71429	70	45.98214	70	76.78571
80	1.589286	80	13.21429	80	63.92857	80	94.64286
90	1.642857	90	17.76786	90	82.85714	90	111.6071
100	3.964286	100	21.42857	100	95.82143	100	133.9286
110	4.5	110	26.16071	110	105.4286	110	155.3571
120	5.839286	120	32.23214	130	140.7143	120	175.8929
130	7.303571	130	38.39286	140	176.7857	130	205.3571
140	10.01786	140	63.03571	150	199.4286	140	230.3571
150	24.375	150	91.60714	160	223.2143	150	270.5357
160	36	170	165.1786	170	249.1071	160	302.6786
170	66.78571	180	185.5714	180	284.8214	170	338.3929
180	96.67857	190	210.2857	190	311.6071	180	390.1786
190	119.9107	200	237.3214	200	346.7857	190	428.5714
200	125.5	230	290.8214	210	378.9286	200	491.0714
210	156.6071	240	310.0784	220	421.7857	210	557.1429
220	175.1429	250	Flashover	230	468.7079	220	610.1071
230	189.875			235	Flashover	228	Flashover
240	199.4107						
250	224.6429						
260	279.8214						
264	Flashover						

Table A7: Breakdown Voltages for Silicone and Glass Insulators.

	POSITIVE DC		NEGATIVE DC	
Corona Source	**Glass (kV)**	**SiR (kV)**	**Glass (kV)**	**SiR (kV)**
Both ends	228	185	252	198
Live end	235	190	256	202
Dead end	250	195	265	207
None	264	198	270	212

Calculation of Basic Insulation Level (U_{10}) for 22 kV SiR Insulator.

$$U_{10} = U_{50}\,(1\text{-}1.3s);$$

Where *s* is the standard deviation of the impulse breakdown voltages measured during the experimental testing and it has a value of 0.03.

Therefore, $U_{10} = U_{50} \times 0.961$

For Dry Positive: U10= 321 x 0.961 = 308 kV

For Dry Negative: U10= 309 x 0.961 = 297 kV

For Wet Positive: U10= 272 x 0.961 = 261 kV

For Wet Negative: U10= 219 x 0.961 = 210 kV

APPENDIX B

Table B1: Circuit Parameter of the HVDC Generator.

Parameters	Value
C1	150 kV, 100nF
C2	300 kV, 50nF
C3	300 kV, 50nF
C4	300 kV, 50nF
D1	300 kV, 20 mA
D2	300 kV, 20 mA
D3	300 kV, 20 mA
D4	300 kV, 20 mA
R1	300 kV, 600 MΩ
R2	300 kV, 600 MΩ
Damping Resistor	10 kΩ
Grounding Resistor	20 kΩ

Table B2: Standard Insulation System Level (According to IEC 60071-1).

Nominal System Voltage (kV)	Power Frequency Withstand Voltage (kV) (r.m.s Value)	Impulse Withstand Voltage 1.2/50 µs (kV) (Peak Value)
22	50	125

Table B3: Precipitation Conditions for Standard Procedure.

Rate of rainfall (Both the vertical and horizontal component)	1mm/min
Conductivity of Water	100 ±15µS/cm
Angle of rainfall	45^0
Temperature	20^0C